alicia.lork@gu.se

Thesis for the Degree of Doctor of Philosophy

Probing the subcellular molecular architecture and turnover of neural cell models using correlative mass spectrometry imaging

Alicia Andrea Lork

UNIVERSITY OF GOTHENBURG

Department of Chemistry and Molecular Biology

Gothenburg, 2024

Thesis for the Degree of Doctor of Philosophy

Probing the subcellular molecular architecture and turnover of neural cell models using correlative mass spectrometry imaging

Alicia Andrea Lork

alicia.lork@gu.se

ISBN: 978-91-8069-637-1 (PRINT)
ISBN: 978-91-8069-638-8 (PDF)
Available online at http://hdl.handle.net/2077/79654

Department of Chemistry and Molecular Biology
University of Gothenburg
SE-405 30 Göteborg, Sweden

Printed by Stema Specialtryck AB

“Look I’m not proud to share this,
but the truth is,
I just kept crawling, and it kept working.”

Jerry Smith

Abstract

Neurons are fascinating cellular units of the nervous system and are responsible for the propagation of signals that let us move and think. Understanding cellular mechanisms that maintain neurons and enable their communication is crucial for a deeper understanding of the nervous system, including diseases that affect it. Elucidating the intricacies of biological processes is a core purpose of analytical methods. However, often the use of one technique does not provide sufficient information to answer scientific questions. Correlative chemical imaging, the combination of two or more imaging modalities, is a useful analytical tool to obtain comprehensive knowledge of a sample that could not be obtained otherwise.

In the work included in this thesis, correlative chemical imaging was used to investigate exocytosis, the process by which neurotransmitter is released from cellular vesicles to the extracellular space to communicate with other cells. The predominantly partial release of neurotransmitters and concurrent chemical transport into vesicles was visualized with correlative transmission electron microscopy (TEM) and nanoscale secondary ion mass spectrometry (NanoSIMS) imaging. Additionally, it was found that the process of partial release is independent of vesicle size. Furthermore, protein turnover, an important mechanism in cells to maintain protein homeostasis was investigated in human stem cell-derived neural progenitor cells (NPCs) and their further differentiation to neurons. Utilizing correlative TEM and NanoSIMS imaging, protein turnover could be tracked at a single organelle level by incubating cells with isotopically labeled amino acids. It was found that protein turnover is heterogeneous across the cell and that different amino acids result in different spatial turnover patterns. In the differentiation from NPCs to neurons it was found that protein turnover overall slowed down and that the protein lifetime of different organelles in different stages of differentiation was highly distinguished which could potentially be used to assess activities of these organelles and their involvement in the regulation of specific cell states. Additionally, it was found with correlative fluorescence microscopy and NanoSIMS imaging that NPCs recovering from stress have reduced protein turnover and that stress granules, organelles that are formed when cells undergo stress, are displaying similar turnover than that in the cytoplasm. Taken together, this thesis provides insights into the biological mechanisms of neural cell models via correlative mass spectrometry imaging.

Sammanfattning på svenska

Neuroner är fascinerande cellulära enheter i nervsystemet och ansvarar för överföring av signaler som gör att vi kan röra oss och tänka. Att förstå de cellulära mekanismer som upprätthåller nervcellerna och möjliggör deras kommunikation är avgörande för en djupare förståelse av nervsystemet, inklusive sjukdomar som påverkar det. Att klargöra de komplicerade biologiska processerna är ett centralt syfte med analytiska metoder. Dock räcker det inte ofta med att använda en enda teknik för att få tillräcklig information för att besvara vetenskapliga frågor. Korrelativ kemisk avbildning, kombinationen av två eller flera avbildningsmetoder, är ett användbart analytiskt verktyg för att få omfattande kunskap om ett prov som inte skulle kunna erhållas på annat sätt.

I det arbete som ingår i denna avhandling användes korrelativ kemisk avbildning för att undersöka exocytos, den process genom vilken neurotransmittorer frisätts från cellulära vesiklar till det extracellulära utrymmet för att kommunicera med andra celler. Den övervägande partiella frisättningen av neurotransmittorer och den samtidiga kemiska transporten in i vesiklarna visualiserades med korrelativ transmissionselektronmikroskopi (TEM) och nanoskalig sekundärjon-masspektrometri (NanoSIMS). Dessutom visade det sig att processen med partiell frisättning är oberoende av vesikalstorleken. Vidare undersöktes proteinomsättning, en viktig mekanism i celler för att upprätthålla proteinhomeostas, i humana stamcellsderiverade neurnala progenitorceller (NPC) och deras vidare differentiering till neuroner. Med hjälp av korrelativ TEM- och NanoSIMS-avbildning kunde proteinomsättningen spåras på en enskild organellnivå genom att cellerna inkuberades med isotopiskt märkta aminosyror. Det visade sig att proteinomsättningen är heterogen över hela cellen och att olika aminosyror resulterar i olika spatiala omsättningsmönster. Vid differentieringen från NPC till neuroner visade det sig att proteinomsättningen generellt sett minskade och att proteinlivslängden för olika organeller i olika differentieringsstadier var mycket olika, vilket kan användas för att bedöma aktiviteter hos dessa organeller och deras inblandning i cellulär reglering av specifika celltillstånd. Dessutom visade det sig med korrelativ fluorescensmikroskopi och NanoSIMS-avbildning att NPC som återhämtar sig från stress har minskad proteinomsättning och att stressgranuler, organeller som bildas när celler genomgår stress, uppvisar liknande omsättning som den i cytoplasman. Sammantaget ger denna

avhandling insikter i de biologiska mekanismerna i neurala cellmodeller via korrelativ masspektrometrisk avbildning.

List of Publications and Contribution Report

I. Visualization of Partial Exocytotic Content Release and Chemical Transport into Nanovesicles in Cells

Tho Duc Khanh Nguyen, Lisa Mellander, Alicia Lork, Aurélien Thomen, Mai Philipsen, Michael E. Kurczy, Nhu T.N. Phan, and Andrew G. Ewing
ACS Nano 2022, 16, 3, 4831–4842

Participated in sample preparation, TEM imaging, and discussion of the results. Edited the manuscript together with the other authors.

II. Characterization of Stress Granule Protein Turnover in Neuronal Progenitor Cells Using Correlative STED and NanoSIMS Imaging

Stefania Rabasco, Alicia A. Lork, Emmanuel Berlin, Tho D.K. Nguyen, Carl Ernst, Nicolas Locker, Andrew G. Ewing, and Nhu T.N. Phan
International Journal of Molecular Sciences 2023, 24(3), 2546

Participated in designing the STED and NanoSIMS experiments, performing the sample preparation, and discussion of the results. Edited the manuscript together with the other authors.

III. Quantitative Nanoscale Secondary Ion Mass Spectrometry (NanoSIMS) Imaging of Individual Vesicles to Investigate the Relation between Fraction of Chemical Release and Vesicle Size

Tho Duc Khanh Nguyen[¥], Stefania Rabasco[¥], Alicia A. Lork, Andre du Toit, and Andrew G. Ewing
Angewandte Chemie Int. Ed. 2023, e202304098

Participated in designing the TEM and NanoSIMS experiments, sample preparation, and discussion of the results. Edited the manuscript together with the other authors.

IV. Subcellular Protein Turnover in Human Neural Progenitor Cells revealed by Correlative Electron Microscopy and Nanoscale Secondary Ion Mass Spectrometry Imaging

Alicia A. Lork, Stefania Rabasco, Carl Ernst, André du Toit, Silvio O. Rizzoli, and Nhu T. N. Phan

Chemical Science, 2024

Participated in designing the experiments, performed the sample preparation and NanoSIMS imaging, analyzed data, and discussed the results. Wrote the manuscript together with N.T.N.P and edited together with the other authors.

V. Elucidation of Subcellular Protein Turnover during Neuronal Differentiation by Correlative Electron Microscopy and NanoSIMS Imaging

Alicia A. Lork, André du Toit, Stefania Rabasco, Carl Ernst, and Nhu T. N. Phan

Manuscript

Participated in designing the experiments, performed the sample preparation and NanoSIMS imaging, analyzed data together with A.T., and discussed the results. Wrote the manuscript together with N.T.N.P and edited it together with the other authors.

[¥] *These authors contributed equally to the work.*

Related Publications not included in the thesis

Potentiometric pH Nanosensor for Intracellular Measurements: Real-Time and Continuous Assessment of Local Gradients
Mohaddeseh Aref, Elias Ranjbari, Juan José García-Guzmán, Keke Hu, Alicia Lork, Gaston A. Crespo, Andrew G. Ewing, and Maria Cuartero

Analytical Chemistry 2021, 93, 47, 15744–15751

Chemical Imaging and Analysis of Single Nerve Cells by Secondary Ion Mass Spectrometry Imaging and Cellular Electrochemistry

Alicia A. Lork, Kim L. L. Vo, and Nhu T. N. Phan

Frontiers in Synaptic Neuroscience, 2022 Volume 14 – 2022

Quantitative Chemical Imaging at the Cellular Level: SIMS, Fluorescence, and Correlative Techniques

Tho D. K. Nguyen[¥], Alicia A. Lork[¥], Andrew G. Ewing, and Nhu T. N. Phan

In: *Single Cell 'Omics of Neuronal Cells. Neuromethods,* Sweedler, J.V., Eberwine, J., Fraser, S.E. (eds). Humana, New York, NY. 2022 vol 184, 219-250.

Lipid Organization and Turnover in the Plasma Membrane of Human Differentiating Neural Progenitor Cells revealed by Time-of-Flight Secondary Ion Mass Spectrometry Imaging

Emmanuel Berlin, Alicia A. Lork, Martin Bornecrantz, Carl Ernst, and Nhu T. N. Phan

Accepted for publication *Talanta*

Partial Dopamine Release Revealed from Single iPSC derived FOXA2 Dopaminergic Neurons by Electrochemistry

Chaoyi Gu[¥], Alicia A. Lork[¥], Soodabeh Majdi[¥], Anna Larsson, Pieter Oomen, Ying Wang, Huashan Peng, Carl Ernst, Andrew G. Ewing

Manuscript in preparation

Understanding the physical functions of stress granules in neurotransmission

Kim L. L. Vo[¥], Keke Hu[¥], André du Toit, Alicia A. Lork, Nikolas Locker, Andrew G. Ewing

Manuscript in preparation

Commentary: Integration of computer vision for correlative imaging of electron microscopy and mass spectrometry imaging

André du Toit, Alicia A. Lork, Nhu T.N. Phan

Manuscript in preparation

[¥] *These authors contributed equally to the work.*

Table of contents

Abbreviations

2D/3D – 2 or 3 Dimensional

A – Adenine

AA – Amino acid

ALK – Anaplastic Lymphoma Kinase

AMP – Adenosine Monophosphate

ATP – Adenosine Triphosphate

ATF – Activating Transcription Factor

BDNF – Brain Derived Neurotropic Factor

BMP – Bone Morphogenetic Protein

C – Cytosine

CLEM – Correlative Light and Electron Microscopy

CLSM – Confocal Laser Scanning Microscopy

DCV – Dense Core Vesicle

DNA – Deoxyribonucleic acid

DESI – Desorption Electrospray Ionization

eIF – Eukaryotic Initiation Factor

EM – Electron Microscopy

ER – Endoplasmic Reticulum

FM – Fluorescence Microscopy

FUS – Fused in Sarcoma

G – Guanine

GA – Glutaraldehyde

GDNF – Glia-derived Neurotrophic Factor

GSK – Glycogen Synthase Kinase

HEK – Human Embryonic Kidney

HRI – Heme Regulated Inhibitor

iPSC – Induced Pluripotent Stem Cell

IRE1 – Inositol-requiring Enzyme 1

LDCV – Large Dense Core Vesicle

L-DOPA – L-3,4-dihydroxyphenylalanine

LLPS – Liquid-liquid Phase Separation

MALDI – Matrix Assisted Laser Desorption Ionization

mRNA – messenger RNA

MS – Mass Spectrometry

MSI – Mass Spectrometry Imaging

mTOR – mammalian/mechanistic target of Rapamycin

m/z – mass to charge

NA – Numerical Aperture

NanoSIMS – Nanoscale Secondary Ion Mass Spectrometry

NGF – Nerve Growth Factor

NPC – Neural Progenitor Cell

OCT – Octamer-binding Transcription Factor 4

PALM – Photoactivated Localization Microscopy

PC12 – Pheochromocytoma 12

PERK – Protein Kinase RNA-like Endoplasmic Reticulum Kinase

PFA – Paraformaldehyde

qPCR – quantitative PCR

RNA – ribonucleic acid

RBP – RNA-binding proteins

RNP – Ribonucleoprotein

ROS – Reactive Oxygen Species

SEM – Scanning Electron Microscopy

SG – Stress Granule

SHH – Sonic Hedgehog

SILAC – Stable Isotope Labeling by Amino Acids in Cell Culture

SIMS – Secondary Ion Mass Spectrometry

SMAD – Small Worm Phenotype Mothers Against Decapentaplegic

SNARE – Soluble *N*-ethylmaleimide-sensitive Factor Attachment Protein Receptor

SSV – Small Synaptic Vesicle

STED – Stimulated Emission Depletion

STORM – Stochastic Optical Reconstruction Microscopy

T – Thymine

TDP-43 – TAR DNA-binding Protein 43

TEM – Transmission Electron Microscopy

TGFβ – Transforming Growth Factor beta

ToF-SIMS – Time-of-Flight Secondary Ion Mass Spectrometry

tRNA – transfer RNA

U – Uracil

UPR – Unfolded Protein Response

WNT – Wingless-related Integration Site

v-ATPase – Vacuolar ATPase

VMAT – Vesicular Monoamine Transporter

VNUT – Vesicular Nucleotide Transporter

CHAPTER 1 Biological processes

Biological processes can be described as a series of molecular, cellular, or physiological events that are the basis for maintenance, growth, development, and reproduction of living organisms. They are essential for the functioning and survival of organisms and require complex interactions of biomolecules and cellular structures such as organelles. In the publications included in this thesis, several cell biological processes were investigated with analytical methods. Protein turnover, cellular differentiation, cellular stress, and exocytosis are introduced in detail in this chapter.

1.1 Protein turnover

Protein turnover is the gradual replacement of old or faulty proteins with newly synthesized ones. Maintaining an intact proteome is a priority of every cell in an organism to function properly as an imbalance of protein turnover or accumulation of faulty proteins can lead to cell death [1], [2]. Protein turnover thereby is a balance of protein synthesis and protein degradation (Fig. 1) [3] and these processes in turn can be modulated in various ways.

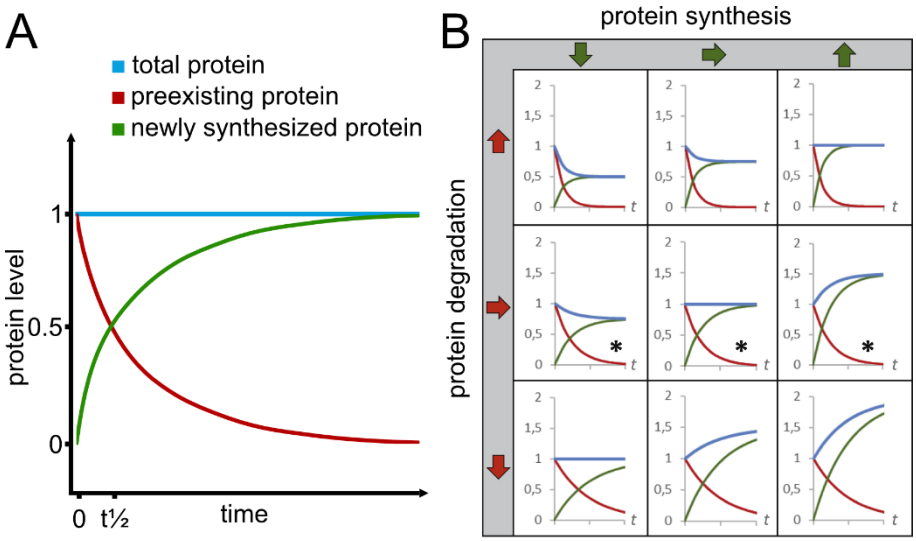

Figure 1. The levels of total cellular protein are dependent on both protein synthesis and degradation (A). If only protein synthesis or protein degradation is altered, the level of total protein changes (B). If both protein synthesis and protein degradation are altered, the level of total protein can

either change or stay at the same level. Figure adapted and reproduced from [3] under the creative commons license.

1.1.1 Protein synthesis

Protein synthesis is the generation of proteins from their building blocks, amino acids. The information for the amino acid sequence of proteins is contained within deoxyribonucleic acid (DNA). DNA is composed of a sugar (deoxyribose), a phosphate group, and different bases containing nitrogen which are adenine (A), cytosine (C), guanine (G), and thymine (T) and these molecules are arranged in a double helix [4]. The order of these four nitrogen bases makes up the genetic code, of which each triplet, also called codon, encodes one amino acid [5]. Importantly, the possible combinations of these codons exceed the number of amino acids so that multiple codons can encode one amino acid. For example, the amino acid leucine is encoded by six codons (TTA, TTG, CTT, CTC, CTA, CTG), however, tryptophan is only encoded by one codon (TGG) [6]. To initiate protein synthesis, a DNA stretch of the respective gene for the protein is transcribed into ribonucleic acid (RNA). The DNA of a eukaryotic cell is contained within the nucleus and is transcribed into messenger RNAs (mRNAs) by RNA polymerase II [7]. In this process, RNA polymerase II accesses the genetic information of a non-coding DNA strand, or so-called antisense strand, to create a complementary strand of the antisense strand. This produces a single-stranded mRNA copy of the sense strand which contains uracil (U) as a nitrogen base instead of thymine. For example, leucine has six possible mRNA codons: UUA, UUG, CUU, CUC, CUA, CUG, and tryptophan has UGG. The RNA then undergoes modifications such as methylation, the addition of a 3’ poly-A-tail, or splicing, which affects its stability and sequence [8], [9]. Once the modifications are completed, the mRNA exits the nucleus through nuclear pores. In the cytoplasm, the mRNA combines with mRNA-binding proteins to form ribonucleoproteins, which influence its stability, cytoplasmic localization, and their translation [10]. The mRNA is then translated into proteins using ribosomes, which are present in the cytoplasm, either in free form or in association with the endoplasmic reticulum (ER) [11]. The partition of mRNAs between those pools of ribosomes was proposed to be a post-transcriptional regulation mechanism [12]. In translation, transfer RNAs (tRNAs) with a complementary sequence to the mRNA assemble with the mRNA and the ribosome (Fig. 2). This is assisted by at least 12 translation factors [13]. The tRNA carries the respective amino acid to the ribosome

which links these amino acids together to form a polypeptide. The polypeptide is post-translationally modified within the cell (phosphorylation, glycosylation, ubiquitination, etc.) and is folded into a three-dimensional (3D) structure to become a protein.

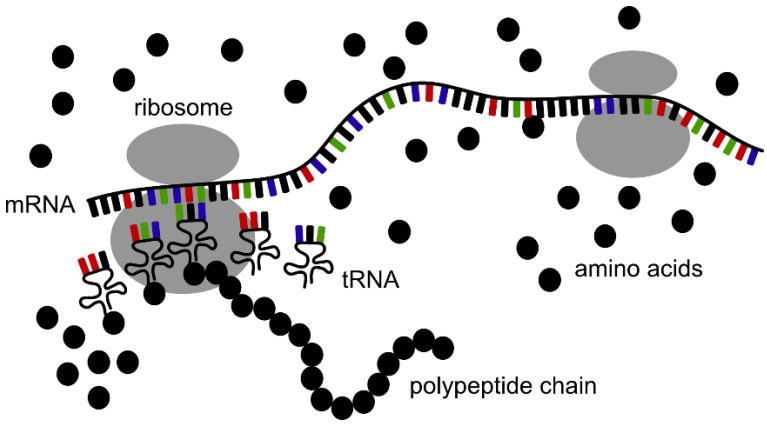

Figure 2. Translation. To translate mRNA into protein the mRNA assembles with ribosome and tRNA. The tRNA carries the respective amino acid. The complementary sequence of tRNA and mRNA attach to each other, and the ribosome facilitates the binding of the amino acids to form a polypeptide chain.

Protein synthesis is influenced by many factors. For example, it has been shown that activation of phosphoinositide 3-kinase (PI3K)/AKT and mitogen-activated protein kinase (MAPK) signaling [14] activate the mammalian or mechanistic target of rapamycin (mTOR) signaling which in turn influences protein synthesis. mTOR signaling is involved in the short-term activation of translation and in increasing translational capacity by increasing the number of ribosomes [15]. mTOR signaling is activated by the level of amino acids, insulin, and growth factors [16], and is suppressed by nutrient and energy deficiency [17]. In addition, protein synthesis is affected by the cell cycle stage, possibly due to the influence of mTOR signaling on cell growth [18]. Translation is also controlled via the phosphorylation of eukaryotic initiation factor 2 (eIF2). eIF2 assembles in a complex, together with methionyl-initiator tRNA, a protein complex, and mRNA. The phosphorylation of eIF2 is induced by kinases (PERK, GCN2, and HRI) and part of the cellular stress response, to induce global inhibition of translation [19], [20].

Protein synthesis can be measured by different methods. A common method is to indirectly assess the cellular mRNA levels using quantitative polymerase chain reaction (qPCR). However, this method could provide misleading results due to a discrepancy between the mRNA and protein levels [21], [22]. Alternatively, protein synthesis is measured by determining the newly synthesized proteins in the cells via an incorporation of radioactive or isotopic labels in combination with mass spectrometry (MS). For example, MS is used to measure nascent proteins in cells treated with puromycin, which induces premature chain termination [23], [24]. Another method is ribosomal profiling for which ribosome-associated mRNAs are sequenced to assess which mRNAs are being translated into proteins which correlates well with protein abundance [25], [26].

1.1.2 Protein degradation

When proteins are old or defective, they must be removed from the cytoplasm and are recycled or degraded. This happens via two distinct pathways: the ubiquitin-proteasome system or lysosomal proteolysis (Fig. 3). The ubiquitin-proteasome system functions by adding ubiquitin to the target proteins with different ubiquitin enzymes which leads to the degradation of the proteins by proteasomes [27], [28]. The ubiquitination is a reversible process as indicated by the presence of deubiquitylating enzymes [29]. The proteasome is a protein complex consisting of two sub-complexes, which have receptors to recognize the ubiquitin chains on the proteins upon which the protein unfolds, and enters the proteasome (Fig. 3A) [30]. Once inside the proteasome, proteins are degraded by proteases into fragments between 3-25 amino acids in length [31]. The fragments are then released into the cytoplasm where they are either reused for new proteins, processed by enzymes, or presented on the cell surface as antigens for the immune system [32]. Importantly, proteasomal degradation is an energy-dependent process requiring adenosine triphosphate (ATP) [33].

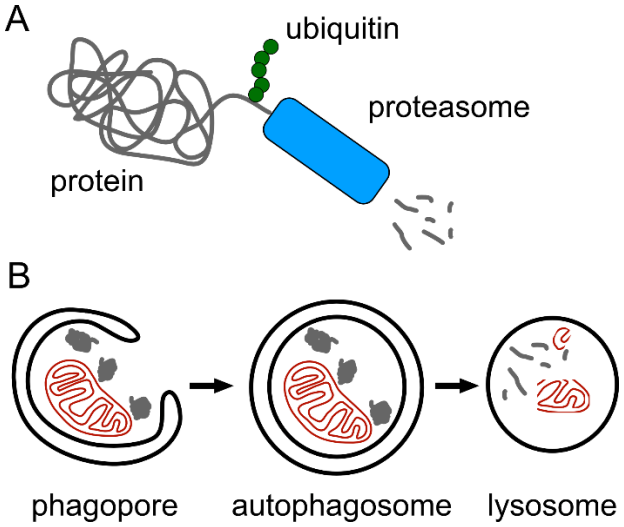

Figure 3. Schematic of the two main mechanisms of protein degradation. A) Degradation of proteins via the ubiquitin-proteasome system. B) Degradation of organelles/proteins via lysosomal proteolysis.

Protein degradation via lysosomal proteolysis on the other hand begins with an engulfment of proteins or organelles by membranes (Fig. 3B). This is considered as non-specific bulk proteolysis [34]. Lysosomal proteolysis can start either from the extracellular space (endocytosis) or from the inside of the cell in case of autophagy, the cellular self-digestion process. The resulting vacuolar structures are then either called endosomes or autophagosomes which, after maturation, fuse with lysosomes. The maturation is thereby defined as the removal of all autophagy-related proteins from the autophagosome surface which might inhibit the fusion with lysosomes [35]. Proton pumps reside on the membrane of lysosomes and create an acidic environment within the lysosome which is ATP-dependent [36]. This activates hydrolytic enzymes such as proteases, nucleases, and lipases [37], [38]. The proteases then break down proteins into peptide fragments and amino acids which are transported out of the lysosome via transporters [39], [40], [41], [42].

Similar to protein synthesis, protein degradation is influenced by many different signaling pathways. Protein degradation via autophagy is influenced by the mTOR pathway, for example, autophagy is induced by scarcity of nutrients [43]. Adenosine monophosphate (AMP) activated protein kinase has also been shown to modulate autophagy in response to

energy deficiency [44]. E3 ubiquitin ligases are often fully activated by posttranscriptional modifications such as phosphorylation, but they can also self-catalyze their own degradation or the degradation of other ubiquitin ligases [45], [46]. In addition, protein phosphorylation by glycogen synthase kinase 3 (GSK3) has been shown to target proteins for degradation. Hence, inhibition of GSK3 by Wingless-related integration site (WNT) signaling leads to protein stabilization and contributes to cell growth during mitosis [47].

Protein degradation can be measured by different approaches. Global degradation can be observed with metabolic labeling via radioactive or isotopic labels. Alternatively, an addition of cycloheximide to cells, which blocks protein synthesis, can be used followed by tracking the decay of proteins by western blot or fluorescence microscopy [48]. However, cycloheximide is toxic leading to cellular stress and cell death which could affect how the cells degrade proteins with differences between short-lived and long-lived proteins [49], [50]. Another method is to measure the degradation of specific proteins by labeling proteins with fluorescent tags and monitoring their decay over time with fluorescent microscopy [48]. Nanoscale secondary ion mass spectrometry (NanoSIMS) imaging has also been employed to study protein degradation/turnover by determining protein age in single lysosomes which was shown to be heterogeneous demonstrating the need for single organelle resolution in turnover studies [51].

1.1.3 Protein turnover

Protein turnover is the complex interplay of protein synthesis and degradation. They are linked via mTOR signaling which affects both, synthesis and degradation, making it an important regulator for protein turnover. It has been found that protein lifetimes in cells of closely related animal species are similar and global protein turnover correlates negatively with species lifetime [52]. Protein turnover was shown to differ between *in vivo* and *in vitro* measurements [49], and varies among tissues [53], and cell types [54]. Cell-to-cell variations in protein turnover have been shown to be due to different global protein degradation rates [18]. In addition, it was shown that the codon sequence could be used to predict protein lifetime, however, the underlying mechanism is not clear [55].

Protein turnover can be studied via the measurement of protein synthesis or degradation as described above. However, it was found that protein

abundance is mainly controlled at the translational level, and thus the indirect method of looking at transcripts via qPCR to draw conclusions about protein abundance is often not sufficient [56]. One common approach is to use a pulse and chase strategy of stable isotope labeling by amino acids (e.g. ^{13}C-, ^{15}N-, amino acid) in cell culture (SILAC) and mass spectrometry proteomics to examine cellular protein turnover [57]. The simultaneous detection of RNA and proteins via SILAC revealed a correlation between mRNA and protein levels, although their half-lives were not correlated [58]. The recycling of labeled amino acids should also be considered as it could lead to an underestimation of the protein synthesis rate [3].

The main limitation of these methods is that they ignore the spatial aspect of protein turnover and the molecular heterogeneity between cells and between subcellular compartments within single cells. Conventional mass spectrometry is performed in bulk measurements which disregard cell-to-cell and organelle-to-organelle variations. Given the heterogeneity between cells, it is possible to sort cells based on fluorescent markers (FACS) [59], or use single-cell proteomics [60]. Recently, proximity labeling has also been combined with SILAC to look at the protein turnover of organelles [61]. In another approach, unnatural amino acids are introduced into the cells allowing fluorescence-based analysis of protein turnover [62]. However, this requires a substantial genetic modification in the cells whose effects on protein folding and function, posttranslational modifications, and protein degradation should be considered.

Subcellular spatial information of protein turnover was found increasingly critical in highly polarized cells, such as neurons where the local translation and degradation occur at single long-distant synapses leading to local turnover [63], [64]. Protein turnover at single synapses was found to closely relate to their synaptic activity [65] implying that local turnover reflects the functional state of cellular compartments. In addition, the same protein could have different turnover corresponding to its subcellular localization and its functional state [66].

1.1.4 Amino acids as building blocks of proteins

Amino acids (AAs) are the building blocks of proteins. There are 20 AAs in the genetic code and the sequence of AAs decides the folding, function, and properties of the protein. Once AAs are deaminated their carbon skeleton can enter metabolic pathways to produce other biomolecules, such as ATP, glucose, and fatty acids, and AAs serve as neurotransmitters or metabolic

precursors to neurotransmitters [67]. AAs are divided into non-essential and essential depending on whether they can be synthesized in the cells to a sufficient amount. Some AAs can be a precursor of other AAs in various molecular pathways. Glutamate, for example, can be converted into other amino acids, such as proline and arginine via ornithine [68]. AAs can be obtained from protein degradation but also from the outside of the cells via plasma membrane transporters. The homeostasis of AAs is regulated for example via mTOR and general control nonderepressible 2/Activating transcription factor 4 (GCN2/ATF4) signaling which affects the expression of amino acid transporters [69]. There are three main classes of AA transporters, namely symporters, antiporters, and uniporters. Most AA transporters are symporters that function by transporting an amino acid together with a cation [70]. Antiporters transport AAs bidirectionally depending on cofactors, and they have been shown to be upregulated in fast-growing cells [71], [72]. Uniporters are not common in mammalian cells, except for cationic AA transporters [70]. The degradation of amino acids involves the removal of the amino group which is then transferred to another molecule or is excreted as NH_3 or NH_4^+. The remaining carbon skeleton is further metabolized in the Krebs cycle [73].

In summary, protein turnover is a complex, tightly regulated process that maintains the proteome within cells. In papers II, IV, and V, protein turnover was studied by incubating cells with isotopically labeled amino acids and tracking their incorporation and clearance at a subcellular scale with NanoSIMS imaging. By combining NanoSIMS with electron or fluorescence microscopy, organelles could be identified, and protein turnover could be attributed to single organelles.

1.2 Cellular differentiation and neuronal development

1.2.1 Early development of an organism, formation of germ layers

The fertilization of two gametes (e.g. egg and sperm cell) gives rise to a zygote in which the genetic material of both (haploid) gametes is unified to make a diploid cell. This zygote is the product of meiosis which in contrast to mitosis is aimed at generating genetic diversity. The zygote is the earliest developmental stage of a new individual organism. By dividing and eventually differentiating into specific cell types in a series of orchestrated events, it makes up an entire organism. The first developmental milestone of the organism is the blastocyst which is reached 5-6 days after fertilization in humans [74]. It was found that the uptake of AAs is altered during the

development of blastocysts, illustrating the significant changes in metabolism in the early development of the embryo [75], [76]. The blastocyst consists of an inner cell mass that is asymmetrically distributed within the blastocyst and the trophectoderm which surrounds the inner cell mass (Fig. 4). The trophectoderm later gives rise to mostly extraembryonic material such as the trophoblast cells in the placenta [77]. The inner cell mass further differentiates into epiblast and hypoblast of which the embryo itself arises from the epiblast contained within the inner cell mass. Embryonic stem cells are usually derived from the inner cell mass of an embryo [78]. The expression of different genes, particularly OCT4, Nanog, CDX2, and GATA6, is critical in early development and well conserved between species although there are differences in the specific timing and localization between species [79]. Without OCT4 expression, for example, the lineage specification from the inner cell mass to epiblast and hypoblast is affected [80].

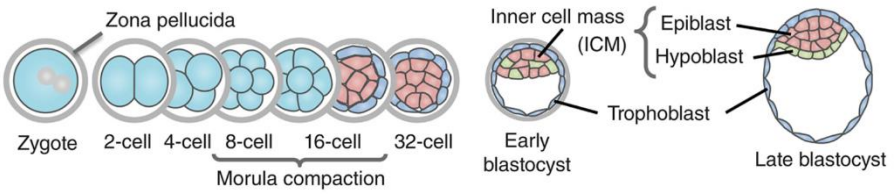

Figure 4. Development from zygote to blastocyst. The zygote undergoes multiple divisions until it reaches the blastocyst stage in which trophoblast and inner cell mass are distinguished. The inner cell mass further develops into epiblast and hypoblast. Figure adapted and reproduced with permission from [77].

The next major process in the development of an embryo is gastrulation in which the epiblast gives rise to the three germ layers: endoderm, mesoderm, and ectoderm [81]. The germ layers give rise to different tissues within the organism. Specifically, the ectoderm will give rise to the nervous system and skin, the mesoderm to the heart, muscles, blood, kidney reproductive organs, microglia, and connective tissue, and the endoderm will make up the intestine, lungs, liver, and pancreas [82]. Due to the commonly employed 14-day rule, a culture of human embryos after 14 days post fertilization, which is the initiation of gastrulation, is mostly prohibited by governments. This aims to establish a boundary for experimentation due to different views on when human life and moral status begin. This results in very limited data

from human embryos after this stage [83] requiring alternative models for experimentation.

Cellular signaling during embryo development is dependent on inductive factors and receptors transmitting the signal given by inductive factors. Inductive factors are signaling molecules that are secreted by (nearby) cells. Receptors on the cell surface respond to inductive factors and trigger an intracellular response via transcription factors, the cytoskeleton, and enzymes. These inductive factors often act in a concentration-dependent manner and a concentration gradient is maintained across the developing organism or tissue. A signaling molecule that acts in a concentration-dependent manner is termed "morphogen" and examples include Sonic hedgehog (SHH) and Bone morphogenetic protein (BMP) [84], [85]. An important concept in embryo development is the competence of a cell because only if a cell expresses all the right receptors/signaling molecules it can respond to certain signals [86], [87]. This means that the same signaling molecule can induce the differentiation of different subgroups of cells, allowing the generation of a variety of cell populations. This enables the creation of an entire organism given relatively few initial signaling molecules, such as BMPs, fibroblast growth factor (FGF), hedgehog, and WNT proteins.

1.2.2 Neural development

After the three germ layers are formed during gastrulation, further differentiation of cells commences. This process is termed organogenesis, during which the body plan is established. A crucial step for an organism is the development of the nervous system beginning with a process termed neurulation (Fig. 5) approximately 18 to 19 days after fertilization in humans [88]. Neurulation begins with the formation of a neural plate derived from the ectoderm. The neural plate is characterized by a suppression of BMP4 signaling [89] and will groove to eventually form the neural tube (Fig. 5). It is surrounded by mesoderm-derived somites and the notochord. In vertebrates, these structures play important roles in further patterning and in defining the anterior-posterior and dorsoventral axis of the neural tube. Dorsoventral patterning is mainly induced by the secretion of SHH from the notochord, and subsequently from the floor plate in the neural tube [90], and by the secretion of dorsalizing BMP and other proteins of the transforming growth factor beta (TGFβ) family from the roof plate [91]. The floor plate

also secretes regional-specific signaling molecules aiding the specification of subsets of cells along the anterior-posterior axis [92], [93]. Concurrently, the formation of the brain vesicles at the anterior end of the neural tube takes place, which later forms the forebrain, midbrain, and hindbrain. The isthmic organizer between midbrain and hindbrain was identified as an organizing center by transplantation experiments and is characterized by the expression of OTX2 and GBX2. It is an important local signaling center to generate polarity in this brain region via FGF8 and WNT1 signaling [94], which are also used *in vitro* to induce specific cell fates [95].

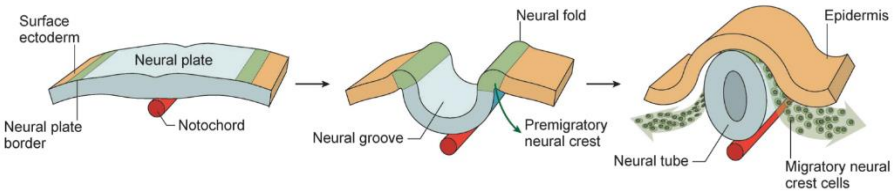

Figure 5. Neurulation. The neural plate groves and forms the neural tube which further develops into the nervous system. Figure adapted and reproduced with permission from [96], [97].

Signaling in the developing brain also influences symmetric or asymmetric cell division. This is crucial to maintain a stem cell population that can self-renew but also generate cells in asymmetric cell division which go on to differentiate into specific cells. For example, radial glia cells give rise to neurons but also self-renew until they differentiate into astrocytes [98]. Interestingly, radial glia cells were found to serve as scaffolds aiding neuronal migration to form the layered structure of the cortex. Once cells have acquired the identity of neurons, they begin to grow axons and dendrites under the guidance of extracellular cues [99], [100]. This process involves the intracellular recruitment of multiple organelles to the site of newly emerging axons [100], [101]. Once a neuron has established its connection with other cells, it will form synapses and communicate with other cells in the neural network.

Neural development is an important step in development. Due to the ethical concerns that are inherent with the use of human embryos, cell models such as human stem cell-derived cells are used to model the cell development processes *in vitro.* Stem cell-derived cells were used in papers II, IV, and V.

In paper V, the cellular changes regarding protein turnover in neural differentiation were analyzed.

1.3 Cellular stress

1.3.1 Cellular stress results in the formation of stress granules

Cells respond to changes in the extracellular environment such as temperature, radiation, and chemical cues. If changes in the extracellular environment are too extreme or persist for extended periods of time, the cell will initiate a stress response to protect and repair macromolecules and restore cell cycle checkpoints. This includes the activation of signaling pathways to coordinate a stress response, expression of stress proteins, cellular repair such as DNA repair, cell cycle arrest, activation of antioxidant pathways, metabolic changes, and activation of cell death pathways such as apoptosis if the stress is too severe [102]. The stress response often includes the formation of so-called stress granules (SGs) which were first observed in tomato cell lines and chicken fibroblasts after heat shock [103], [104], and they comprise mainly proteins and RNAs. SGs are "membrane-less" organelles meaning they separate from the cytoplasm without a membrane in a process involving liquid-liquid phase separation (LLPS) and oligomerization of ribonucleoproteins (RNPs). The assembly of SGs occurs rapidly after stress within several minutes and has been shown to be ATP-dependent [105], [106]. LLPS is a common mechanism within the cell to compartmentalize or separate small reaction volumes. Further examples of membrane-less organelles are nucleoli and P-bodies. SGs were found to have sub-structures including a stable core and a dynamic outer shell [105]. They contain RNPs which are complexes of RNA and RNA binding proteins (RBPs) influencing RNA processing [107], [108]. It has been suggested that intrinsically disordered regions in RBPs promote phase separation at a high concentration, and thus influence stress granule assembly [109], [110], [111], [112]. Besides RNPs, SGs also contain ribosomal subunits, translation initiation factors, and signaling molecules [113], [114]. Increasing levels of mRNPs, due to the inhibition of protein synthesis during cellular stress, drive the assembly of SGs [115]. The sequestration of signaling molecules, such as TOR complex 1 (TORC1), is thought to influence cell signaling by controlling the translation machinery [116]. T-cell intracellular antigen-1 (TIA1) and RasGAPSH3 binding protein (G3BP) are essential constituents for SG formation and thus are commonly used as marker proteins of SGs inside cells [117].

SGs have been shown to interact with P-bodies to exchange RNA and proteins [118] highlighting the dynamic nature of the organelles. There is a difference in the protein mobility between SGs and the cytoplasm and that mobility depends on the protein itself [117]. When the cell is recovered from stress, SGs resolve within a timespan of several minutes to a few hours. During this process, mRNPs can either return to translation or be targeted for autophagy [119], [120]. In neurons, mRNP granules appear in both synapse and soma [121] possibly due to the increased need for spatially restricted gene expression. SGs have also been linked to neurodegenerative diseases [115], [122], [123]. TAR DNA binding protein 43 (TDP43) and fused in sarcoma (FUS) are proteins, that are known to localize in SGs, and have been implicated with neurodegenerative diseases such as amyotrophic lateral sclerosis, frontotemporal lobar degeneration, and Alzheimer's disease [124], [125]. Upon stress, TDP43 and FUS translocate from the nucleus to the cytoplasm and associate with SGs. In neurodegenerative disease models, the nucleocytoplasmic localization of FUS and TDP43 is disturbed and the disassembly of SGs is impaired [126] leading to pathological aggregation of RBPs [127].

1.3.2 Different stressors result in different cellular stress responses

Cellular stress can be induced by various mechanisms which will lead to specific responses of the cell to the stressor. Common types of stresses for cells are oxidative, ER, mitochondrial, osmotic, hypoxic, and temperature stress. SGs can be classified into different groups based on their differential composition which is stressor-dependent [128]. However, the common step in SG assembly across different stressors is the disassembly of polysomes which can be mediated by the stressors through the phosphorylation of eIF2α and the attenuation of translation [108], [129].

Oxidative stress by reactive oxygen species (ROS) results in the damage of DNA and/or other biomolecules within the cells. An increased level of ROS results in an increase in autophagy activity to remove mitochondria as one of the main endogenous contributors of ROS [130]. In addition, heme-regulated inhibitor (HRI) kinase is required to phosphorylate eIF2α, inhibit protein synthesis, and induce SG formation in oxidative stress [131]. On the other hand, heat shock-induced stress results in an increase in the number of unfolded/entangled proteins, unspecific aggregation of proteins, damage to the cytoskeleton, fragmented ER or Golgi, and a decrease in lysosomes and mitochondria, which leads to a decrease of ATP levels in the cells [132]. Stress signaling after heat shock was shown to involve HRI kinase-

dependent phosphorylation of eIF2α [133] via heat shock protein 90 (HSP90) [134].

In the occurrence of ER stress, many proteins remain unfolded due to improper functioning of the ER. ER stress can be triggered for example by viral infections or molecules such as thapsigargin (Fig. 6). Thapsigargin causes the depletion of Ca^{2+} ions in the ER via the inhibition of the Sarcoplasmic/endoplasmic reticulum calcium ATPase (SERCA) pump [135], [136]. The cells counteract this effect with the unfolded protein response (UPR) via the ER chaperone GRP78 in an association with three signaling molecules, inositol requiring enzyme 1 (IRE1), protein kinase RNA-like ER kinase (PERK) and activating transcription factor 6 (ATF6) [102], [133]. Upon dissociation of GRP78, the inhibition of the three signaling molecules IRE1, PERK, and ATF6 is stopped and downstream signaling is activated leading to increased transcription of chaperones and increased mRNA degradation to reduce the amount of protein in the ER lumen [137], [138]. In addition, translation can be downregulated via these signaling cascades (via eIF2α) and an induction of apoptosis can take place if UPR persists for a prolonged time and ER function cannot be restored [139].

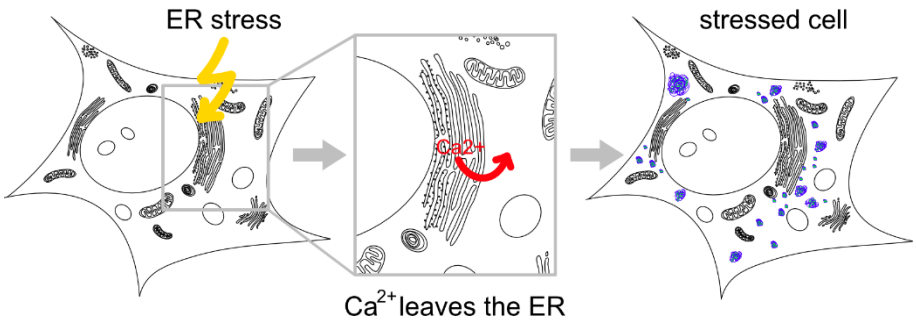

Figure 6. Schematic of ER stress by thapsigargin (yellow). ER stress leads to the depletion of Ca^{2+} storage (red) within the ER inducing signaling by IRE1, PERK, and ATF6. The stress eventually leads to the formation of SGs (blue) in the cell. These SGs were found to associate with or be in close proximity to the ER [140].

Overall, the mechanisms of formation, presence, and removal of SGs is very important in cell biological and medical research as these intricate cellular processes affect RNA localization, translation, and degradation and have been linked to neurodegenerative diseases and cancer. In paper II, the protein

turnover of SGs was investigated in neuronal progenitor cells using different stress paradigms. The results show that the protein turnover of SGs is similar to that of the cytoplasm. In addition, it was shown that after SG disassembly, cellular protein turnover is still significantly inhibited indicating the stress effects remain even after SG clearance.

1.4 Exocytosis

In an organism, cells are continuously communicating with each other, transmitting information to allow the organism to function. This communication can take place in various ways. Extracellular vesicles such as exosomes, microvesicles, or apoptotic bodies are types of intercellular communication but electrical signals and molecules such as hormones, cytokines, growth factors, and neurotransmitters can also transmit signals between cells. Extracellular vesicles are secreted as whole vesicles which contain, for example, nucleic acids, proteins, and lipids [141], [142]. Hormones, cytokines, growth factors, and neurotransmitters are usually stored in vesicles and are released from the vesicle upon stimulation of the cell and vesicular fusion with the cell membrane (Fig. 7). This process of release of the vesicle content is called exocytosis.

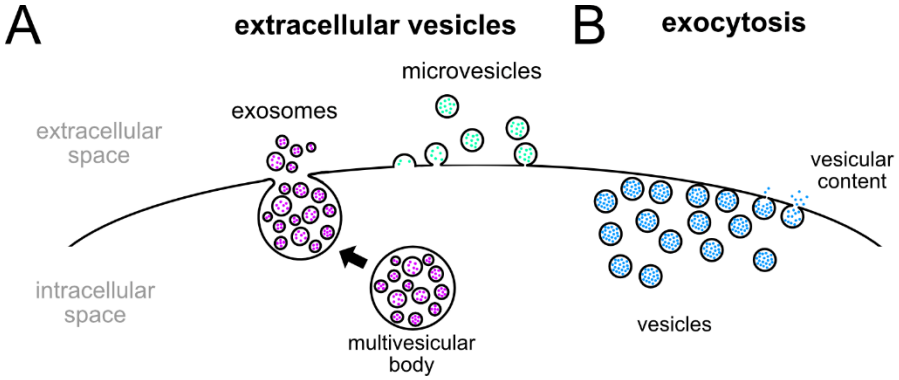

Figure 7. Different types of cellular communication via vesicles. A) Cellular communication via extracellular vesicles. Exosomes are secreted via the fusion of a multivesicular body with the plasma membrane. Microvesicles bud from the plasma membrane directly. B) Cellular communication via exocytosis: vesicular content is released from vesicles to the extracellular space.

1.4.1 Secretory vesicles

Secretory vesicles are complex organelles within cells that are formed through vesicle budding from the *trans*-Golgi network [143]. Vesicles enclose their contents with a lipid bilayer. This layer of phospholipids has been proposed to contain an enriched presence of triacyl glycerols and sphingomyelins compared to the synaptosome membrane [144]. In addition, a variety of proteins are located in and on the vesicle membrane which fulfill different functions. Some of the membrane proteins found on secretory vesicle membranes are part of the soluble N-ethylmaleimide-sensitive factor attachment receptor (SNARE) complex which is responsible for vesicle docking and fusion to the plasma membrane and is further described in the exocytosis section below [145]. Further vesicle membrane proteins include the proton pump vacuolar ATPase (v-ATPase) to maintain an acidic environment (pH ~5.5) within the vesicle (Fig. 8A). The ATPase contains two domains that mediate H^+ transport across the vesicle membrane via ATP hydrolysis which triggers a rotational mechanism within the v-ATPase [146]. Another membrane protein on secretory vesicles is the vesicular nucleotide transporter (VNUT) which translocates ATP into the vesicle lumen [147]. The transport of neurotransmitters into the vesicle is mediated via transmembrane proteins such as vesicular monoamine transporter (VMAT), vesicular glutamate transporter (VGLUT), or vesicular acetylcholine receptor (VAChT) and is often pH dependent. They actively transport their substrate across the vesicular membrane against the concentration gradient in exchange for protons [148], [149], [150].

The size of secretory vesicles typically ranges from 30-350 nm. Based on size and appearance they can be divided into small synaptic vesicles (SSVs) up to about 50 nm in size [151] and large dense core vesicles (LDCVs) ranging up to 500 nm in size [152]. LDCVs are not only characterized by their size but also by a protein-rich content, which appears as a dark and dense structure within the vesicle when imaged in transmission electron microscopy after staining with heavy metals like osmium. SSVs generally appear lighter in electron microscopy indicating less protein content compared to LDCVs (Fig. 8B). Additionally, a third class of small dense core vesicles with an average size of ~110 nm was suggested [153].

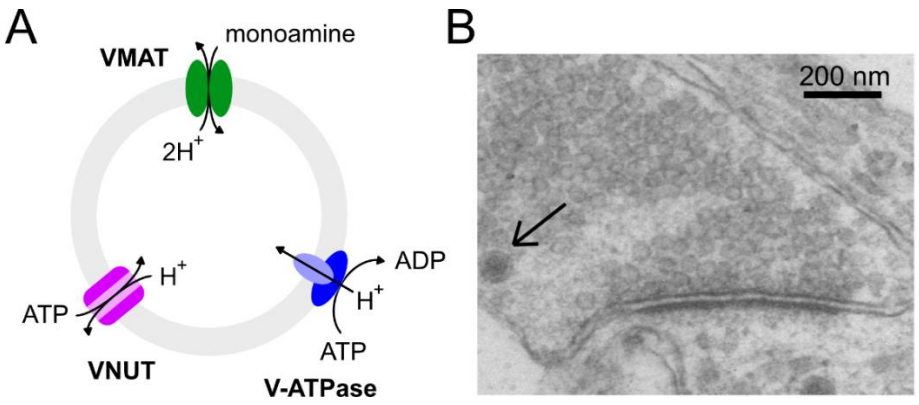

Figure 8. A) Schematic depicting a secretory vesicle with different membrane transporter proteins such as VMAT, VNUT, and v-ATPase. B) TEM image of SSVs and an LDCV (indicated with black arrow) in a hippocampal neuron, reproduced under the creative commons license from reference [154].

LDCVs contain neurotransmitters, ATP, different ions (Ca^{2+}, H^{+}, and Mg^{2+}), neuropeptides, and proteins [155], [156]. The most abundant proteins within LDCVs are chromogranins [157]. They are packaged into the vesicle in the *trans*-Golgi network and aid in the packaging of high concentrations of neurotransmitters within the vesicle. Dopamine has been shown to bind to the dense protein core due to electrostatic forces between the protonated dopamine and the negatively charged amino acid residues of the chromogranin proteins. The binding of catecholamine to chromogranins is thought to relieve the osmotic pressure within the vesicle [158]. This is also in agreement with the finding that a majority of dopamine localizes within the dense core of vesicles [159]. Newly synthesized vesicles are transported to the release site via microtubules and motor proteins such as kinesins facilitate this transport [160]. At the synapse, synaptic vesicles cluster via LLPS of synapsin which confines them to a cluster but retains their mobility within the cluster [161]. Once vesicles undergo exocytosis they have been shown to release/recycle around 200 times before reaching an inactive state and are subsequently degraded [162].

1.4.2 Exocytosis

Exocytosis is the fusion of the vesicle membrane with the plasma membrane leading to the release of vesicular content into the extracellular space. This process can be divided into three steps, namely docking, priming, and fusion.

Exocytosis is Ca^{2+} dependent and is mediated by a variety of vesicle and plasma membrane proteins, the SNARE proteins [163]. Those proteins act together in a zipper-like mechanism to pull the membranes closer together and aid in the fusion of the vesicle to the plasma membrane.

SNARE proteins are an important class of proteins involved in exocytosis as they form a complex to provide the necessary force for vesicle fusion. SNARE proteins include synaptobrevin, syntaxin, and synaptosome-associated protein 25 (SNAP25). Synaptobrevin is localized on the vesicle membrane whereas syntaxin and SNAP25 are located on the target membrane [164]. During priming, these SNARE proteins will form a partially zippered *trans*-SNARE complex which is facilitated by the interaction of munc18 with syntaxin [165]. Synaptotagmin is a protein residing on the vesicle membrane and acts as a calcium sensor. Isoforms of synaptotagmin have different sensitivities to Ca^{2+} and have been proposed to influence the release mode [166]. Upon binding of synaptotagmin with Ca^{2+}, it interacts with the SNARE proteins and phospholipids, ultimately leading to the opening of the fusion pore and the expulsion of vesicular content [167].

Depending on how much of the vesicular content is released, three main modes of exocytosis have been proposed: kiss and run partial release, and full release (Fig. 9). During kiss and run exocytosis the fusion pore is not fully established, and only about 2 nm in size [168]. The flickering of the fusion pore allows for only a small amount of neurotransmitter to leave the vesicle before the fusion pore closes. During partial release (also named "opened and closed", "sub quantal release", and "selective secretion") the fusion pore is larger, and more neurotransmitter is expelled into the extracellular space. Full release, as the name suggests, results in the release of all the stored neurotransmitter into the extracellular space and the collapse of the vesicle into the plasma membrane (Fig. 9) [169].

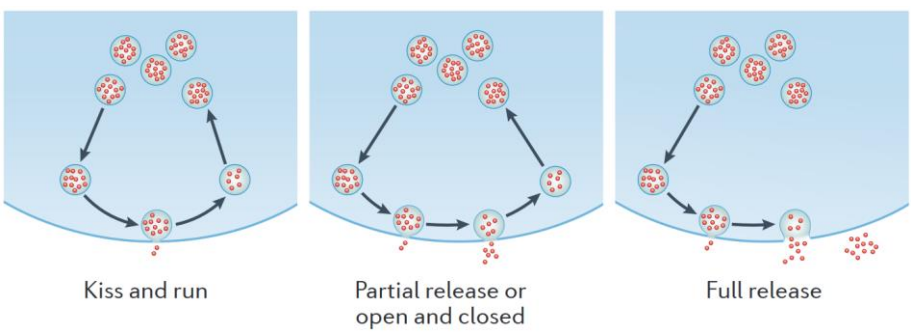

Figure 9. Schematic depicting different modes of exocytosis. Kiss and run only allows a small fraction of transmitter to be released. Partial release can lead to the release of a large proportion of neurotransmitter. Full release leads to the expulsion of all the content of the vesicle. Figure reproduced with permission from [169].

In summary, exocytosis is a highly conserved communication mechanism in cells to release vesicular content into the extracellular space. In the work for this thesis, correlative TEM and NanoSIMS imaging was used to visualize partial release using a stimulation paradigm with a substance to observe entry into the open vesicle in publication I. This led to calculations of the fraction released that correlated nicely to those from amperometry. In a follow-up study, these methods were used to study the effect of vesicle size on the fraction of release in publication III.

CHAPTER 2 Cell models

Cell models are used to model biological processes and diseases but are also used for testing drugs and their mechanisms of action. They offer advantages such as the highly controllable but also modifiable environment (e.g. culture medium, temperature), and different surfaces the cells can be cultured on (glass, plastic with or without different coatings but also microfluidic devices, etc.). Two-dimensional (2D) cell cultures do not model the *in vivo* environment in the same way that organoids, acute or organotypic brain slices, or harvested tissues do. The 3D environment present in the latter systems accounts for cell-cell interactions and effects of the extracellular matrix, however, it increases the complexity of the experiments due to, for example, the concentration gradients within the tissue or organoid when they are treated with chemicals. In addition, these models suffer from higher batch-to-batch variation due to intricacies during the sample preparation, less controllable microenvironments, or differences between animals used to collect tissues. Choosing the right model system therefore depends on the scientific question for example if a basic, highly conserved intracellular mechanism is investigated or whether it is a mechanism that involves the interplay of different cells and the extracellular environment.

One type of 2D cell culture includes stable cell lines, often derived from cancerous tissue. Commonly used cell lines are human embryonic kidney (HEK) 293 cells which is an immortalized cell line derived from embryonic kidney tissue in the 1970s [170] and HeLa cells which were derived from the cervical cancer of a 31-year-old woman called Henrietta Lacks in the 1950s [171]. Cell lines are easy to culture and genetically manipulate and can be used for the production of adenoviruses (HEK293 cells). The advantages of cell lines are their ease of use and the extensive amount of data available from many laboratories. Given their continuous division and cancerous origin, however, cell lines are prone to developing subclones, and their cellular metabolism is altered compared to cells that do not display these cancerous characteristics [172].

Another type of cells are primary cells which are isolated from tissue and then cultured for a certain period, but they usually cannot be kept in culture as long as the stable cell lines. They have the advantage that specific cells from a tissue of interest can be extracted and cultured which might represent the closest *in vitro* analogue of that cell type. Also, it is particularly useful when the cell type of interest does not have an available cell line. Primary

cells can be isolated from laboratory animals that have a specific genetic background (e.g. disease models) or from patients during a surgery. However, the cost and amount of labor to culture primary cells are often higher, and the batch-to-batch variation might be larger compared to those of stable cell lines. It was found that the metabolome of primary cells changes significantly in the first 24 h of culture after the isolation from the tissue [173].

Since the discovery of induced pluripotent stem cells (iPSCs), iPSC-derived cells have quickly become a very useful model system. Applications of iPSC-derived cells include drug testing, disease modeling, and personalized medical treatments as the cells can be generated from the tissue of any human being, thus different genetic backgrounds, e.g., disease related backgrounds, can easily be obtained. The iPSCs can be further differentiated into potentially any cell type of the three germ layers, however, it is challenging to ensure a proper differentiation and they require a high amount of maintenance. Stem cells can be obtained from somatic cells but also from a blastocyst, generating embryonic stem cells. This however raises an ethical concern due to the destruction of the early-stage embryo.

In summary, different cell models have different benefits and ultimately the choice of cell model is dependent on scientific question, cost, ease of use, and availability. In the following, the PC12 cell line and human iPSCs and their derived cells are discussed in more detail as PC12 and iPSC-derived neuronal progenitor cells (NPCs) were used in this thesis work.

2.1 PC12 cells

2.1.1 Types of PC12 cells and their differentiation

Pheochromocytoma (PC12) cells are an immortal cell line that was first created in 1972 by Greene and Tischler [174]. It is derived from a cancerous tissue in the rat (*Rattus norvegicus*) adrenal medulla. PC12 cells can be cultured and propagated for many passages due to their proliferative capacities given their cancerous origin. Different variants of PC12 cells exist today, namely adherent and nonadherent PC12. Both adherent and nonadherent cells cannot synthesize epinephrine due to the lack of phenylethanolamine M-methyltransferase enzyme [175] but they store other catecholamines namely dopamine and norepinephrine inside their vesicles. PC12 cells can also be differentiated into neuron-like cells with the addition of nerve growth factor (NGF) to the culture medium [174]. This leads to a

significant change in morphology. Whereas undifferentiated PC12 are characterized by roundness and growth in clusters, differentiated PC12 cells after a few days of culture with NGF display a neuron-like morphology with thin neurites growing out of the cell body and the formation of varicosities [174] on which exocytosis takes place [176]. Interestingly, the expression of synapsin I, a synaptic vesicle protein, although already present in undifferentiated PC12 cells, increases during differentiation with NGF [177], [178]. Synaptic vesicle proteins (isoforms of synaptotagmin) have also been shown to localize to different subgroups of vesicles and determine release modes in PC12 cells [179]. Notably, not only NGF can induce differentiation of PC12 cells, but also glucocorticoid can induce differentiation and affect the release machinery inducing fast exocytosis and endocytosis [180].

2.1.2 Vesicles in PC12 cells

PC12 cells are an ideal model to study the basic mechanisms of neuronal communication. They contain vesicles for the storage of neurotransmitters (Fig. 10A, C). Vesicles are responsible for releasing the transmitters from one cell to communicate with neighboring cells, the so-called exocytosis process. The average release event of a vesicle of an undifferentiated PC12 cell has been shown to release around 114300 molecules of catecholamine [181]. This exocytosis is Ca^{2+} dependent [182] similar to neurons thus it can be used as a model for exocytosis in neurons. Exocytosis in PC12 cells can be triggered by an application of K^+, which leads to the depolarization of the plasma membrane, an influx of Ca^{2+}, and an expulsion of vesicular content. Other mechanisms of stimulation via nicotinic and muscarinic receptors also result in neurotransmitter release but display increased latency compared to K^+ [183]. Vesicles inside PC12 cells can be classified into two groups: small vesicles containing acetylcholine and dense core vesicles (DCVs) containing catecholamines, which are mostly dopamine but also norepinephrine [182], [184], [185]. It has also been suggested that DCVs can be divided into two subpopulations (small DCVs and LDCVs), which are different in vesicle size and neurotransmitter content [186], [187]. LDCVs possess VMATs on their membrane which transports dopamine from the cytoplasm into the vesicle. It was shown that the vesicle size decreases when VMAT is blocked by reserpine, but this effect can be reversed after cells are co-incubated with reserpine and the dopamine precursor L-3,4-dihydroxyphenylalanine (L-DOPA) [188]. Incubation of the cells with L-DOPA alone leads to a significant increase in vesicle size, predominantly the halo compartment of LDCVs which surrounds the dense core (Fig. 10B, D). Upon release,

dopamine binds to receptors of neighboring cells to conduct signals, and to D2 auto-receptors. The activation of the D2 receptor in turn regulates the number of neurotransmitters released in subsequent exocytosis events [189].

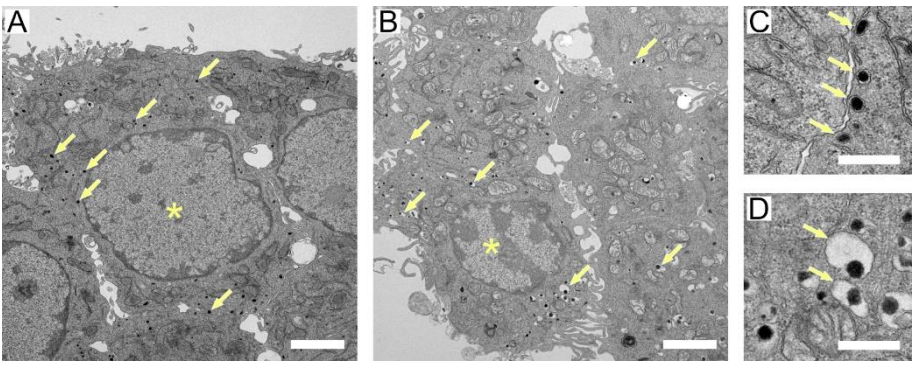

Figure 10. TEM images of PC12 cells containing LDCVs. A) regular (control) PC12 cells, B) PC12 cells incubated with 150 µM L-DOPA for 6 h leading to an increase in LDCV size, C) A detailed image of LDCVs in a control cell D) A detailed image of LDCVs of PC12 cells after an incubation with 150 µM L-DOPA for 6 h illustrating an increase LDCV size mainly in the halo compartment. Yellow arrows indicate LDCVs and asterixis indicate nuclei. Scale bars are 2 µm for A, B, and 500 nm for C, D.

2.1.3 PC12 cells are a common cell model for exocytosis

The mechanism of exocytosis has been conserved among multicellular organisms. Hence, PC12 cells have previously been used for many studies on vesicles and exocytosis [190]. Using electrochemical techniques, such as single-cell amperometry and intracellular vesicular impact electrochemical cytometry, the amount of catecholamine inside vesicles and the amount released to the extracellular space could be measured. It has been found that the amount of molecules released from undifferentiated compared to NGF-differentiated PC12 cells is similar, with a more homogenous population of vesicles in differentiated PC12 cells [176]. More recently, it has been found that repetitively stimulated PC12 cells with K^+ change the release dynamics of vesicles indicating plasticity at the level of single vesicles [191]. In addition, many studies have investigated the effects of pharmacological manipulation on vesicle content and release [192], [193], [194], [195], [196], [197]. Using correlative TEM and NanoSIMS imaging, multiple studies have investigated the vesicular content of LDCVs in PC12 cells and found a differential distribution of dopamine within the vesicle [198], and

determined the absolute concentration of dopamine in the vesicle [199] and its sub compartments, dense core and halo [159].

In summary, PC12 cells are a highly useful model to study the basic mechanism of exocytosis and different pharmacological and genetic manipulations of the process. In this thesis, additional insight into the release mechanism of PC12 cells was obtained using correlative TEM and NanoSIMS imaging on PC12 cells in publication I & III.

2.2 Induced pluripotent stem cells (iPSCs) and neural differentiation

Pluripotent stem cells are cells that can self-renew and differentiate into almost any cell in an organism. Pluripotent (derived from Latin; "pluri" meaning many and "potent" meaning having power/being able) hereby refers to the ability of the cells to differentiate into cells of any of the three germ layers of an organism. Totipotent cells (derived from Latin; "toti" meaning all) on the other hand can create an entire organism from itself. The best example of totipotent cells is a zygote, which is a cell formed upon the fertilization of two gametes, e.g., egg cell and sperm cell. In the 2000s, the discovery that cultured cells such as fibroblasts can be induced to become pluripotent stem cells by the Yamanaka group [200], [201], [202] has created the ability for researchers to potentially create any cell of an organism in a dish. This is particularly interesting for human tissues as drugs can be tested on specific human cells which cannot be obtained otherwise, and on patient-specific cells [203]. This reprogramming of somatic cells to become induced pluripotent stem cells (iPSCs) can be achieved by an overexpression of the so-called Yamanaka factors which are transcription factors, OCT3/4, SOX2, KLF4, and c-MYC.

2.2.1 Reprogramming of somatic cells to iPSCs

The over-expression of the Yamanaka factors in somatic cells can be achieved with multiple methods. The first group of methods to generate iPSCs utilizes integrating vectors such as retroviral and lentiviral transduction to reprogram cells [201], [204]. Early difficulties of combining multiple vectors have been overcome and the integration of vectors into the genome could be reversed by the Cre/loxP [205] or piggyBac system [206], but the efficiency of these methods is low and they are time-consuming [207]. Another group of methods to reprogram somatic cells uses non-integrating vectors, such as adenoviruses [208], Sendai viruses [209], DNA

transfection [210], Epstein-Barr virus-derived OriP/EBNA1 DNA [211], and minicircle DNA [212]. Non-DNA methods for reprogramming include modified RNA [213], microRNAs [214], [215], and recombinant proteins [216], [217] to circumvent the problems of integrating DNA. In addition to these groups of reprogramming methods, small molecules have been investigated for their ability to enhance the reprogramming of somatic cells. Small molecules that have been used for this purpose are histone deacetylase inhibitors [218], [219], two inhibitor (2i) cocktails [220], [221], [222], kenpaullone [223], TGF-β inhibitors [224], [225], histone and DNA methyl transferase inhibition [222], [226], [227], and ROCK inhibition [228]. The success of reprogramming is determined by the expression of the Yamanaka factors and by the ability to differentiate the reprogrammed cells (iPSC) into any of the three germ layers. This can be tested by qPCR experiments, and immunocytochemical staining followed by fluorescent imaging. Another method to test pluripotency is teratoma (tumor) formation which can be observed after an implantation of the reprogrammed cells into a lab animal.

2.2.2 Neural and dopaminergic differentiation of iPSCs

Pluripotent cells can be differentiated into many different cell types using different combinations of growth factors and small molecules. A large variety of protocols are available for the generation of the same cell type, leading to different characteristics of the same cell type, making it difficult to compare results between different labs [229]. However, a commonly used approach to achieve neuroectodermal fate is dual SMAD inhibition as it has been shown to be highly effective in the neural conversion of stem cells [230]. SMAD refers to the SMA gene “small worm phenotype” from *Caenorhabditis elegans* and the MAD gene “mothers against decapentaplegic” from *Drosophila melanogaster*. SMADs are a family of proteins of the TGFβ superfamily relevant for cell development and growth.

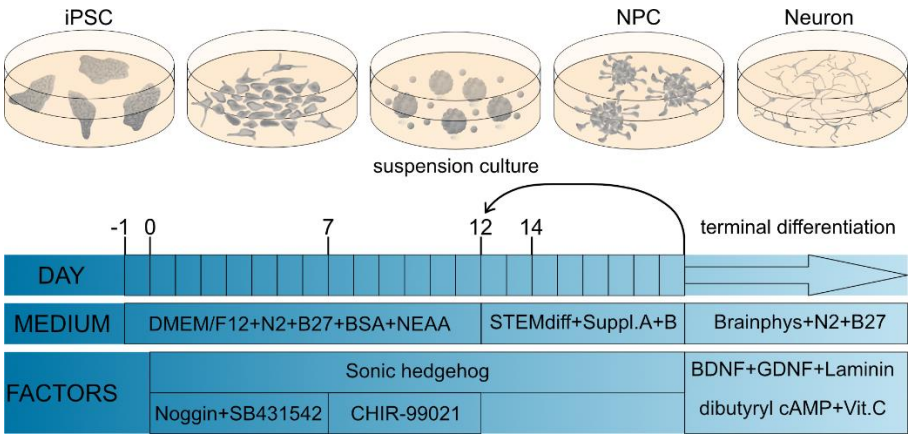

Figure 11. Timeline of the neural induction of human iPSCs and the subsequent differentiation of NPCs into dopaminergic neurons. iPSCs will be treated with Noggin and SB431542 for dual SMAD inhibition to induce neuroectodermal fate. CHIR-99021 is added for WNT activation and SHH is added for ventralization. Terminal differentiation to neurons is completed by adding neurotrophic factors BDNF and GDNF, Laminin, dibutyryl cyclic AMP, and ascorbic acid.

This SMAD inhibition is usually carried out with Noggin and SB431542 with which iPSCs are incubated for ~7 days (Fig. 11). SB431542 acts by blocking phosphorylation of anaplastic lymphoma kinase (ALK) 4, ALK5, and ALK7 to inhibit the Lefty/Activin/TGFβ pathways [231]. Noggin inhibits BMP signaling by binding to different BMPs and it has been previously shown to be crucial for neural development [232]. The combination of SB431542 and Noggin treatment of iPSCs has yielded more neuroectodermal cells (>80 % positive cells) than either one of them alone [230]. To maintain neurogenic propensity, CHIR99021 can be added to inhibit GSK3, which is an inhibitor of WNT signaling. Therefore, CHIR99021 activates WNT signaling [233] and enhances neural proliferation. Exposing cells with the SHH during dual SMAD inhibition and subsequent WNT activation leads to the generation of midbrain neural progenitor cells (NPCs). SHH is a morphogen meaning that it acts in a concentration-dependent matter and in development it is needed for ventralization of the neural tube [234].

The result of the neural induction of iPSCs after ~ 20 days are NPCs which can self-renew or differentiate into a restricted amount of neuronal cell types and glia. NPCs have regional characteristics (e.g. midbrain) that separate

them from other progenitor domains and each domain is characterized by a unique expression pattern of transcription factors. For example, NPCs are characterized by lacking the expression of pluripotency marker OCT4 whereas midbrain NPCs are characterized by the expression of FOXA2, LMX1A, or OTX2. In culture, the selective adhesion of homotypic cells has been shown to be an efficient way to purify the NPCs [235]. From the NPC stage, the cells can be terminally differentiated into a specific type of neurons. The addition of neurotrophins brain-derived neurotrophic factor (BDNF) and glial cell line-derived neurotrophic factor (GDNF) enhances neuronal survival and dopaminergic differentiation. The homodimeric GDNF promotes dopamine uptake and differentiation into midbrain neurons and their survival [236]. BDNF was discovered in 1982 as a neurotrophin that acts through the tropomyosin receptor kinase B [237], [238]. It is used to maintain motoneurons and to differentiate dopaminergic and cholinergic neurons [239]. It has been shown to mediate dendritic growth and branching [240]. The successful differentiation of dopaminergic neurons can be confirmed by the expression of tyrosine hydroxylase, a rate-limiting enzyme in dopamine production.

In summary, iPSCs and their derived cells, NPCs, and differentiated neurons, are complex cell models and their differentiation and maintenance are intricate processes. However, they offer great potential in modeling biological processes of human cells *in vitro*. Human NPCs and differentiated neurons derived from human iPSCs were used for studying protein turnover in publications II, IV, and V of this thesis.

CHAPTER 3. Microscopy

Microscopy is used to discern sample features that are undiscernible by the human eyes. There are many different types of microscopies, such as optical, electron, scanning probe, and x-ray microscopy, and they are in constant development to visualize targeted structures with improved spatial resolution. These techniques utilize different beams (e.g., light and electron beams) and probes to interact with the sample, generating images with increased resolution, and providing us with information of subcellular structures. Each microscopy technique is suitable for specific applications or scientific questions, and samples need to be prepared to be suitable for the chosen method. In this chapter, fluorescence and electron microscopy will be discussed in more detail, as they were used in the work included in this thesis.

3.1 Fluorescence microscopy (FM)

Fluorescence microscopy (FM) is a common imaging technique in biology and biochemistry for localizing biomolecules of interest within cell or tissue samples. FM requires fluorescent molecules, or so-called fluorophores, which can be excited with a specific wavelength of light, which stimulates the emission of photons. In brief, the molecule absorbs the energy of the light beam at a specific wavelength to jump up to its excited state, and then it relaxes to the lowest level of the excited state via vibrational relaxation; finally, it returns to the ground state by emitting photons of another specific wavelength (Fig. 12A). This phenomenon usually occurs within a few nanoseconds. The emitted photons typically have a longer wavelength and less energy than those of the exciting light. The difference between the two excitation and emission wavelengths is called Stokes shift [241]. These fluorophores are usually introduced into the samples to mark specific molecules or cellular structures for visualizing them with fluorescence imaging. This can be done with various approaches which will be described in more detail in the sample preparation section below.

3.1.1 FM techniques to overcome the diffraction limit

Spatial resolution is an important aspect in FM and refers to the ability to distinguish between two closely spaced objects. The diffraction limit is thereby the physical constraint imposed by optics to resolve two points in an image. The diffraction limit was originally defined by Abbe in 1873 [242]. It

states the relation between the wavelength (λ), the numerical aperture (NA), and the minimum resolvable distance (d):

$$d = \frac{\lambda}{2n \sin \theta} = \frac{\lambda}{2NA} \qquad \text{(eq. 1)}$$

where n represents the refractive index and θ stands for the half-angular aperture subtended by the objective lens.

Given the wavelength of visible light (400-700 nm) the theoretical resolution of optical microscopy is limited to around 200 nm. Confocal laser scanning microscopy (CLSM) is an FM technique; its setup was optimized compared to traditional widefield fluorescence microscopy, to achieve the best spatial resolution within the diffraction limit. In CLSM, a sample is scanned with a laser beam of a specific wavelength pixel by pixel, and the fluorescence from the emitting molecules in the sample is detected after passing through a pinhole (Fig. 12C). The function of the pinhole is to filter the fluorescence emitted from the out-of-focus sample planes, which helps to significantly reduce the background signal. Theoretically, the spatial resolution in the x and y direction of CLSM can reach the diffraction limit of ~200 nm. This barrier has been overcome with several types of super-resolution techniques that can circumvent the diffraction limit in different ways.

Each super-resolution technique, while overcoming the diffraction limit, compromises between temporal resolution, spatial resolution, contrast, and specimen health. Generally, super-resolution techniques can be divided into coordinate-stochastic and coordinate-targeted techniques. Coordinate-stochastic methods include photo-activated localization microscopy (PALM) [243] and stochastic optical reconstruction microscopy (STORM) [244]. The principle for these techniques is to turn on only a subset of fluorescent molecules at a time, record them, and repeat this over many cycles after which an image is reconstructed [245]. A spatial resolution of tens of nanometers can routinely be achieved with these techniques (~ 20-30 nm for STORM). Early limitations in image acquisition time have been overcome so that an image can be acquired in seconds, however, disadvantages of those techniques include that adjacent pixels are not temporally correlated, and a good photon yield is required to accurately determine the fluorophore's position [246], [247]. The first coordinate-targeted method to have been developed, and the first super-resolution microscopy technique, is called stimulated emission depletion (STED) microscopy [248], [249] which achieves a spatial resolution of 20-50 nm in fixed and live cells [250]. STED utilizes a donut-shaped depletion laser beam (STED beam), with a zero-laser

intensity at the beam center, as an additional laser beam to the CLSM setup (Fig. 12D). In the STED setup, the STED beam is superimposed on the excitation laser beam. When the fluorophores in the samples are excited by the excitation laser beam, this coupling of the two lasers will force the fluorophores surrounding the beam center to return to the ground state via stimulated emission without emitting their fluorescence (Fig. 12B). The fluorophores at the center (where the STED intensity is 0) do not undergo the effects of the STED beam and thus return to the ground state by emitting fluorescence. Hence, the spot size from which the fluorescence is emitted is reduced extensively [248], [251]. STED offers the advantage of live cell imaging, and importantly, high imaging speed from milliseconds to minutes [247], [252]. In addition, STED has the advantage that the adjacent imaged pixels are temporally correlated resulting in better images of moving objects at a high resolution. However, STED requires more stable fluorophores due to higher intensities of the lasers [253]. Another disadvantage, especially for live imaging, is phototoxicity due to the powerful lasers that could lead to cell damage [254]. Nonetheless, the use of longer wavelengths and the addition of a reducing agent (e.g., ascorbic acid) to the imaging medium are ways to circumvent phototoxicity in live fluorescence imaging [255]. Since the development of STED, other coordinate-targeted methods have been developed, including reversible saturable/switchable optical linear fluorescence transition (RESOLFT) and minimal photon fluxes (MINFLUX) microscopy [246]. The main advantage of these techniques is a reduction of the laser intensities reducing cytotoxicity. However, this prolongs the acquisition time or limits the field of view for imaging. In addition, the equipment cost is relatively high [247].

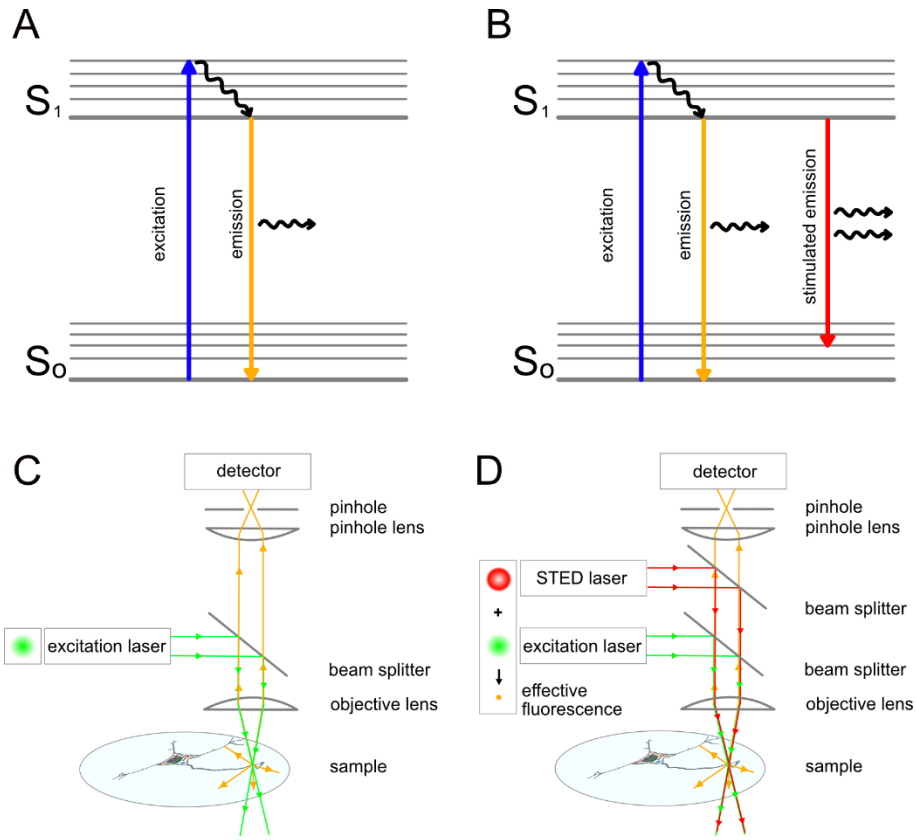

Figure 12. A) Jablonski diagram for normal fluorescence B) Jablonski diagram for STED microscopy. S_0 refers to the ground state and S_1 to the excited state. C) and D) Simplified schematic diagrams of the setups of C) a confocal microscope and D) a STED microscope. In the confocal microscope, an excitation laser is directed onto a sample, and the emitted fluorescence light is directed through a pinhole to the detector. The pinhole allows only the fluorescence from the focal plane to pass through and reach the detector. For STED, a second depletion laser beam is superimposed onto the excitation laser beam, and they are directed onto the sample, allowing only the fluorophore at the center of the beams to emit fluorescence, and be detected. This results in an improved lateral resolution beyond the diffraction limit.

3.1.2 Sample preparation for FM

Labeling is a crucial part of an FM experiment as it allows specific molecules to be visualized under the microscope. Ideally, it should be highly

selective and produce low background fluorescence. Various techniques to introduce fluorescent labels are available, for example, genetic overexpression, live labeling dyes, or immunolabeling, and their uses depend on scientific questions and the availability of microscopes.

One main advantage of FM is its ability to perform live cell imaging. This requires the use of non-toxic, cell-permeable fluorescent labels or genetic modification to express a fluorescent protein tag [256], [257]. Cell permeable dyes are very useful and simple to use, but not many are available for target biomolecules within cells or tissues [253]. Genetic overexpression of fluorescent proteins is also a relatively simple fluorescent labeling method, but its suitability depends highly on whether the studied cell line can be transfected to express the fluorescent label. Also, the overexpression of fluorescent proteins could disturb cellular processes, such as the localization or function of the protein of interest. Live cell imaging may also cause phototoxicity to the imaged cells. In addition, it usually requires a complex setup to maintain the cells in controlled temperature and atmospheric conditions during imaging [258].

Fixed cell imaging is a common FM imaging approach owing to its advantage that the samples can be imaged after the cell has been preserved, and a variety of fluorescent labels are commercially available. The samples are first chemically fixed using fixatives, and then permeabilized and immunolabeled against specific proteins with fluorescent labels. Post-fixation is an optional step to better preserve the fluorophores on the samples after immunolabeling, and it is used especially for correlative imaging methods. The choice of fixative ultimately depends on the target molecules. Common fixatives for FM include aldehydes and organic solvents. Alcohols, such as ethanol, and methanol, or acetone in combination with aldehyde fixation are often used to fix cytoskeletal epitopes [259], [260]. Alcohols fix the sample by dehydration and protein denaturation which ultimately preserves the cells. However, alcohol fixation potentially causes sample shrinkage and washes away certain cellular lipids. For aldehyde fixation, proteins are crosslinked with the aldehyde molecules inhibiting cellular biochemical processes. The mechanism of aldehyde fixation is further discussed in the electron microscopy sample preparation section. Aldehydes commonly used for fixation include formaldehyde, paraformaldehyde (PFA), glutaraldehyde (GA), and glyoxal [261]. It was found that aldehyde fixation can block/lose certain epitopes preventing the binding with antibodies [262]. In this case, the epitopes can be recovered via antigen retrieval, a process, in

which the samples are submersed into a buffer (e.g., citrate buffer) to change the pH and, to a lesser extent, molarity; this is often combined with a raise in temperature [263]. After fixation, the cells are permeabilized allowing antibodies to enter the cells through the membrane. This is followed by blocking unspecific binding, then incubating with a primary antibody for a specific protein and subsequently with a secondary antibody containing a fluorophore. Afterwards, the samples are mounted on a microscope slide for FM imaging. Often a nucleic acid staining (4′,6-Diamidin-2-phenylindol (DAPI)/Hoechst) is included to facilitate cell identification and/or counting.

For super-resolution microscopy to visualize nanometer-sized objects, fluorescent labeling is a critical factor for a successful measurement. First, the fluorophores should have high and long-lasting brightness (for STED) or should be photo-switchable (for PALM/STORM). Second, the size of the fluorescent label must be sufficiently small. Traditional antibodies are around 9x15 nm in size [264], which can significantly distort the localization of individual proteins especially when more than one label is used. Therefore, camelid single domain antibodies, or so-called nanobodies, with a size of around 2.5x4 nm can be employed to facilitate the labeling for super-resolution FM [265].

In summary, FM offers high molecular specificity, high sensitivity (detectable at single molecules), and high imaging resolution. FM is an excellent choice for correlative imaging owing to its non-destructive property and the possibility of optical sectioning. In this thesis, FM was used to identify SGs for the correlation with NanoSIMS imaging in paper II, to determine transfection efficiency to modulate vesicle size in paper III, and to track the expression of marker proteins in neuronal differentiation in paper V.

3.2 Electron microscopy (EM)

Electron microscopy (EM) was developed in the 1930s by Knoll and Ruska to overcome the theoretical resolution limit of ~200 nm in optical light microscopes [266], [267]. It utilizes an electron beam to generate a sample image. This was based on the discovery of the wave properties of electrons and the ability to focus and manipulate the direction of electron beams. Transmission EM (TEM) attains resolutions down to 0.5 Ångström, or 50 pm, with aberration-corrected EM to image single gold atoms [268]. Given its excellent spatial resolution, EM is an invaluable tool for discerning subcellular morphological features within cells and tissues. EM is mainly

divided into scanning EM (SEM) and TEM, depending on which electrons are used for detection, particularly, the backscattered and secondary electrons, or the transmitted ones, respectively. The principles of EM and sample preparation of EM will be further discussed below.

3.2.1 Principles of EM

In EM, a sample is exposed to a highly focused electron beam in a high vacuum chamber. There are two main types of electron sources, particularly, thermionic and field emission sources. The thermionic electron sources are either tungsten filaments or solid-state hexaboride crystals, whereas the field emission guns are either cold field emission sources operated at room temperature, or Schottky field emission sources operated at elevated temperatures [269]. The electrons emitted from the source are focused to a small beam and directed onto the sample surface where they interact with the atoms within the sample. The focusing/defocusing of the beam is achieved by electromagnetic lenses where the beam size is dependent on the strength of the electromagnetic field. In addition, deflectors and stigmators are used to manipulate the beam shape, such as the symmetricity and tilt (Fig 3.2A).

The use of electrons in EM instead of a light beam in FM allows a substantial improvement in the spatial resolution. The wavelength of an electron can be determined using the De Broglie equation, which states that the wavelength (λ) is inversely proportional to the momentum (p), h is the Plank constant:

$$\lambda = h/p \qquad \text{(eq. 2)}$$

The momentum in turn depends on the speed of the electron (as the mass of an electron is constant), and thus the speed of the electron determines its wavelength. Therefore, higher electron speed leads to shorter electron wavelength resulting in better spatial resolution, within limits: faster electrons pass through the sample more efficiently, which reduces image contrast and lowers image quality.

SEM can be operated in two different modes, imaging either the low energy secondary electrons ejected from the sample surface providing information about the surface topography, or the high energy electrons backscattered from the bulk of the sample providing the compositional/density information of the sample [270], [271]. On the other hand, TEM employs a camera situated beneath the sample (Fig. 13A) to detect the electrons transmitted through the sample. The diffraction pattern that is created by the interactions

with the electrons and different atoms in the sample is then used to reconstruct an image. Heavier atoms thereby create darker areas in the image, and this is why heavy metals are often used in the preparation of biological samples to increase the image contrast. In addition, cutting samples into thin sections (70-300 nm) is needed to allow the electrons to pass through the sample efficiently. These sections are usually placed on copper grids before transferring the sample into the TEM instrument (Fig. 13B). A common voltage applied for TEM is 120 keV to achieve a theoretical resolution of 0.2 nm, which is more than sufficient to discern the ultrastructure of the cell (Fig. 13C). In practice, this is rarely achieved with biological samples, as resolution also depends on the sample preparation, radiation damage and aberrations [272].

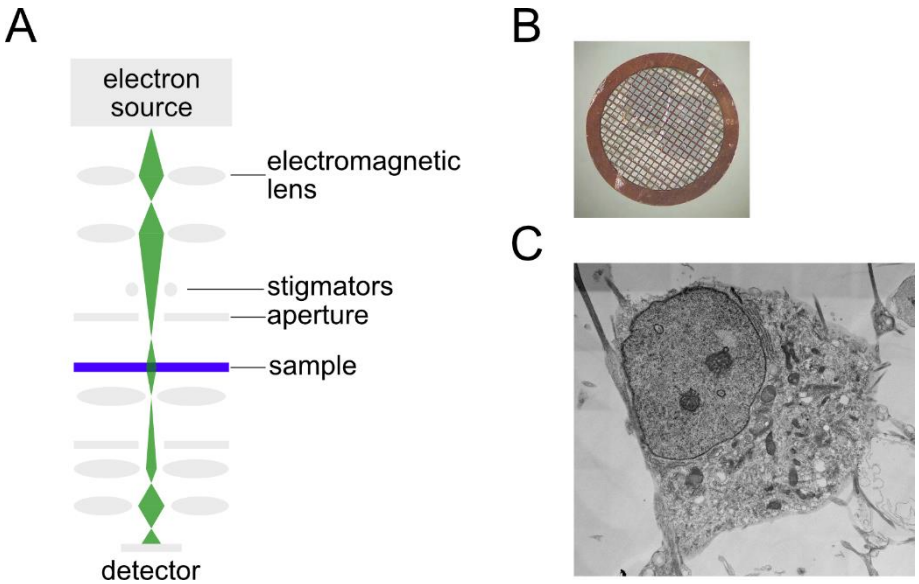

Figure 13. Principle of TEM and its application in subcellular imaging. A) Simplified schematic of a TEM instrument. B) Example image of a copper grid containing sample sections on top. C) Example image of a neural progenitor cell imaged by TEM allowing the identification of different organelles.

3.2.2 Sample preparation for transmission EM

Samples for TEM should be compatible with high vacuum conditions and provide high contrast. The first step in a conventional sample preparation for TEM requires chemical fixation to preserve the ultrastructure of biological

samples, commonly using GA. Other aldehydes, such as PFA, have been used in correlative TEM and FM, but do not preserve the ultrastructure as efficiently as GA. In general, aldehyde fixation leads to crosslinking between the aldehyde and mostly the amino groups of biomolecules. The mechanism of formaldehyde fixation involves the formation of methylene bridges between amino groups. It penetrates the tissues/cells quickly due to its small size, but some reversibility of the reaction has been observed [273]. In contrast, GA has shown less reversibility of the crosslinking at pH 7-9 [274] and a slower penetration into tissue compared to formaldehyde [275]. The detailed crosslinking mechanism of GA is not fully understood but is likely to involve different mechanisms (e.g. Schiff base formation, aldol condensation, and Michael type addition) rather than a single mechanism [276], [277]. GA and PFA can also be used together in mixtures (such as in Karnovsky's fixative) to combine the advantages of both fixatives regarding the fast penetration of PFA and the stable crosslinking of GA [278]. The disadvantages of chemical fixation include shrinkage of samples, possible alterations of the cellular nanostructures [279], and its inability to crosslink all biomolecules within cells/tissues [276]. However, it is an inexpensive and simple method that is widely used and as such it is additionally very useful for data comparison and relation with previous published findings.

Cryofixation techniques, such as high-pressure freezing followed by freeze substitution or rapid freezing for cryogenic EM are often valuable alternatives to chemical fixation methods. High-pressure freezing combined with freeze substitution has been shown to preserve the samples closer to their native state and has therefore been considered as the gold standard of sample preparation for TEM. In brief, a sample is rapidly cooled to -196 °C at high pressure of about ~1200 bar to avoid the formation of ice crystals [280]. An organic solvent is then introduced at low temperature to dehydrate the sample followed by a resin embedding. During the embedding period, the temperature of the sample is slowly raised to room temperature. Due to the low temperature, this method ceases cellular processes immediately and prevents the movement of biomolecules leading to a better preservation of the native state of the sample. High-pressure freezing is advantageous for effectively freezing larger sample volume without the formation of ice crystals when compared to conventional rapid freezing [281]. However, high-pressure freezing requires a specialized instrumental setup which is more expensive.

TEM often requires good contrast of the sample to easily observe ultrastructures. This is achieved by a deposition of heavy metals (e.g., osmium, uranium) into the sample [282]. These metals in turn react with the biomolecules providing a secondary fixation [282]. Osmium tetroxide, a common heavy metal compound for sample preparation in EM, reacts with the double bonds of unsaturated lipids resulting in significant staining of cell membranes [283]. Another common reagent is uranyl acetate, which reacts with proteins and lipids by binding to phosphate and amino groups, providing additional contrast. In addition, samples can be treated with lead citrate which reacts with negatively charged molecules to further enhance contrast [282].

TEM imaging is performed at ultrahigh vacuum, thus the samples need to be dehydrated and embedded in resin unless a cryogenic analysis is carried out. Sample dehydration is achieved by washing the sample with increasing concentrations of an organic solvent, such as ethanol or acetone, in an aqueous solution. A slow increment in the ratio of organic solvent helps to minimize sample shrinkage. Afterward, a resin, for example, acrylic or epoxy resin, is infiltrated into the sample, replacing the solvent. Following resin infiltration, resin polymerization is induced by heat or UV light. The embedded sample is cut into thin sections with an ultramicrotome, and the sections are then placed on copper grids for TEM imaging. Epoxy resin produces very hard blocks with minimal shrinkage, which proves advantageous for this type of preparation. However, because of its strong crosslinking abilities, epoxy resin was shown to cause structural changes that may reduce antigenicity [284]. On the other hand, acrylic resin produces softer resin blocks compared to epoxy, thus it is more difficult to section them, and they can be less stable under the TEM beam. Still, acrylic resin generates less autofluorescence, making it better suited for correlative light microscopy and EM (CLEM) [285].

In summary, TEM sample preparation needs careful consideration depending on the application, availability of instruments, molecules of interest, and the option for correlative multimodal imaging. In this thesis, TEM was used in papers I, III, IV, and V in correlation with NanoSIMS to study the vesicular content and its release in PC12 cells and the protein turnover of different organelles in stem cell-derived cells.

CHAPTER 4. Secondary Ion Mass Spectrometry (SIMS)

4.1. Mass Spectrometry imaging (MSI)

Mass spectrometry imaging (MSI) is a group of powerful imaging techniques to elucidate the chemical distribution of the sample surface. The technique originates from the findings of J.J. Thompson who discovered that charged particles can be emitted from surfaces, setting the foundation for the various imaging technologies in the field today [286]. Different emerging MSI techniques are specified by their methods of ion generation at the sample surface, the achievable spatial resolutions, and the fragmentation level of analytes (Fig. 14). Spatial resolution in MSI is defined as the ability to distinguish signals between two adjacent sample features and it depends not only on the capability of the instruments but also on the sample properties.

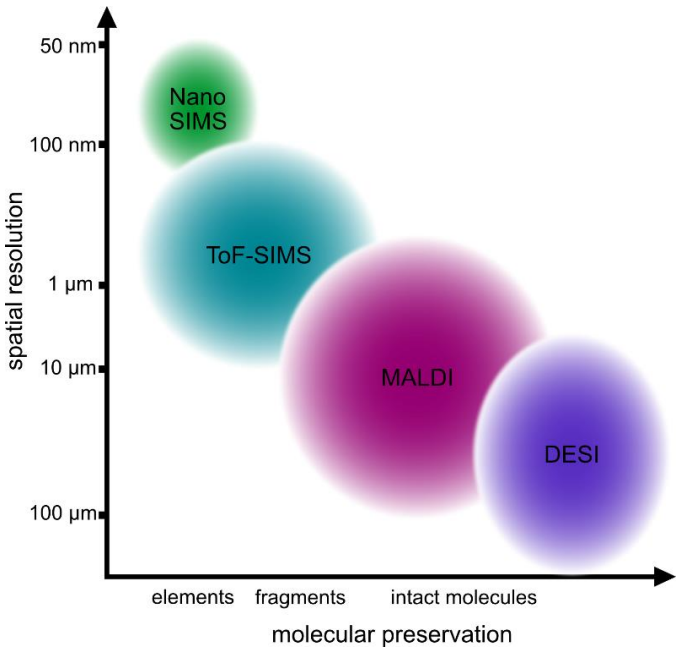

Figure 14: Schematic diagram illustrating the relationship between spatial resolution and molecular preservation across different MSI techniques.

A common MSI technique is matrix-assisted laser desorption/ionization (MALDI) imaging which was introduced in the 1990s [287]. It requires the application of a matrix layer onto the sample surface to absorb the energy of

a radiating laser which then transfers the energy to sample molecules to generate molecular ions with a small amount of fragmentation. MALDI is a commonly used technique to investigate the spatial distribution of molecules, especially proteins, and peptides, in clinical samples [288]. Spatial resolutions down to 10-200 μm are routinely achieved [289], and more recently, subcellular spatial resolution of ~0.6 μm could be obtained with MALDI-2 [290]. On the other hand, desorption electrospray ionization (DESI) imaging, first described in the 2000s [291], ionizes the samples in ambient conditions and often does not require any sample preparation. In DESI, charged droplets of solvent are directed onto the sample surface at a certain angle where secondary charged particles containing the analyte are generated. During the evaporation of the droplets, the analytes are ionized due to a decrease in surface area without a decrease in surface charge. The typical spatial resolution of DESI is 40-200 μm. More recently, nano-DESI has been developed and optimized utilizing smaller capillaries to achieve a spatial resolution of 7 μm [292]. DESI is also a soft ionization technique that is suitable for detecting large molecules such as peptides, proteins and lipids. Another common type of MSI technique is secondary ion mass spectrometry (SIMS) [293]. SIMS employs a focused primary ion beam to sputter the sample surface ionizing sample molecules. Depending on the type of primary ion beam, the analytes can range from monoatomic and diatomic ions, small, fragmented ions, metabolites, lipids, and even small peptides with mass to charge (m/z) up to 2000 using matrix-enhanced SIMS [294]. SIMS provides good spatial resolution (several tens of nm to a few μm) often allowing to discern subcellular compartments. One of the highest lateral resolutions (~50 nm) can be obtained by NanoSIMS. Other types of MSI techniques, such as liquid extraction surface analysis (LESA) [295], laser ablation electrospray ionization (LAESI) [296], laser ablation inductively coupled plasma mass spectrometry (LA-ICP-MS) [297] have been developed and applied in biological research.

In this thesis, NanoSIMS combined with isotopic labels is the main analytical approach used to interrogate the subcellular chemical composition of biological species in the context of neural cell biology, thus the principles of SIMS and NanoSIMS as well as the sample preparation procedures for SIMS will be discussed below.

4.2 Principles of SIMS imaging

In SIMS, a sample surface is bombarded with primary ions pixel by pixel. This bombardment results in particles, including ions being ejected from the sample surface. The ejection of particles from the sample surface is termed sputtering. These sputtered sample ions, termed secondary ions, are then extracted, focused with ion optics, and transferred into a mass analyzer where they are separated according to their m/z ratios. After the primary beam rasters the entire sample surface, images depicting the intensity and distribution of different detected ions can be created and used to spatially localize analytes of interest.

4.2.1. Ion generation in SIMS

Once primary ions impact a sample surface, sputtering of material takes place, resulting in positive ions, negative ions, and neutral particles being ejected. Depending on the type of primary ion beam, different sputtering mechanisms have been proposed. With atomic and small cluster ion beams, a so-called collision cascade within the sample surface takes place. In this process, primary ions collide with the neighboring atoms transferring their energy to these atoms. Subsequently, these atoms are displaced as the kinetic energy from the primary ions is sufficient to break chemical bonds within the molecules leading to a fragmentation of molecules. The displaced atoms in turn can recoil or collide with other atoms leading to a collision cascade and the ejection of particles from the surface [298]. With bigger cluster ion beams, effusive desorption, and fluid flow have been proposed as the main sputtering mechanisms [299].

Sputtering and ionization of the analytes are also influenced by the surrounding material: this is termed matrix effect. This is an important factor in any SIMS experiment, as the difference in the matrix between a standard and a biological sample, as well as between areas of a heterogenous sample could significantly influence the secondary ion yield and the signal of the analytes. The matrix effect is specific to the analyte of interest and thus must be considered for individual analytes.

4.2.2. Main factors influencing SIMS measurements

The basic equation of SIMS (equation 3) is presented showing that the detected secondary ion current (I_s) depends on the primary ion current (I_p), the total sputter yield of the analyte of interest (S), the ionization probability

of the analyte (α), the fractional concentration of the analyte in the sample surface (θ), and the transmission of the instrument (η):

$$I_s = I_p * S * \alpha * \theta * \eta \qquad \text{(eq. 3)}$$

The first factor influencing the secondary ion yield is the primary ion current. A variety of primary ions are available with different performances for example, regarding the obtained lateral resolution, depth resolution, and the extension of sample damage. The secondary ion yield has been found to be a function of cluster size and kinetic energy of primary ions [300]. Monoatomic ion beams such as Cs^+ are advantageous for obtaining high lateral resolution with a spot size down to ~2 nm [301], however, the fragmentation that occurs due to the high kinetic energy per atom limits the detected masses to mainly mono and diatomic species. Small cluster beams (e.g. Bi_3^+, Au_3^+, C_{60}^+) induce less fragmentation and increase the yield compared to monoatomic ion beams, especially for higher mass ions [302]. Larger cluster ion beams, e.g. gas cluster ion beams (GCIBs), with large cluster sizes produce even less fragmentation, and thus preserve the molecular ions of intact lipids (m/z ~700-900) and other molecules with m/z up to ~2000 [294], [303], [304]. GCIBs typically generate clusters of ~2000-20000 component atoms/molecules and are accelerated up to ~70 kV [305], [306], [307]. This energy spreads among the cluster particles resulting in a low kinetic energy of each particle which is often not sufficient to break chemical bonds to produce fragmented ions. In addition, the low kinetic energy per primary particle results in less mixing of the surface with the layers below compared to monoatomic or small cluster beams (Fig. 15) which is beneficial for 3D imaging [300], [308], [309]. A disadvantage of the GCIBs is difficulty focusing the beam size to a nanometer scale. The best spatial resolution obtained with GCIBs is thus around 1-3 μm [304], [310]. In addition, despite a good desorption for ionization, the ionization efficiency is relatively poor with low-energy GCIBs [304]. For subcellular measurements in biology especially at the organelle level, monoatomic or small cluster ion beams are preferred.

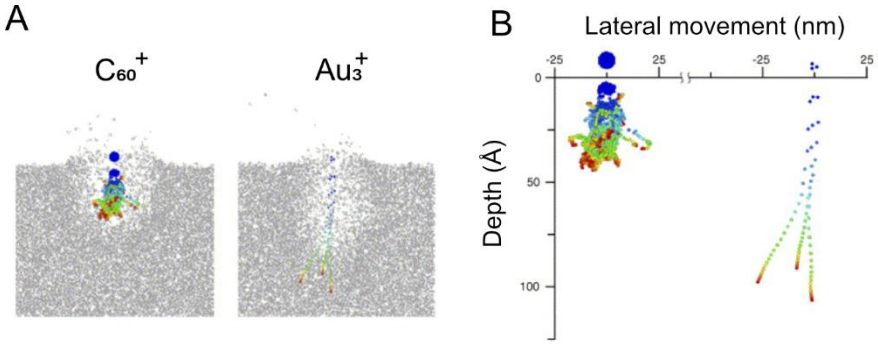

Figure 15. An illustration of the impact of two different primary ion beams on the sample surface. Monoatomic or small cluster ion beams, such as Au_3^+, cause less damage on the sample surface but penetrate deeper into the surface, and induce more atomic mixing in the layers beneath the surface. Larger ion beams, such as the C_{60}^+, induce lesser interlayer mixing but leave a larger crater on the sample surface. Color represents time. Figure adapted and reproduced from [311].

Based on the primary ion dose, SIMS has been divided into static and dynamic SIMS. The separation is based on the so-called static limit which is defined as the primary ion dose at which each single primary ion impacts a pristine sample area. If each impact influences around 10 nm^2 surface area, the static limit is found to be 10^{13} ions/cm^2. Anything above this primary ion dose is defined as dynamic SIMS and causes measurable damage to the sample surface [298].

4.2.3. Mass analyzers in SIMS

Among the particles that are ejected from the samples, only a small fraction is ionized [312]. These secondary ions are then collected into an extraction lens, focused via ion optics, and subsequently transferred to a mass analyzer before being recorded by detectors. Different mass analyzers are available providing different mass resolutions, a term for the ability to distinguish two adjacent mass peaks with similar m/z ratios [313]. Magnetic sector mass analyzers function by accelerating secondary ions through a magnetic field in which smaller ions are deflected more than larger ones resulting in separated travel paths for ions with different m/z. A mass resolution of ~10000 is often achieved in NanoSIMS which is sufficient to resolve isobaric species. On the other hand, in a time of flight (ToF) mass analyzer, all ions are accelerated to the same kinetic energy before traveling in a flight

tube to reach the detector. Owing to the same kinetic energy, ions with different m/z possess different velocities and thus reach a detector at different times. The mass resolution is ~10000 with delayed extraction (in an IONTOF instrument) or a buncher (in the Ionoptika J105 instrument) [314], [315]. A more recent SIMS instrument has been coupled with an Orbitrap mass analyzer offering higher mass resolution (>240000 at m/z 200) and therefore a more accurate molecular identification [316]. Fourier transform ion cyclotron resonance (FTICR) analyzers identify the m/z of ions by detecting the frequencies of their oscillations within a strong magnetic/electric field providing much higher mass resolution (>1000000), however, their drawbacks are high costs and long acquisition times [317].

The availability of high-resolution mass analyzers allows SIMS to be a powerful label-free imaging technique. However, due to high fragmentation especially with monoatomic and small cluster primary ion beams, rare isotopic or rare element labels are often used to accommodate the tracking of the distribution of large molecules, such as proteins, or cellular processes at the subcellular level [51], [199], [318], [319], [320], [321], [322].

4.3 NanoSIMS

Nanoscale SIMS (NanoSIMS) is a type of dynamic SIMS capable of delivering a spatial resolution of ~50 nm. The instrument comprises a primary column, a central column, a coaxial column, matching optics, an electrostatic magnetic sector mass analyzer, and a multicollection system (Fig. 16A). The main feature of NanoSIMS is a coaxial design in the primary ion and secondary ion paths allowing the primary ion beam to impact the sample surface at a 90° angle (Fig. 16B). This allows the last focusing lens and the extraction lens to be in close proximity to the sample surface, maximizing the collection of secondary ions therefore optimizing the transmission of the instrument, as well as minimizing abberations.

The NanoSIMS is equipped with two primary ion sources, a Cs^+ source and an O^- source. Cesium has been shown to be a well-suited material for the primary ion source due to its low electronegativity and low ionization energy. The Cs^+ beam is generated by heating Cs_2CO_3 to 400 °C to generate a cesium vapor. The ionization of cesium takes place at a tungsten plate which is heated to 1100 °C. Cs^+ ions are then exposed to an electric field, extracted, and accelerated into ion optics to obtain a finely focused Cs^+ beam. The Cs^+ primary ion source is suitable for analysis of negative secondary ions, such as $^{12}C^{12}C^-$, $^{13}C^{12}C^-$, $^{12}C^{14}N^-$, $^{12}C^{15}N^-$, $^{31}P^-$, $^{32}S^-$, $^{127}I^-$. In

addition, it can be focused better than the O^- ion beam (~50 nm for Cs^+ beam, ~150 nm for O^+ beam).

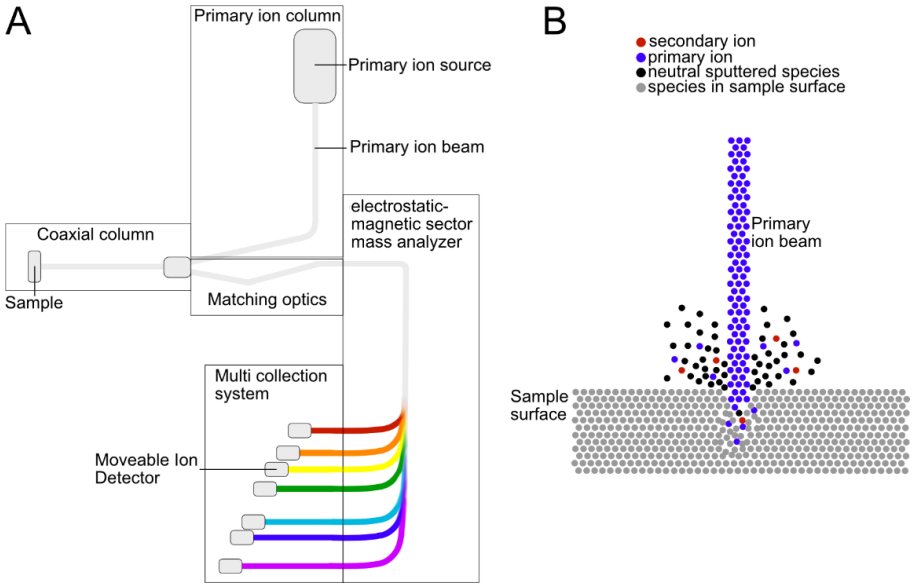

Figure 16: A) Schematic of the main components of the NanoSIMS instrument. Primary ions are focused onto the sample surface at a 90° angle. Secondary ions are extracted in the same path to increase spatial resolution. B) Schematic of the sputtering process in NanoSIMS imaging. Primary Cs^+ ions impact the surface orthogonally and result in secondary particles. Of these, secondary ions are then extracted, focused, separated by the mass analyzer, and detected by the multicollection system.

In NanoSIMS, when the sample surface is impacted by the primary ion beam, a displacement of ions within the sample surface occurs, resulting in the sputtering of particles from the surface (Fig. 16B). This sputtering is not stable on a new surface thus it is important to implant it with primary ions before analysis. A steady state is reached after a certain number of primary ions have been implanted into the surface. Steady state thereby is the state in which the rate of primary ion implantation equals the rate of primary ion sputtering. The period before the steady state is known as a transient state. The enhancement of sputtering in the steady state compared to the transient state has been mostly ascribed to a change in the work function/ionization potential in the surface due to the increased amount of Cs^+ in the sample [298]. It follows that some analytes are more susceptible to these changes than others due to the differences in their electron affinity [199], [323].

High mass resolution (~ 10000) can be obtained with NanoSIMS allowing the separation of isobaric interferences [324]. The NanoSIMS has a double-focusing mass spectrometer consisting of an electrostatic sector and a magnetic sector, based on the development of Mattauch and Herzog in 1934 [325]. Secondary ions are filtered according to their kinetic energies and focused based on their m/z ratios. Seven electron multipliers are used as detectors, of which six are movable. Therefore, up to seven masses can be detected at the same time. This limits the number of detected ions compared to other SIMS methods, however, due to the high fragmentation in NanoSIMS such that only mono-, di-, and tri-atomic ions are produced, seven detectors are sufficient for many experimental designs. The deadtime of the electron multipliers, which is the time that the detector cannot respond and produce a signal after an ion has reached it, must also be considered in image processing. In NanoSIMS, the deadtime of the detectors is 44 ns. In addition, the quasi-simultaneous arrival (QSA) factor in the ion detection with NanoSIMS should be considered. This is particularly relevant to high-abundance ions which have a higher probability of two ions reaching the detector at the same time, leading to an underestimation of the count rate [326].

NanoSIMS has been used for a variety of biological applications in single mammalian cells, for example, mapping the distributions of different lipids across single-cell plasma membranes [327], [328], iron uptake into lung macrophages [329], heart renewal [330], subcellular chemotherapeutic distribution [331], dopamine uptake and storage in nanovesicles of PC12 cells [159], [198], [199], protein turnover in synapses [65], and absolute intracellular drug concentration and metabolism [322], [332]. Additionally in 2023, the development of CryoNanoSIMS was published, allowing correlated cryo-SEM and CryoNanoSIMS of samples in their most pristine state retaining even soluble compounds [333].

Owing to the excellent performance of NanoSIMS regarding the spatial resolution, sensitivity, and capability to resolve isobaric and isotopic species, NanoSIMS was utilized as a main analytical tool in the work included in this thesis to interrogate dopamine storage and release in nanovesicles of PC12 cells, as well as the protein turnover in stress granules and organelles in human iPSC derived cells.

4.4 Sample preparation for SIMS imaging

Sample preparation for SIMS imaging is critical as it helps preserve the sample as close to the native state as possible while making it compatible for high vacuum analysis. Sample preparation depends heavily on the types of analytes and the research questions that might require a correlation of SIMS with other imaging techniques. A basic sample preparation protocol for biological samples involves air drying to dehydrate the cells. Typically, cells are chemically fixed prior to air drying, using various fixation agents such as aldehydes and/or osmium tetroxide [328]. The main advantage of this technique is that no special equipment for sample preparation is needed, and sample handling is relatively easy. Air drying however has been shown to cause shrinkage and altered topography of the sample. Another simple method to preserve biological samples is freeze drying. In this case, the samples are first either chemically fixed or washed with ammonium formate/acetate to remove residues of cell culture medium [334], then plunge-frozen in liquid isopentane, ethane, or propane (cooled down with liquid nitrogen) to avoid the formation of ice crystals, which would cause changes in cell structures. Afterward, the samples are placed in a vacuum chamber where the temperature of the samples is slowly raised, leading to the sublimation of water from the sample. This is a simple, reproducible method for preserving the localization of sample analytes well and maintaining sample morphology [335]. However, it has been shown that molecular delocalization occurs at the subcellular level during the freeze-drying process and over a long period of sample storage [336], [337]. Frozen hydrated samples are supposed to result in the best sample preservation in terms of morphology and localization of analytes: samples are plunge frozen and then imaged in a frozen condition at ~ -185 °C. A drawback of this method is the challenge in sample handling leading to a low reproducibility of the imaging results [338]. In addition, not many SIMS instruments, especially NanoSIMS, are equipped for cryo-measurements. Freeze-fracture is a part of the frozen hydrated method by which the subcellular compartments can be exposed in situ for imaging without cryo-ultramicrotome sectioning, or eroding the sample surface with the primary ion beam. The samples are analyzed in a frozen state [339], or after being freeze-dried [340]. For the correlation of SIMS with other imaging techniques, sample preparation has to be adapted to be compatible with all modalities. For example, a typical procedure for TEM imaging can be used for correlative TEM-SIMS imaging, which includes chemical fixation,

dehydration, and embedding of samples into resin, and subsequently cutting samples into sections with nanometer thickness [341]. The advantage of this method is that the procedure is well established, and additionally, resin-embedded samples can be stored for long periods of time. However, chemical fixation can cause sample distortions or artifacts due to for example osmotic pressure, extraction of lipid constituents of membranes, or temperature/pH variation [342]. In addition, small analytes such as lipids and small metabolites, which cannot be fixed completely by regular fixatives, can be washed away during sample preparation. Moreover, chemical fixation and labeling also affect the isotopic enrichment in some cases due to the dilution of the isotope-enriched biomass [343]. Another approach used for EM that has also been used in correlative TEM-NanoSIMS is high-pressure freezing and freeze substitution for which the samples are quickly frozen in liquid nitrogen at a high pressure followed by an infiltration with a fixative (e.g. GA) and resin to minimize the sample shrinkage [285] This method preserves the samples more closely to their native state, however, it requires a more specialized setup leading to higher cost. Further considerations for sample preparation in correlative imaging, particularly EM-NanoSIMS and FM-NanoSIMS are described in the following chapter.

CHAPTER 5 Correlative imaging

The combination or correlation of two or more imaging techniques is termed correlative imaging. When one imaging modality cannot characterize a sample sufficiently, correlating it to an additional technique can help answer specific scientific questions. Correlative imaging is commonly employed in biology for example in CLEM in which the strength of FM to image by labeling specific proteins or other biomolecules is combined with the strength of EM to obtain ultrastructural features of a sample. Also, correlative NanoSIMS imaging is increasingly used to study biological samples [344], [345]. In fact, this has become a standard procedure with NanoSIMS.

Correlative imaging requires careful planning of the experiment to ensure the compatibility of all methods with each other. When performing correlative EM/FM and SIMS imaging, usually EM or FM is done first as they are usually not destructive. Then the same sample is imaged in SIMS during which the sample is eroded with the ion beam. Careful consideration should also be taken with sample preparation as standard procedures for EM or FM preparation might alter the chemical nature of the sample and thereby affect the SIMS measurements. In essence, correlative imaging complicates imaging due to increased concerted efforts in sample preparation, planning of experiments, and data analysis, but the advantages of increased information make correlative imaging an invaluable tool that was used in all publications of this thesis to investigate biological mechanisms in neural cell models.

5.1 Correlative EM-NanoSIMS

NanoSIMS imaging is commonly correlated with EM when imaging biological specimens. In biological samples, NanoSIMS alone is often not sufficient to accurately identify regions of interest such as organelles. EM is helpful as it can be used to identify many different organelles/ultrastructural features at the same time with high spatial resolution, allowing efficient correlation of the images from both modalities. As mentioned above, EM is performed before NanoSIMS imaging due to the latter being destructive. An advantage of correlative EM-NanoSIMS is that for EM, the standard sample preparations are aimed at the high vacuum inside the microscope which is also required for NanoSIMS. Therefore, standard EM sample preparations can be used for correlative EM-NanoSIMS given that the analyte of interest

is preserved during this EM preparation. However, high levels of metal in the sample (e.g. osmium, copper) have been observed to lead to a matrix effect affecting the ionization/sputtering of analytes [51]. This should be considered for each analysis. Another challenge of correlative imaging is to image the exact same areas in both modalities. Finder grids with a labeled grid pattern (Fig. 13B) are a useful tool in correlative EM-NanoSIMS to facilitate and expedite finding the same analysis area in both techniques (Fig. 17). The images can then be overlayed; sometimes mirroring and turning the images may be required for accurate overlays; it may also be necessary to stretch one of the images as TEM and/or NanoSIMS imaging can stretch the section in some cases, due to the force of the focused beams onto the thin sample sections.

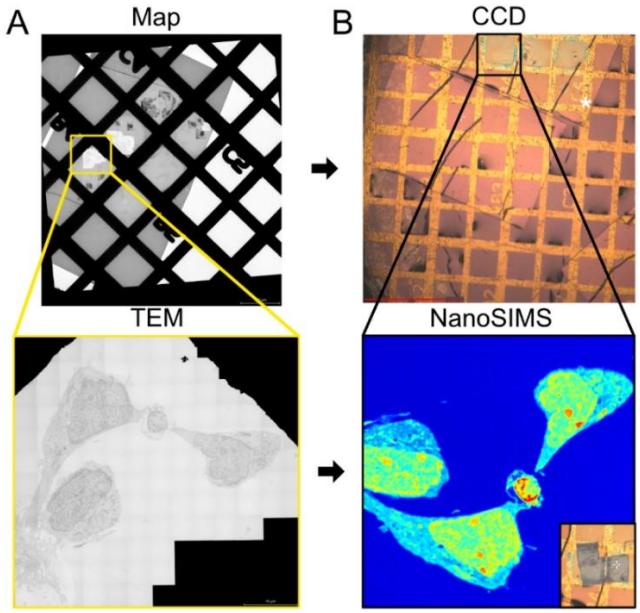

Figure 17. Correlative TEM and NanoSIMS imaging during which the same region of interest is imaged with two modalities. A) First a TEM image is taken, and then an overview/map of the surrounding area is obtained to facilitate the identification of the imaged area in the NanoSIMS. B) To image the area in the NanoSIMS it is localized with the help of the CCD camera inside the NanoSIMS, after which the NanoSIMS image is taken. One of the images must be mirrored and turned during data processing to overlay both images. The NanoSIMS measurement erodes the sample as seen with the CCD camera after the measurement (bottom right insert) illustrating the need to perform TEM before NanoSIMS imaging.

Many different clinically relevant molecules have been studied in their (subcellular) distribution with the help of correlative TEM and NanoSIMS imaging. Examples include cholesterol, lipoprotein lipase, arsenic trioxide, and oxaliplatin [346], [347], [348], [331]. The localization of lipoprotein lipase in murine endothelial cells was assessed by combining the immunogold labeling as such that the localization of gold could be tracked in both TEM and NanoSIMS imaging [347]. Tracking the subcellular localization of chemotherapeutic oxaliplatin in colon cancer cells on the other hand was possible due to the ability of NanoSIMS to directly measure rare isotopes (^{13}C) and elements such as platinum in the oxaliplatin molecule [331]. Nucleic acid-based therapeutics are a new class of drugs that have also been studied with correlative EM-NanoSIMS imaging. This allowed the study of both the uptake and distribution of these therapeutics [349] and their intracellular absolute quantification within lysosomes of hepatocytes using external standards [332]. The study of nanosized, neurotransmitter-carrying vesicles within cells has also been of interest. The vesicle structure was discerned with TEM and the isotopically labeled neurotransmitter content was then localized to the specific sub-compartments of the vesicle [198], in which the content could be absolutely quantified [159], [199].

These examples demonstrate the increasing use of correlative EM-NanoSIMS imaging in the life science/medical science field. In recent years it has become evident that it is a valuable tool to study the localization and quantification of molecules at the subcellular scale which would otherwise remain elusive.

5.2 Correlative FM-NanoSIMS

In correlative FM-NanoSIMS the molecular specificity of FM, as compared to EM, is an advantage as it allows visualization of targets that are not discernable in EM. The molecular specificity allows to define regions of interest for NanoSIMS imaging based on specific proteins. Stress granules, for example, are usually not discernible in EM images so they are commonly imaged with fluorescent microscopy. In addition, sub-compartments such as the core and shell of stress granules, or subsets of organelles can be defined based on marker proteins on the surface or within organelles.

Traditional sample preparation for FM is not vacuum compatible requiring an extra step of e.g., resin embedding to make the sample suited for subsequent NanoSIMS analysis. Analogous to EM-NanoSIMS preparation, careful consideration is needed to be sure the sample preparation procedure

will preserve the analyte localization and the fluorescence signal. Some epoxy resins have shown autofluorescence and generally lead to more denaturation of proteins affecting antigenicity/fluorescence and are therefore not commonly used for correlative FM-NanoSIMS. Acrylic resins do not interact with the biological material as strongly and therefore affect fluorescence/antigenicity less. However, the use of some acrylic resins can lead to a loss in fluorescence due to their high acidity [350]. When using the acrylic London resin (LR) white, the loss in fluorescence can be reversed by alkaline buffer in some cases [351]. In addition, some acrylic resins can be cured in cold conditions and have been shown to work well for FM [350]. The resin can also significantly affect the photo-switching abilities of fluorophores [352]. Dual labeling probes (with fluorescent and rare element labels) have also been developed to ease the identification of structures with FM and SIMS. However, it should be noted that the labeling with fluorescent probes can affect the ion count rates in NanoSIMS [343]. Some molecules commonly used in sample preparation can fluoresce such as uranyl acetate [350]. This is especially useful when combining EM, FM, and NanoSIMS (CLEM-SIMS) together on the same section to help the identification of the same structures in multiple modalities [285].

Correlating the same area in correlative FM-NanoSIMS can be more challenging compared to EM-NanoSIMS. FM is usually not performed with finder grids, instead, samples are placed on other types of substrates, such as silicon wafers. The identification of the area of interest is often more challenging when doing FM-NanoSIMS as the imaged area is not discernible after imaging as seen after TEM. Instead, areas of interest can be marked with a high-power laser or features of the sections can aid in orientation in the sample section [354].

Correlative FM-NanoSIMS has been used to address multiple different scientific questions in the life sciences. Jähne and colleagues [65], labeled pre- and post-synapse of murine hippocampal neurons with fluorescent marker proteins to determine protein turnover of the different compartments via ^{15}N-leucine incorporation (Fig. 18A, B). In addition to proteins, mRNA transcripts can also be targeted via fluorescence *in situ* hybridization (FISH) (Fig. 18C) allowing, for example, the phylogenetic labeling of target cells when morphological differences are absent [355], [356]. Mammalian heart renewal has also been investigated with correlative FM-NanoSIMS via the incorporation of ^{15}N thymidine into dividing cardiomyocytes in combination with a GFP reporter mouse line [357].

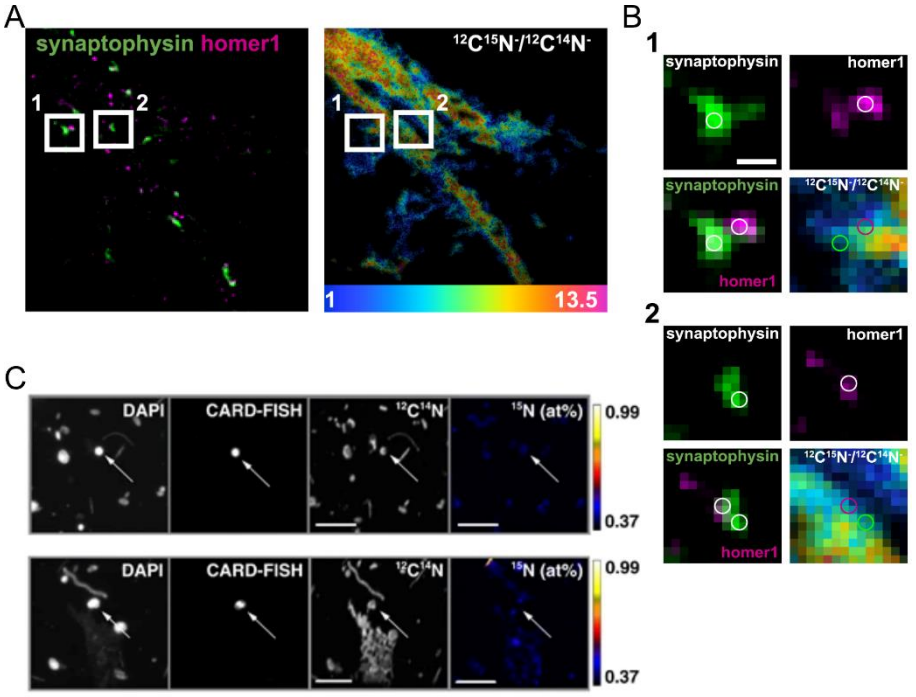

Figure 18. Example of correlative FM-NanoSIMS. A) Labeling of pre- and post-synapses with antibodies against synaptophysin and homer. NanoSIMS $^{12}C^{15}N/^{12}C^{14}N$ images display localization of ^{15}N-leucine incorporation and therefore newly synthesized proteins. B) Zoom-ins of areas depicted in A) showing a single pre- and post-synapse each. C) Nuclei of cells were labeled with DAPI and *Deltaproteobacteria* were labeled with FISH. NanoSIMS images depicting $^{12}C^{14}N$ and enrichment of the ^{15}N isotope could be obtained of the same area allowing assessment of differences between $^{15}N_2$ fixation capabilities of different bacterial strains. Scale bars 5 µm. Figures reproduced with permission from [65], [356].

In conclusion, the correlation of NanoSIMS with FM allows the localization and correlation of specific target molecules such as proteins or mRNA transcripts, which are usually not discernible in EM. This allows for studying a variety of target molecules and organelles to answer different scientific questions. In some of the work included in this thesis, correlative FM-NanoSIMS was used to localize SGs in NPCs via FM and to characterize their protein turnover via NanoSIMS imaging.

CHAPTER 6. Summary of papers

The overarching goal of my thesis was to use correlative imaging to study protein turnover in different cellular organelles in stem cell-derived cells and vesicular content and its release in PC12 cells.

In **papers I & III,** the dopamine content of vesicles was determined with correlative TEM and NanoSIMS imaging to obtain insights into exocytosis mechanisms. By incubating PC12 cells with the ^{13}C-labeled dopamine precursor L-DOPA, the neurotransmitter content inside vesicles could be quantified. This was combined with a stimulation paradigm to induce exocytosis with KCl. The main findings are presented in the following:

In **paper I**, visual proof of partial release was obtained by observing a reduction of ^{13}C-dopamine in vesicles after KCl stimulation combined with the presence of ^{127}I-amiodarone inside some vesicles which was applied externally only during the stimulation. This allowed confirmation of partial release by NanoSIMS imaging. The partial release process had previously mostly been described with electrochemical methods. Furthermore, by using NanoSIMS to quantify the neurotransmitter content from vesicles before and after stimulation (in different cells), it was possible to determine the fraction of transmitter released and this was in full agreement with electrochemical data for the same cell line.

In **paper III**, vesicle size was modulated to see how it affects neurotransmitter release, hence exploiting the visual information that can be obtained with correlative TEM and NanoSIMS imaging. By applying the same stimulation paradigm as above to PC12 cells with differently sized vesicles, we found that there is no correlation between vesicle size and fraction of release.

In **paper II**, correlative STED and NanoSIMS imaging were employed to investigate the protein turnover of SGs in NPCs. Correlative STED and NanoSIMS imaging allowed visualization of SGs with a fluorescent marker targeting the G3BP protein. Protein turnover was visualized by incubating NPCs with ^{15}N-labeled leucine and tracking its incorporation with NanoSIMS imaging. By stressing cells with the endoplasmic reticulum stressor, thapsigargin, the cells formed SGs and thapsigargin was used in various incubation schemes together with ^{15}N-leucine incubation. This work provided evidence that cellular stress affects protein turnover on a timescale beyond commonly used recovery times. Moreover, protein turnover in SGs

is largely similar to that in the cytoplasm, indicating a dynamic nature of SGs and that SGs predominantly recruit their constituents from the cytoplasm.

In **papers IV & V**, the subcellular distribution of protein turnover was investigated in detail in NPCs and during their differentiation to matured neurons. Using correlative TEM and NanoSIMS imaging, different organelles were identified, and their turnover was determined. The protein turnover was found to be heterogeneous across organelles. In addition, it was shown that different amino acids lead to a different subcellular distribution of protein turnover in NPCs revealing a possible lysine bias in the protein turnover studies using the SILAC method, where most studies primarily use a single amino acid (lysine) as a protein precursor. Furthermore, turnover was observed to slow down with the differentiation moving towards midbrain neurons. Finally, the protein half-lives of different organelles were found to be heterogenous at different stages of differentiation and found to increase slower in nucleus, nucleolus, and Golgi during the differentiation process. The findings suggest a close relation between the protein turnover and cellular activity at the organelle level during cellular differentiation. This gives an important insight into the functional remodeling process during neuronal differentiation.

CHAPTER 7 Concluding remarks and future outlook

The focus of this work has been the use of correlative SIMS imaging to probe the subcellular architecture of neural cell models to understand neural cells/neurons and the intracellular mechanisms that allow them to function and communicate. This is especially important for neurons as they do not regenerate at the same levels that other cells in a mammalian organism do. Correlative NanoSIMS imaging, as used in this thesis, provides insights into neuronal communication and protein turnover in regular culture or stress conditions. However, one of the challenges remaining with NanoSIMS is its low throughput. Increasing the throughput of NanoSIMS would allow for larger sample sizes leading to more robust data. In addition, data analysis in SIMS and NanoSIMS can be challenging and time-consuming. Currently, an increasing number of artificial intelligence tools are available to handle great amounts of complex data and condense them into simple outputs. In the future, these tools can increasingly be exploited to increase throughput, correct for imaging artifacts, and condense information to aid in easier understanding of data.

The work in this thesis demonstrates that single-cell and single-organelle spatial resolution of SIMS is an exquisite tool to uncover insights into (neural) cell biology. Subcellular MSI options are therefore the preferred option for cell biological questions. Looking forward, improving instrumentation to achieve high spatial resolution with less fragmentation to obtain better molecular information is desirable. Instruments such as SIMS:Zero [358] and CryoNanoSIMS [333], are interesting developments due to their increased resolution and ability to perform measurements under cryogenic conditions, which can further improve our understanding of cellular processes, possibly in correlation with other imaging methods. Also, approaches to artificially increase image resolution in correlative SIMS imaging by “image fusion” [359] could potentially give better insights due to more detailed mapping of the SIMS information to the microscopy image. These developments might be especially helpful in iPSC/organoid biology to understand/characterize developmental stages and subpopulations of cells that require high spatial resolution chemical imaging.

Correlative SIMS imaging has also been demonstrated to be a useful tool to investigate drug metabolism such as the absolute quantification of molecules. This approach can be employed for different (new) types of drugs

and aid the field of pharmacology to further improve the dosage of medication and understand their subcellular trafficking and mode of action.

In summary, correlative chemical imaging is a valuable tool in understanding biological mechanisms. Further advancements in instrumentation, throughput, and data analysis can increase its benefit in an even larger variety of applications, giving more insights into previously elusive target analytes. The use of correlative mass spectrometry to uncover the spatial organization of turnover processes at a subcellular scale was shown to be important as heterogenous patterns of turnover were observed. Further studies are required to understand the underlying processes leading to different turnover patterns with respect to different amino acids, signaling pathways, and cellular differentiation. This can lead to a more detailed understanding of how turnover is controlled at the subcellular scale.

Acknowledgments

I am profoundly grateful to numerous people whose contributions, support, and encouragement have made this thesis possible!

First, I would like to thank my supervisor **Asst. Prof. Nhu Phan** for giving me the opportunity to do my PhD in her lab and supporting me during all this time. You gave me the chance to dive into the interesting field of mass spectrometry imaging which gave me new (scientific) perspectives and provided an environment for professional and personal growth. Thank you for making all of this possible! In addition, I would like to thank my second supervisor **Prof. Andrew Ewing** for his encouraging words and his advice whenever I needed it. Thank you also to my third supervisor **Prof. Marica Ericson** for supporting me during my studies. I am also very grateful to my examiner **Prof. John Fletcher** who guided me throughout my studies.

To Dr. **Stefania Rabasco** and Dr. **Duc Khanh Tho Nguyen**: thank you for being the best office partners for (most of) our PhD time. I owe so much to you both and I cherish our friendship. You taught me so many things and our office discussions were indispensable to this thesis, and you made every day at work so much more fun to be around!

Thank you to both the Ewing and Phan research groups for being such a nice team to work with. It was fun to collaborate with anyone. The fikas, BBQs and after works were really awesome and I gained many friends! Special thanks to Dr. **Chaoyi Gu,** for helping so much with various things and for trying so many different lunch places together. Thank you to (soon-to-be Dr.) **Kim Long Le Vo**; writing our thesis together was such a special experience and your positive outlook was inspiring many times. Thank you for making sure I would always have something or the other to snack on during this time! Thank you also to Dr. **Andre du Toit** for investing so much time into my projects and always keeping me on top of my sarcasm. Thank you to Dr. **Alex Lima**, and **Emmanuel Berlin** for helping me in different ways along the way. I am also grateful to Dr. **Anna Larsson** and Dr. **Pieter Oomen** for sharing their experience with the NPCs in the early days of my PhD.

To all my **co-authors**, thank you for all the stimulating discussions and all the work you did without which none of the projects would have been the same.

Thank you to **Dr. Aurelién Thomen**, **Dr. Michael Kurczy,** and **Dr. Elias Ranjbari** for teaching and supporting me in all things NanoSIMS. I have learned so much from all of you. Also thank you to **Dr. Massimo Micaroni**, **Dr. Jens Bengtson**, **Dr. Charlotte Blomquist,** and **Dr. Anna Pielach** for assistance during sample preparation and TEM. I would like to acknowledge the **Centre for Cellular Imaging** at Gothenburg University for assistance in sample preparation and TEM and the **NanoSIMS facility** at Gothenburg University, located at the AstraZeneca BioVentureHub for the assistance in NanoSIMS imaging.

Thank you also to **Simon Uzoni** & **Sonali Chavan** for all the uplifting conversations during my thesis writing.

To all my **advisors/supervisors/mentors** I had along the way during my studies. You inspired me to go for the PhD and I learned many things from each one of you and all these things helped me accomplish this thesis. I am very grateful to you!

Thank you to all my **friends** for always being there for me, listening, and giving advice or encouragement whenever I need it. It means so much to me.

To my **family** and **family-in-law**: Thank you for all the love and support that you have given me all those years. I am the person I am today because of you, and I am so grateful to all of you.

To **Aarush**, you manage to put a smile on my face in every situation and you make my heart feel so full. This wouldn't have been possible without you. I cannot wait for many more chapters in our life together!

References

[1] G. Biolo, R. Antonione, R. Barazzoni, M. Zanetti, and G. Guarnieri, "Mechanisms of altered protein turnover in chronic diseases: A review of human kinetic studies," *Curr Opin Clin Nutr Metab Care*, vol. 6, no. 1, pp. 55–63, 2003, doi: 10.1097/00075197-200301000-00009.

[2] Y. C. Wang, E. Lauwers, and P. Verstreken, "Presynaptic protein homeostasis and neuronal function," *Curr Opin Genet Dev*, vol. 44, pp. 38–46, 2017, doi: 10.1016/j.gde.2017.01.015.

[3] A. B. Ross, J. D. Langer, and M. Jovanovic, "Proteome Turnover in the Spotlight: Approaches, Applications, and Perspectives," *Mol. and Cell. Proteomics*, vol. 20, pp. 1–17, 2021, doi: 10.1074/mcp.R120.002190.

[4] J. D. Watson and F. H. C. Crick, "Genetical Implications of the Structure of Deoxyribonucleic Acid," *Nature*, vol. 171, pp. 964–967, 1953, doi: 10.1007/BF00434693.

[5] F. H. C. Crick, F.R.S., L. Barnett, S. Brenner, and R. J. Watts-Tobin, "General Nature of the Genetic Code for Proteins," *Nature*, vol. 192, pp. 1227–1232, 1961, doi:https://doi.org/10.1038/1921227a0

[6] P. F. Agris, "Decoding the genome: A modified view," *Nucleic Acids Res*, vol. 32, no. 1, pp. 223–238, 2004, doi: 10.1093/nar/gkh185.

[7] A. Sentenac, "Eukaryotic RNA polymerase," *Crc Crit Rev Biochem Mol Biol*, vol. 18, no. 1, pp. 31–90, 1985, doi: 10.3109/10409238509082539.

[8] A. Dome, M. Dymova, V. Richter, and G. Stepanov, "Post-Transcriptional Modifications of RNA as Regulators of Apoptosis in Glioblastoma," *Int J Mol Sci*, vol. 23, no. 16, 2022, doi: 10.3390/ijms23169272.

[9] L. A. Passmore and J. Coller, "Roles of mRNA poly(A) tails in regulation of eukaryotic gene expression," *Nat Rev Mol Cell Biol*, vol. 23, no. 2, pp. 93–106, 2023, doi: 10.1038/s41580-021-00417-y.

[10] P. De Magistris, "The great escape: mRNA export through the nuclear pore complex," *Int J Mol Sci*, vol. 22, no. 21, 2021, doi: 10.3390/ijms222111767.

[11] C. M. Redman, "Biosynthesis of serum proteins and ferritin by free and attached ribosomes of rat liver.," *J Biol Chem*, vol. 244, no. 16, pp. 4308–4315, 1969, doi: 10.1016/s0021-9258(18)94321-8.

[12] D. W. Reid and C. V. Nicchitta, "Primary role for endoplasmic reticulum-bound ribosomes in cellular translation identified by ribosome profiling," *Journal of Biological Chemistry*, vol. 287, no. 8, pp. 5518–5527, 2012, doi: 10.1074/jbc.M111.312280.

[13] W. C. Merrick and G. D. Pavitt, "Protein synthesis initiation in eukaryotic cells," *Cold Spring Harb Perspect Biol*, vol. 10, no. 12, pp. 1–22, 2018, doi: 10.1101/cshperspect.a033092.

[14] P. P. Roux and I. Topisirovic, "Signaling Pathways Involved in the Regulation of mRNA Translation," *Mol Cell Biol*, vol. 38, no. 12, pp. 1–26, 2018, doi: 10.1128/mcb.00070-18.

[15] A. Gentilella, S. C. Kozma, and G. Thomas, “A liaison between mTOR signaling, ribosome biogenesis and cancer,” *Biochim Biophys Acta*, vol. 1849, no. 7, pp. 812–820, 2015, doi: 10.1016/j.bbagrm.2015.02.005.

[16] M. Laplante and D. M. Sabatini, “MTOR signaling in growth control and disease,” *Cell*, vol. 149, no. 2, pp. 274–293, 2012, doi: 10.1016/j.cell.2012.03.017.

[17] X. Wang and C. G. Proud, “The mTOR pathway in the control of protein synthesis,” *Physiology*, vol. 21, no. 5, pp. 362–369, 2006, doi: 10.1152/physiol.00024.2006.

[18] A. B. Alber, E. R. Paquet, M. Biserni, F. Naef, and D. M. Suter, “Single Live Cell Monitoring of Protein Turnover Reveals Intercellular Variability and Cell-Cycle Dependence of Degradation Rates,” *Mol Cell*, vol. 71, no. 6, pp. 1079-1091.e9, 2018, doi: 10.1016/j.molcel.2018.07.023.

[19] A. E. Koromilas, “Roles of the translation initiation factor eIF2α serine 51 phosphorylation in cancer formation and treatment,” *Biochim Biophys Acta*, vol. 1849, no. 7, pp. 871–880, 2015, doi: 10.1016/j.bbagrm.2014.12.007.

[20] A. G. Hinnebusch, I. P. Ivanov, and N. Sonenberg, “Translational control by 5’-untranslated regions of eukaryotic mRNAs,” *Science*, vol. 352, pp. 1413–1416, 2016, doi: 10.1126/science.aad9868.Translational.

[21] C. Vogel *et al.*, “Sequence signatures and mRNA concentration can explain two-thirds of protein abundance variation in a human cell line,” *Mol Syst Biol*, vol. 6, no. 400, pp. 1–9, 2010, doi: 10.1038/msb.2010.59.

[22] A. Ghazalpour *et al.*, “Comparative analysis of proteome and transcriptome variation in mouse,” *PLoS Genet*, vol. 7, no. 6, 2011, doi: 10.1371/journal.pgen.1001393.

[23] R. Aviner, “The science of puromycin: From studies of ribosome function to applications in biotechnology,” *Comput Struct Biotechnol J*, vol. 18, pp. 1074–1083, 2020, doi: 10.1016/j.csbj.2020.04.014.

[24] C. M. Forester *et al.*, “Revealing nascent proteomics in signaling pathways and cell differentiation,” *Proc Natl Acad of Sci USA*, vol. 115, no. 10, pp. 2353–2358, 2018, doi: 10.1073/pnas.1707514115.

[25] N. T. Ingolia, S. Ghaemmaghami, J. R. S. Newman, and J. S. Weissman, “Genome-wide analysis in vivo of translation with nucleotide resolution using ribosome profiling,” *Science*, vol. 324, no. 5924, pp. 218–223, 2009, doi: 10.1126/science.1168978.

[26] G. A. Brar and J. S. Weissman, “Ribosome profiling reveals the what, when, where and how of protein synthesis,” *Nat Rev Mol Cell Biol*, vol. 16, no. 11, pp. 651–664, 2015, doi: 10.1038/nrm4069.

[27] Y. Tu, C. Chen, J. Pan, J. Xu, Z. G. Zhou, and C. Y. Wang, “The ubiquitin proteasome pathway (UPP) in the regulation of cell cycle control and DNA damage repair and its implication in tumorigenesis,” *Int J Clin Exp Pathol*, vol. 5, no. 8, pp. 726–738, 2012.

[28] A. Hershko, H. Heller, S. Elias, and A. Ciechanover, “Components of ubiquitin-protein ligase system. Resolution, affinity purification, and role in protein breakdown.,” *Journal of Biological Chemistry*, vol. 258, no. 13, pp. 8206–8214, 1983, doi: 10.1016/s0021-9258(20)82050-x.

[29] K. Tanaka, “The proteasome: Overview of structure and functions,” *Proc Jpn Acad Ser B Phys Biol Sci*, vol. 85, no. 1, pp. 12–36, 2009, doi: 10.2183/pjab.85.12.

[30] C. Pohl and I. Dikic, “Cellular quality control by the ubiquitin-proteasome system and autophagy,” *Science (1979)*, vol. 366, no. 6467, pp. 818–822, 2019, doi: 10.1126/science.aax3769.

[31] A. V. Sorokin, E. R. Kim, and L. P. Ovchinnikov, “Proteasome system of protein degradation and processing,” *Biochemistry (Moscow)*, vol. 74, no. 13, pp. 1411–1442, 2009, doi: 10.1134/S000629790913001X.

[32] A. L. Goldberg and K. L. Rock, “Proteolysis, proteasomes and antigen presentation,” *Nature*, vol. 357, no. 6377, pp. 375–379, 1992, doi: 10.1038/357375a0.

[33] A. Hershko, E. Leshinsky, D. Ganoth, and H. Heller, “ATP-dependent degradation of ubiquitin-protein conjugates,” *Proc Natl Acad Sci USA*, vol. 81, no. 6, pp. 1619–1623, 1984, doi: 10.1073/pnas.81.6.1619.

[34] C. S. Pillay, E. Elliott, and C. Dennison, “Endolysosomal proteolysis and its regulation,” *Biochem J*, vol. 363, no. 3, pp. 417–429, 2002, doi: 10.1042/0264-6021:3630417.

[35] F. Reggiori and C. Ungermann, “Autophagosome Maturation and Fusion,” *J Mol Biol*, vol. 429, no. 4, pp. 486–496, 2017, doi: 10.1016/j.jmb.2017.01.002.

[36] J. L. Mego, “The ATP-Dependent Proton Pump In Lysosome Membranes,” *FEBS Lett*, vol. 107, no. 1, pp. 113–116, 1979. doi: 10.1016/0014-5793(79)80475-5.

[37] T. Kolter and K. Sandhoff, “Lysosomal degradation of membrane lipids,” *FEBS Lett*, vol. 584, no. 9, pp. 1700–1712, 2010, doi: 10.1016/j.febslet.2009.10.021.

[38] C. Arsenis and O. Touster, “Purification and properties of an acid nucleotidase from rat liver lysosomes.,” *J of Biol Chem*, vol. 243, no. 21, pp. 5702–5708, 1968, doi: 10.1016/s0021-9258(18)91923-x.

[39] P. Bohley and P. O. Seglen, “Proteases and proteolysis in the lysosome,” *Experientia*, vol. 48, no. 2, pp. 151–157, 1992, doi: 10.1007/BF01923508.

[40] J. A. Schneider and R. L. Pisoni, “Amino Acid Transport By Lysosomes,” In: Kilberg, M.S., Häussinger, D. (eds) Mammalian Amino Acid Transport. Springer, Boston, MA. pp. 89–90, 1992, doi: 10.1007/978-1-4899-1161-2_6.

[41] C. Sagné *et al.*, “Identification and characterization of a lysosomal transporter for small neutral amino acids,” *Proc Natl Acad Sci USA*, vol. 98, no. 13, pp. 7206–7211, 2001, doi: 10.1073/pnas.121183498.

[42] Ö. Demirel *et al.*, "Identification of a lysosomal peptide transport system induced during dendritic cell development," *J of Biol Chem*, vol. 282, no. 52, pp. 37836–37843, 2007, doi: 10.1074/jbc.M708139200.

[43] Y. Wang and H. Zhang, "Regulation of Autophagy by mTOR Signaling Pathway" *Adv Exp Med Biol*, vol. 1206. pp. 67-83. 2019. doi: 10.1007/978-981-15-0602-4_3.

[44] J. Kim, M. Kundu, B. Viollet, and K. L. Guan, "AMPK and mTOR regulate autophagy through direct phosphorylation of Ulk1," *Nat Cell Biol*, vol. 13, no. 2, pp. 132–141, 2011, doi: 10.1038/ncb2152.

[45] N. Zheng and N. Shabek, "Ubiquitin ligases: Structure, function, and regulation," *Annu Rev Biochem*, vol. 86, pp. 129–157, 2017, doi: 10.1146/annurev-biochem-060815-014922.

[46] P. De Bie and A. Ciechanover, "Ubiquitination of E3 ligases: Self-regulation of the ubiquitin system via proteolytic and non-proteolytic mechanisms," *Cell Death Differ*, vol. 18, no. 9, pp. 1393–1402, 2011, doi: 10.1038/cdd.2011.16.

[47] S. P. Acebron, E. Karaulanov, B. S. Berger, Y. L. Huang, and C. Niehrs, "Mitotic Wnt Signaling Promotes Protein Stabilization and Regulates Cell Size," *Mol Cell*, vol. 54, no. 4, pp. 663–674, 2014, doi: 10.1016/j.molcel.2014.04.014.

[48] A. B. Alber and D. M. Suter, "Dynamics of protein synthesis and degradation through the cell cycle," *Cell Cycle*, vol. 18, no. 8, pp. 784–794, 2019, doi: 10.1080/15384101.2019.1598725.

[49] E. F. Fornasiero *et al.*, "Precisely measured protein lifetimes in the mouse brain reveal differences across tissues and subcellular fractions," *Nat Commun*, vol. 9, no. 1, 2018, doi: 10.1038/s41467-018-06519-0.

[50] A. Geier, R. Beery, M. Haimshon, R. Hemi, and B. Lunenfeld, "Serum and insulin inhibit cell death induced by cycloheximide in the human breast cancer cell line MCF-7," *In Vitro Cell Dev Biol Anim*, vol. 28 A, no. 6, pp. 415–418, 1992, doi: 10.1007/BF02634045.

[51] D. P. Narendra, C. Guillermier, F. Gyngard, X. Huang, M. E. Ward, and M. L. Steinhauser, "Coupling APEX labeling to imaging mass spectrometry of single organelles reveals heterogeneity in lysosomal protein turnover," *J Cell Biol*, vol. 219, pp. 1–15, 2020, doi: 10.1083/jcb.201901097.

[52] K. Swovick, K. A. Welle, J. R. Hryhorenko, A. Seluanov, V. Gorbunova, and S. Ghaemmaghami, "Cross-species comparison of proteome turnover kinetics," *Mol Cell Proteomics*, vol. 17, no. 4, pp. 580–591, 2018, doi: 10.1074/mcp.RA117.000574.

[53] J. Hasper, K. Welle, J. Hryhorenko, S. Ghaemmaghami, and A. Buchwalter, "Turnover and replication analysis by isotope labeling (TRAIL) reveals the influence of tissue context on protein and organelle lifetimes," *Mol Syst Biol*, vol. 19, no. 4, pp. 1–19, 2023, doi: 10.15252/msb.202211393.

[54] A. R. Dörrbaum, L. Kochen, J. D. Langer, and E. M. Schuman, "Local and global influences on protein turnover in neurons and glia," *Elife*, vol. 7, 2018, doi: 10.7554/eLife.34202.

[55] S. Mandad *et al.*, "The codon sequences predict protein lifetimes and other parameters of the protein life cycle in the mouse brain," *Sci Rep*, vol. 8, no. 1, pp. 1–19, 2018, doi: 10.1038/s41598-018-35277-8.

[56] T. Maier, M. Güell, and L. Serrano, "Correlation of mRNA and protein in complex biological samples," *FEBS Lett*, vol. 583, no. 24, pp. 3966–3973, 2009, doi: 10.1016/j.febslet.2009.10.036.

[57] M. K. Doherty, D. E. Hammond, M. J. Clague, S. J. Gaskell, and R. J. Beynon, "Turnover of the human proteome: determination of protein intracellular stability by dynamic SILAC," *J Proteome Res*, vol. 8, pp. 104–112, 2009. doi: 10.1021/pr800641v.

[58] B. Schwanhäusser *et al.*, "Global quantification of mammalian gene expression control," *Nature*, vol. 473, no. 7347, pp. 337–342, 2011, doi: 10.1038/nature10098.

[59] D. R. Parks and L. A. Herzenberg, "Fluorescence - Activated Cell Sorting: Theory , Experimental Optimization, and Applications in Lymphoid Cell Biology" 1984. *Methods Enzymol*, vol. 108, pp. 197–241, doi: 10.1016/s0076-6879(84)08086-1

[60] H. M. Bennett, W. Stephenson, C. M. Rose, and S. Darmanis, "Single-cell proteomics enabled by next-generation sequencing or mass spectrometry," *Nat Methods*, vol. 20, no. 3, pp. 363–374, 2023, doi: 10.1038/s41592-023-01791-5.

[61] F. Yuan, Y. Li, X. Zhou, P. Meng, and P. Zou, "Spatially resolved mapping of proteome turnover dynamics with subcellular precision," *Nat Commun*, vol. 14, no. 7217, pp. 1–13, 2023, doi: 10.1038/s41467-023-42861-8.

[62] D. C. Dieterich *et al.*, "In situ visualization and dynamics of newly synthesized proteins in rat hippocampal neurons," *Nat Neurosci*, vol. 13, no. 7, pp. 897–905, 2010, doi: 10.1038/nn.2580.

[63] R. Cagnetta, C. K. Frese, T. Shigeoka, J. Krijgsveld, and C. E. Holt, "Rapid Cue-Specific Remodeling of the Nascent Axonal Proteome," *Neuron*, vol. 99, no. 1, pp. 29-46.e4, 2018, doi: 10.1016/j.neuron.2018.06.004.

[64] C. Sun and E. M. Schuman, "Logistics of neuronal protein turnover: Numbers and mechanisms," *Mol Cell Neurosci*, vol. 123, no. November, p. 103793, 2022, doi: 10.1016/j.mcn.2022.103793.

[65] S. Jähne *et al.*, "Presynaptic activity and protein turnover are correlated at the single-synapse level," *Cell Rep*, vol. 34, no. 108841, pp. 1–9, 2021, doi: 10.1016/j.celrep.2021.108841.

[66] R. Yousefi, K. Jevdokimenko, V. Kluever, D. Pacheu-grau, and E. F. Fornasiero, "Influence of Subcellular Localization and Functional State on Protein Turnover," *Cells*, vol. 10, no. 7, 2021. doi: 10.3390/cells10071747.

[67] N. S. Chandel, “Amino acid metabolism,” *Cold Spring Harb Perspect Biol*, vol. 13, no. 4, pp. 1–17, 2021, doi: 10.1101/CSHPERSPECT.A040584.

[68] M. E. Jones, “Conversion of glutamate to ornithine and proline: Pyrroline-5-carboxylate, a possible modulator of arginine requirements,” *J Nutr*, vol. 115, no. 4, pp. 509–515, 1985, doi: 10.1093/jn/115.4.509.

[69] M. S. Kilberg, M. Balasubramanian, L. Fu, and J. Shan, “The transcription factor network associated with the amino acid response in mammalian cells,” *Adv Nutr*, vol. 3, no. 3, pp. 295–306, 2012, doi: 10.3945/an.112.001891.

[70] G. Gauthier-Coles *et al.*, “Quantitative modelling of amino acid transport and homeostasis in mammalian cells,” *Nat Commun*, vol. 12, no. 1, pp. 1–18, 2021, doi: 10.1038/s41467-021-25563-x.

[71] B. C. Fuchs and B. P. Bode, “Amino acid transporters ASCT2 and LAT1 in cancer: Partners in crime?,” *Semin Cancer Biol*, vol. 15, no. 4, pp. 254–266, 2005, doi: 10.1016/j.semcancer.2005.04.005.

[72] G. Gauthier-Coles, S. J. Fairweather, A. Bröer, and S. Bröer, “Do Amino Acid Antiporters Have Asymmetric Substrate Specificity?,” *Biomolecules*, vol. 13, no. 2, 2023, doi: 10.3390/biom13020301.

[73] R. G. Sawers, “Amino Acid Degradation,” *eLS*, 2015, doi: 10.1002/9780470015902.a0001388.pub3.

[74] J. Rossant and P. P. L. Tam, “Early human embryonic development: Blastocyst formation to gastrulation,” *Dev Cell*, vol. 57, no. 2, pp. 152–165, 2022, doi: 10.1016/j.devcel.2021.12.022.

[75] D. K. Gardner and A. J. Harvey, “Blastocyst metabolism,” *Reprod Fertil Dev*, vol. 27, no. 4, pp. 638–654, 2015, doi: 10.1071/RD14421.

[76] L. J. Van Winkle, A. L. Campione, J. M. Gorman, and B. D. Weimer, “Changes in the activities of amino acid transport systems b0,+ and L during development of preimplantation mouse conceptuses,” *Biochim Biophys Acta*, vol. 1021, no. 1, pp. 77–84, 1990, doi: 10.1016/0005-2736(90)90387-4.

[77] S. R. Frankenberg, F. R. O. de Barros, J. Rossant, and M. B. Renfree, “The mammalian blastocyst,” *Wiley Interdiscip Rev Dev Biol*, vol. 5, no. 2, pp. 210–232, 2016, doi: 10.1002/wdev.220.

[78] M. Amit and J. Itskovitz-Eldor, “Derivation and spontaneous differentiation of human embryonic stem cells,” *J Anat*, vol. 200, pp. 225–232, 2002, doi: 10.1046/j.1469-7580.2002.00032.x.

[79] K. K. Niakan and K. Eggan, “Analysis of human embryos from zygote to blastocyst reveals distinct gene expression patterns relative to the mouse,” *Dev Biol*, vol. 375, no. 1, pp. 54–64, 2013, doi: 10.1016/j.ydbio.2012.12.008.

[80] G. C. Le Bin *et al.*, “Oct4 is required for lineage priming in the developing inner cell mass of the mouse blastocyst,” *Development*, vol. 141, no. 5, pp. 1001–1010, 2014, doi: 10.1242/dev.096875.

[81] E. S. Bardot and A. K. Hadjantonakis, “Mouse gastrulation: Coordination of tissue patterning, specification and diversification of cell fate,” *Mech Dev*, vol. 163, p. 103617, 2020, doi: 10.1016/j.mod.2020.103617.

[82] J. Muhr, T. Arbor, and K. M. Ackerman, “Embyology, Gastrulation,” 2023.

[83] K. R. W. Matthews and D. Moralí, “National human embryo and embryoid research policies: A survey of 22 top research-intensive countries,” *Regen Med*, vol. 15, no. 7, pp. 1905–1917, 2020, doi: 10.2217/rme-2019-0138.

[84] L. Wolpert, “Positional information and the spatial pattern of cellular differentiation,” *J Theor Biol*, vol. 25, no. 1, pp. 1–47, 1969, doi: 10.1016/S0022-5193(69)80016-0.

[85] E. Dessaud, A. P. McMahon, and J. Briscoe, “Pattern formation in the vertebrate neural tube: A sonic hedgehog morphogen-regulated transcriptional network,” *Development*, vol. 135, no. 15, pp. 2489–2503, 2008, doi: 10.1242/dev.009324.

[86] R. S. Darken and P. A. Wilson, “Axis induction by Wnt signaling: Target promoter responsiveness regulates competence,” *Dev Biol*, vol. 234, no. 1, pp. 42–54, 2001, doi: 10.1006/dbio.2001.0253.

[87] R. T. Moon and J. L. Christian, “Competence modifiers synergize with growth factors during mesoderm induction and patterning in xenopus,” *Cell*, vol. 71, no. 5, pp. 709–712, 1992, doi: 10.1016/0092-8674(92)90545-N.

[88] R. O’Rahilly and F. Müller, “Neurulation in the normal human embryo” *Ciba Found Symp*, vol. 181, pp. 70–82 1994, doi: 10.1002/9780470514559.ch5.

[89] K. J. Lee and T. M. Jessell, “The specification of dorsal cell fates in the vertebrate central nervous system,” *Annu Rev Neurosci*, vol. 22, pp. 261–294, 1999, doi: 10.1146/annurev.neuro.22.1.261.

[90] T. Yamada, M. Placzek, H. Tanaka, J. Dodd, and T. M. Jessell, “Control of cell pattern in the developing nervous system: Polarizing activity of the floor plate and notochord,” *Cell*, vol. 64, no. 3, pp. 635–647, 1991, doi: 10.1016/0092-8674(91)90247-V.

[91] A. Liu and L. A. Niswander, “Bone morphogenetic protein signalling and vertebrate nervous system development,” *Nat Rev Neurosci*, vol. 6, no. 12, pp. 945–954, 2005, doi: 10.1038/nrn1805.

[92] G. La Manno *et al.*, “Molecular architecture of the developing mouse brain,” *Nature*, vol. 596, no. 7870, pp. 92–96, 2021, doi: 10.1038/s41586-021-03775-x.

[93] M. Placzek and J. Briscoe, “The floor plate: Multiple cells, multiple signals,” *Nat Rev Neurosci*, vol. 6, no. 3, pp. 230–240, 2005, doi: 10.1038/nrn1628.

[94] W. Wurst and L. Bally-cuif, “Neural Plate Patterning: Upstream and Downstream of the Isthmic Organizer,” vol. 2, no. 2, pp. 99–108, 2001. doi: 10.1038/35053516.

[95] I. Allodi and E. Hedlund, “Directed midbrain and spinal cord neurogenesis from pluripotent stem cells to model development and disease in a dish,” *Front Neurosci*, vol. 8, no. 8, pp. 1–18, 2014, doi: 10.3389/fnins.2014.00109.

[96] S. Fitriasari and P. A. Trainor, “Diabetes, Oxidative Stress, and DNA Damage Modulate Cranial Neural Crest Cell Development and the Phenotype Variability of Craniofacial Disorders,” *Front Cell Dev Biol*, vol. 9, pp. 1–16, 2021, doi: 10.3389/fcell.2021.644410.

[97] M. Simões-Costa and M. E. Bronner, “Establishing neural crest identity: a gene regulatory recipe,” *Development*, vol. 142, no. 2, pp. 242–257, 2015, doi: 10.1242/dev.105445.

[98] G. Chanas-Sacre, B. Rogister, G. Moonen, and P. Leprince, “Radial glia phenotype: Origin, regulation, and transdifferentiation,” *J Neurosci Res*, vol. 61, no. 4, pp. 357–363, 2000, doi: 10.1002/1097-4547(20000815)61:4<357::AID-JNR1>3.0.CO;2-7.

[99] F. Polleux, T. Morrow, and A. Ghosh, “Semaphorin 3A is a chemoattractant for cortical apical dendrites,” *Nature*, vol. 404, no. 6778, pp. 567–573, 2000, doi: 10.1038/35007001.

[100] A. Gärtner *et al.*, “N-cadherin specifies first asymmetry in developing neurons,” *EMBO J*, vol. 31, no. 8, pp. 1893–1903, 2012, doi: 10.1038/emboj.2012.41.

[101] J. F. Zmuda and R. J. Rivas, “The Golgi apparatus and the centrosome are localized to the sites of newly emerging axons in cerebellar granule neurons in vitro,” *Cell Motil Cytoskeleton*, vol. 41, pp. 18–38, 1998, doi: 10.1002/(SICI)1097-0169(1998)41:1<18::AID-CM2>3.0.CO;2-B.

[102] L. Galluzzi, T. Yamazaki, and G. Kroemer, “Linking cellular stress responses to systemic homeostasis,” *Nat Rev Mol Cell Biol*, vol. 19, no. 11, pp. 731–745, 2018, doi: 10.1038/s41580-018-0068-0.

[103] N. C. Collier and M. J. Schlesinger, “The dynamic state of heat shock proteins in chicken embryo fibroblasts,” *J Cell Biol*, vol. 103, no. 4, pp. 1495–1507, 1986, doi: 10.1083/jcb.103.4.1495.

[104] L. Nover, K. D. Scharf, and D. Neumann, “Formation of Cytoplasmic Heat Shock Granules in Tomato Cell Cultures and Leaves,” *Mol Cell Biol*, vol. 3, no. 9, pp. 1648–1655, 1983, doi: 10.1128/mcb.3.9.1648-1655.1983.

[105] S. Jain, J. R. Wheeler, R. W. Walters, A. Agrawal, A. Barsic, and R. Parker, “ATPase-Modulated Stress Granules Contain a Diverse Proteome and Substructure,” *Cell*, vol. 164, no. 3, pp. 487–498, 2016, doi: 10.1016/j.cell.2015.12.038.

[106] J. R. Wheeler, T. Matheny, S. Jain, R. Abrisch, and R. Parker, “Distinct stages in stress granule assembly and disassembly,” *Elife*, vol. 5, pp. 1–25, 2016, doi: 10.7554/eLife.18413.

[107] S. L. Erickson and J. Lykke-Andersen, “Cytoplasmic mRNP granules at a glance,” *J Cell Sci*, vol. 124, no. 3, pp. 293–297, 2011, doi: 10.1242/jcs.072140.

[108] S. Hofmann, N. Kedersha, P. Anderson, and P. Ivanov, “Molecular mechanisms of stress granule assembly and disassembly,” *Biochim Biophys Acta Mol Cell Res*, vol. 1868, no. 1, p. 118876, 2021, doi: 10.1016/j.bbamcr.2020.118876.

[109] S. Elbaum-Garfinkle *et al.*, “The disordered P granule protein LAF-1 drives phase separation into droplets with tunable viscosity and dynamics,” *Proc Natl Acad Sci USA*, vol. 112, no. 23, pp. 7189–7194, 2015, doi: 10.1073/pnas.1504822112.

[110] Y. Lin, D. S. W. Protter, M. K. Rosen, and R. Parker, “Formation and Maturation of Phase-Separated Liquid Droplets by RNA-Binding Proteins,” *Mol Cell*, vol. 60, no. 2, pp. 208–219, 2015, doi: 10.1016/j.molcel.2015.08.018.

[111] A. Molliex *et al.*, “Phase Separation by Low Complexity Domains Promotes Stress Granule Assembly and Drives Pathological Fibrillization,” *Cell*, vol. 163, no. 1, pp. 123–133, 2015, doi: 10.1016/j.cell.2015.09.015.

[112] T. J. Nott *et al.*, “Phase Transition of a Disordered Nuage Protein Generates Environmentally Responsive Membraneless Organelles,” *Mol Cell*, vol. 57, no. 5, pp. 936–947, 2015, doi: 10.1016/j.molcel.2015.01.013.

[113] N. Kedersha *et al.*, “Evidence That Ternary Complex (eIF2-GTP-tRNAi Met)– Deficient Preinitiation Complexes Are Core Constituents of Mammalian Stress Granules,” *Mol Biol Cell*, vol. 13, no. 6, pp. 2170–2179, 2002, doi: 10.1091/mbc.01.

[114] T. Takahara and T. Maeda, “Transient Sequestration of TORC1 into Stress Granules during Heat Stress,” *Mol Cell*, vol. 47, no. 2, pp. 242–252, 2012, doi: 10.1016/j.molcel.2012.05.019.

[115] D. S. W. Protter and R. Parker, “Principles and Properties of Stress Granules,” *Trends Cell Biol*, vol. 26, no. 9, pp. 668–679, 2016, doi: 10.1016/j.tcb.2016.05.004.

[116] J. R. Buchan, A. P. Capaldi, and R. Parker, “TOR-tured Yeast Find a New Way to Stand the Heat,” *Mol Cell*, vol. 47, no. 2, pp. 155–157, 2012, doi: 10.1016/j.molcel.2012.07.005.

[117] N. Bley *et al.*, “Stress granules are dispensable for mRNA stabilization during cellular stress,” *Nucleic Acids Res*, vol. 43, no. 4, 2015, doi: 10.1093/nar/gku1275.

[118] N. Kedersha *et al.*, “Stress granules and processing bodies are dynamically linked sites of mRNP remodeling,” *J Cell Biol*, vol. 169, no. 6, pp. 871–884, 2005, doi: 10.1083/jcb.200502088.

[119] M. Brengues, D. Teixeira, and R. Parker, “Cell biology: Movement of eukaryotic mRNAs between polysomes and cytoplasmic processing bodies,”

Science, vol. 310, no. 5747, pp. 486–489, 2005, doi: 10.1126/science.1115791.

[120] J. R. Buchan, R. M. Kolaitis, J. P. Taylor, and R. Parker, "Eukaryotic stress granules are cleared by autophagy and Cdc48/VCP function," *Cell*, vol. 153, no. 7, p. 1461, 2013, doi: 10.1016/j.cell.2013.05.037.

[121] S. A. Barbee *et al.*, "Staufen- and FMRP-Containing Neuronal RNPs Are Structurally and Functionally Related to Somatic P Bodies," *Neuron*, vol. 52, no. 6, pp. 997–1009, 2006, doi: 10.1016/j.neuron.2006.10.028.

[122] M. Ramaswami, J. P. Taylor, and R. Parker, "XAltered ribostasis: RNA-protein granules in degenerative disorders," *Cell*, vol. 154, no. 4, pp. 727–736, 2013, doi: 10.1016/j.cell.2013.07.038.

[123] A. C. Fan and A. K. L. Leung, "RNA Granules and Diseases - A Case Study of Stress Granules in ALS and FTLD" *Adv Exp Med Biol*. vol. 176, no. 3. 2016. doi: 10.1007/978-3-319-29073-7.

[124] L. Liu-Yesucevitz *et al.*, "Tar DNA binding protein-43 (TDP-43) associates with stress granules: Analysis of cultured cells and pathological brain tissue," *PLoS One*, vol. 5, no. 10, 2010, doi: 10.1371/journal.pone.0013250.

[125] T. Vanderweyde *et al.*, "Contrasting pathology of the stress granule proteins TIA-1 and G3BP in Tauopathies," *J Neurosci*, vol. 32, no. 24, pp. 8270–8283, 2012, doi: 10.1523/JNEUROSCI.1592-12.2012.

[126] Y. R. Li, O. D. King, J. Shorter, and A. D. Gitler, "Stress granules as crucibles of ALS pathogenesis," *J Cell Biol*, vol. 201, no. 3, pp. 361–372, 2013, doi: 10.1083/jcb.201302044.

[127] B. Wolozin and P. Ivanov, "Stress granules and neurodegeneration," *Nat Rev Neurosci*, vol. 20, no. 11, pp. 649–666, 2019, doi: 10.1038/s41583-019-0222-5.

[128] J. R. Buchan, J. H. Yoon, and R. Parker, "Stress-specific composition, assembly and kinetics of stress granules in Saccharomyces cerevisiae," *J Cell Sci*, vol. 124, no. 2, pp. 228–239, 2011, doi: 10.1242/jcs.078444.

[129] P. P. Lamichhane and P. Samir, "Cellular Stress: Modulator of Regulated Cell Death," *Biology*, vol. 12, no. 9, p. 1172, 2023, doi: 10.3390/biology12091172.

[130] G. Filomeni, D. De Zio, and F. Cecconi, "Oxidative stress and autophagy: The clash between damage and metabolic needs," *Cell Death Differ*, vol. 22, no. 3, pp. 377–388, 2015, doi: 10.1038/cdd.2014.150.

[131] E. McEwen *et al.*, "Heme-regulated inhibitor kinase-mediated phosphorylation of eukaryotic translation initiation factor 2 inhibits translation, induces stress granule formation, and mediates survival upon arsenite exposure," *J Biol Chem*, vol. 280, no. 17, pp. 16925–16933, 2005, doi: 10.1074/jbc.M412882200.

[132] K. Richter, M. Haslbeck, and J. Buchner, "The Heat Shock Response: Life on the Verge of Death," *Mol Cell*, vol. 40, no. 2, pp. 253–266, 2010, doi: 10.1016/j.molcel.2010.10.006.

[133] L. Lu, A.-P. Han, and J.-J. Chen, “Translation Initiation Control by Heme-Regulated Eukaryotic Initiation Factor 2α Kinase in Erythroid Cells under Cytoplasmic Stresses,” *Mol Cell Biol*, vol. 21, no. 23, pp. 7971–7980, 2001, doi: 10.1128/mcb.21.23.7971-7980.2001.

[134] S. K. Berwal, V. Bhatia, A. Bendre, C. G. Suresh, S. Chatterjee, and J. K. Pal, “Activation of HRI is mediated by Hsp90 during stress through modulation of the HRI-Hsp90 complex,” *Int J Biol Macromol*, vol. 118, pp. 1604–1613, 2018, doi: 10.1016/j.ijbiomac.2018.06.204.

[135] O. Thastrup, P. J. Cullen, B. K. Drobak, M. R. Hanley, and A. P. Dawson, “Thapsigargin, a tumor promoter, discharges intracellular Ca2+ stores by specific inhibition of the endoplasmic reticulum Ca2+-ATPase,” *Proc Natl Acad Sci USA*, vol. 87, no. 7, pp. 2466–2470, 1990, doi: 10.1073/pnas.87.7.2466.

[136] J. Lytton, M. Westlin, and M. R. Hanley, “Thapsigargin inhibits the sarcoplasmic or endoplasmic reticulum Ca-ATPase family of calcium pumps,” *J Biol Chem*, vol. 266, no. 26, pp. 17067–17071, 1991, doi: 10.1016/s0021-9258(19)47340-7.

[137] M. Maurel, E. Chevet, J. Tavernier, and S. Gerlo, “Getting RIDD of RNA: IRE1 in cell fate regulation,” *Trends Biochem Sci*, vol. 39, no. 5, pp. 245–254, 2014, doi: 10.1016/j.tibs.2014.02.008.

[138] K. R. Bhattarai, T. A. Riaz, H. R. Kim, and H. J. Chae, “The aftermath of the interplay between the endoplasmic reticulum stress response and redox signaling,” *Exp Mol Med*, vol. 53, no. 2, pp. 151–167, 2021, doi: 10.1038/s12276-021-00560-8.

[139] G. C. Shore, F. R. Papa, and S. A. Oakes, “Signaling cell death from the endoplasmic reticulum stress response,” *Curr Opin Cell Biol*, vol. 23, no. 2, pp. 143–149, 2011, doi: 10.1016/j.ceb.2010.11.003.

[140] J. R. Child, Q. Chen, D. W. Reid, S. Jagannathan, and C. V. Nicchitta, “Recruitment of endoplasmic reticulum-targeted and cytosolic mRNAs into membrane-associated stress granules,” *RNA*, vol. 27, no. 10, pp. 1241–1256, 2021, doi: 10.1261/rna.078858.121.

[141] E. R. Abels and X. O. Breakefield, “Introduction to Extracellular Vesicles: Biogenesis, RNA Cargo Selection, Content, Release, and Uptake,” *Cell Mol Neurobiol*, vol. 36, no. 3, pp. 301–312, 2016, doi: 10.1007/s10571-016-0366-z.

[142] T. Skotland, K. Sagini, K. Sandvig, and A. Llorente, “An emerging focus on lipids in extracellular vesicles,” *Adv Drug Deliv Rev*, vol. 159, pp. 308–321, 2020, doi: 10.1016/j.addr.2020.03.002.

[143] S. A. Tooze, T. Flatmark, J. Tooze, and W. B. Huttner, “Characterization of the immature secretory granule, an intermediate in granule biogenesis,” *J Cell Biol,* vol. 115, no. 6, pp. 1491–1503, 1991, doi: 10.1083/jcb.115.6.1491.

[144] K. T. Lewis, K. R. Maddipati, A. R. Naik, and B. P. Jena, “Unique Lipid Chemistry of Synaptic Vesicle and Synaptosome Membrane Revealed Using Mass Spectrometry,” *ACS Chem Neurosci*, vol. 8, no. 6, pp. 1163–1169, 2017, doi: 10.1021/acschemneuro.7b00030.

[145] R. Jahn and R. H. Scheller, “SNAREs - Engines for membrane fusion,” *Nat Rev Mol Cell Biol*, vol. 7, no. 9, pp. 631–643, 2006, doi: 10.1038/nrm2002.

[146] M. Forgac, “Vacuolar ATPases: Rotary proton pumps in physiology and pathophysiology,” *Nat Rev Mol Cell Biol*, vol. 8, no. 11, pp. 917–929, 2007, doi: 10.1038/nrm2272.

[147] Y. Moriyama, M. Hiasa, S. Sakamoto, H. Omote, and M. Nomura, “Vesicular nucleotide transporter (VNUT): appearance of an actress on the stage of purinergic signaling,” *Purinergic Signal*, vol. 13, no. 3, pp. 387–404, 2017, doi: 10.1007/s11302-017-9568-1.

[148] K. Wimalasena, “Vesicular Monoamine Transporters: Structure-Function, Pharmacology, and Medicinal Chemistry,” *Med Res Rev*, vol. 31, no. 4, pp. 483–519, 2010. doi: 10.1002/med.20187.

[149] S. D. Meriney and E. E. Fanselow, “Amino acid neurotransmitters,” *Synaptic Transmission*, pp. 399–419, 2019, doi: 10.1016/B978-0-12-815320-8.00018-1.

[150] B. M. de Castro *et al.*, “The Vesicular Acetylcholine Transporter Is Required for Neuromuscular Development and Function,” *Mol Cell Biol*, vol. 29, no. 19, pp. 5238–5250, 2009, doi: 10.1128/mcb.00245-09.

[151] L. Qu, Y. Akbergenova, Y. Hu, and T. Schikorski, “Synapse-to-synapse variation in mean synaptic vesicle size and its relationship with synaptic morphology and function,” *J Comp Neurol*, vol. 514, no. 4, pp. 343–352, 2009, doi: 10.1002/cne.22007.

[152] Z. Lin *et al.*, “Tuning the Size of Large Dense-Core Vesicles and Quantal Neurotransmitter Release via Secretogranin II Liquid–Liquid Phase Separation,” *Adv Sci*, vol. 9, no. 27, pp. 1–16, 2022, doi: 10.1002/advs.202202263.

[153] R. D. Adams and A. B. Harkins, “PC12 cells that lack synaptotagmin 1 exhibit loss of a subpool of small dense core vesicles,” *Biophys J*, vol. 107, no. 12, pp. 2838–2849, 2014, doi: 10.1016/j.bpj.2014.10.060.

[154] N. Dominguez, J. R. T. van Weering, R. Borges, R. F. G. Toonen, and M. Verhage, “Dense-core vesicle biogenesis and exocytosis in neurons lacking chromogranins A and B,” *J Neurochem*, vol. 144, no. 3, pp. 241–254, 2018, doi: 10.1111/jnc.14263.

[155] R. Borges, J. D. Machado, C. Alonso, M. A. Brioso, and J. F. Gómez, “Functional role of chromogranins: The intragranular matrix in the last phase of exocytosis,” *Adv Exp Med Biol*, vol. 482, pp. 69–81, 2000. doi: 10.1007/0-306-46837-9_5.

[156] H. Fathali, J. Dunevall, S. Majdi, and A. S. Cans, “Extracellular Osmotic Stress Reduces the Vesicle Size while Keeping a Constant Neurotransmitter

Concentration," *ACS Chem Neurosci*, vol. 8, no. 2, pp. 368–375, 2017, doi: 10.1021/acschemneuro.6b00350.

[157] J. Estevez-Herrera, M. R. Pardo, N. Dominguez, D. Pereda, J. D. Machado, and R. Borges, "The role of chromogranins in the secretory pathway," *Biomol Concepts*, vol. 4, no. 6, pp. 605–609, 2013, doi: 10.1515/bmc-2013-0020.

[158] K. B. Helle, R. K. Reed, K. E. Pihl, and G. Serck-Hanssen, "Osmotic properties of the chromogranins and relation to osmotic pressure in catecholamine storage granules," *Acta Physiol Scand*, vol. 123, no. 1, pp. 21–33, 1985, doi: 10.1111/j.1748-1716.1985.tb07556.x.

[159] S. Rabasco, T. D. K. Nguyen, C. Gu, M. E. Kurczy, N. T. N. Phan, and A. G. Ewing, "Localization and absolute quantification of dopamine in discrete intravesicular compartments using nanoSIMS imaging," *Int J Mol Sci*, vol. 23, no. 1, 2022, doi: 10.3390/ijms23010160.

[160] G. Q. Bi, R. L. Morris, G. Liao, J. M. Alderton, J. M. Scholey, and R. A. Steinhardt, "Kinesin- and myosin-driven steps of vesicle recruitment for Ca2+- regulated exocytosis," *J Cell Biol*, vol. 138, no. 5, pp. 999–1008, 1997, doi: 10.1083/jcb.138.5.999.

[161] C. Hoffmann *et al.*, "Synapsin condensation controls synaptic vesicle sequestering and dynamics," *Nat Commun*, vol. 14, no. 1, pp. 1–13, 2023, doi: 10.1038/s41467-023-42372-6.

[162] S. Truckenbrodt *et al.*, "Newly produced synaptic vesicle proteins are preferentially used in synaptic transmission," *EMBO J*, vol. 37, no. 15, pp. 1–24, 2018, doi: 10.15252/embj.201798044.

[163] K. Hu, J. Carroll, S. Fedorovich, C. Rickman, A. Sukhodub, and B. Davletov, "Vesicular restriction of synaptobrevin suggests a role for calcium in membrane fusion," vol. 415, pp. 646–650, 2002. doi: 10.1038/415646a

[164] T. C. Südhof and J. E. Rothman, "Membrane fusion: Grappling with SNARE and SM proteins," *Science*, vol. 323, no. 5913, pp. 474–477, 2009, doi: 10.1126/science.1161748.

[165] P. Burkhardt, D. A. Hattendorf, W. I. Weis, and D. Fasshauer, "Munc18a controls SNARE assembly through its interaction with the syntaxin N-peptide," *EMBO Journal*, vol. 27, no. 7, pp. 923–933, 2008, doi: 10.1038/emboj.2008.37.

[166] Z. Zhang *et al.*, "Release mode of large and small dense-core vesicles specified by different synaptotagmin isoforms in PC12 cells," *Mol Biol Cell*, 2011, doi: 10.1091/mbc.E11-02-0159.

[167] T. C. Südhof, "Neurotransmitter release: The last millisecond in the life of a synaptic vesicle," *Neuron*, vol. 80, no. 3, pp. 675–690, 2013, doi: 10.1016/j.neuron.2013.10.022.

[168] R. Borges, C. Gu, J. D. Machado, and A. G. Ewing, "The dynamic nature of exocytosis from large secretory vesicles. A view from electrochemistry and

imaging," *Cell Calcium*, vol. 110, no. January, 2023, doi: 10.1016/j.ceca.2023.102699.

[169] N. T. N. Phan, X. Li, and A. G. Ewing, "Measuring synaptic vesicles using cellular electrochemistry and nanoscale molecular imaging," *Nat Rev Chem*, vol. 1, pp. 1–18, 2017, doi: 10.1038/s41570-017-0048.

[170] F. L. Graham, J. Smiley, W. C. Russell, and R. Nairn, "Characteristics of a human cell line transformed by DNA from human adenovirus type 5," *J Gen Virol*, vol. 36, no. 1, pp. 59–72, 1977, doi: 10.1099/0022-1317-36-1-59.

[171] W. F. Scherer, J. T. Syverton, and G. O. Gey, "Studies on the Propagation in vitro of Poliomyelitis Viruses," *J Exp Med*, 1953. vol. 97, no. 5, pp. 695-710

[172] N. D. Amoêdo, J. P. Valencia, M. F. Rodrigues, A. Galina, and F. D. Rumjanek, "How does the metabolism of tumour cells differ from that of normal cells," *Biosci Rep*, vol. 33, no. 6, pp. 865–873, 2013, doi: 10.1042/BSR20130066.

[173] P. Nemes, A. M. Knolhoff, S. S. Rubakhin, and J. V. Sweedler, "Single-cell metabolomics: Changes in the metabolome of freshly isolated and cultured neurons," *ACS Chem Neurosci*, vol. 3, no. 10, pp. 782–792, 2012, doi: 10.1021/cn300100u.

[174] L. A. Greene and A. S. Tischler, "Establishment of a Noradrenergic Clonal Line of Rat Adrenal Pheochromocytoma Cells which Respond to Nerve Growth Factor," *Proc Natl Acad Sci USA*, vol. 73, no. 7, pp. 2424–2428, 1976.

[175] D. J. Anderson and A. Michelsohn, "Role of glucocorticoids in the chromaffin-neuron developmental decision," *Int Dev Neurosci*, vol. 7, no. 5, 1989, doi: 10.1016/0736-5748(89)90007-5.

[176] S. E. Zerby and A. G. Ewing, "Electrochemical monitoring of individual exocytotic events from the varicosities of differentiated PC12 cells," *Brain Res*, vol. 712, no. 1, pp. 1–10, 1996, doi: 10.1016/0006-8993(95)01383-0.

[177] K. P. Das, T. M. Freudenrich, and W. R. Mundy, "Assessment of PC12 cell differentiation and neurite growth: A comparison of morphological and neurochemical measures," *Neurotoxicol Teratol*, vol. 26, no. 3, pp. 397–406, 2004, doi: 10.1016/j.ntt.2004.02.006.

[178] J. -H Tao-Cheng, A. Dosemeci, J. P. Bressler, M. W. Brightman, and D. L. Simpson, "Characterization of synaptic vesicles and related neuronal features in nerve growth factor and ras oncogene differentiated PC12 cells," *J Neurosci Res*, vol. 42, no. 3, pp. 323–334, 1995, doi: 10.1002/jnr.490420306.

[179] Z. Zhang *et al.*, "Release mode of large and small dense-core vesicles specified by different synaptotagmin isoforms in PC12 cells," *Mol Biol Cell*, 2011, doi: 10.1091/mbc.E11-02-0159.

[180] A. Elhamdani, M. E. Brown, C. R. Artalejo, and H. C. Palfrey, "Enhancement of the dense-core vesicle secretory cycle by glucocorticoid differentiation of PC12 cells: Characteristics of rapid exocytosis and

endocytosis," *J Neurosci*, vol. 20, no. 7, pp. 2495–2503, 2000, doi: 10.1523/jneurosci.20-07-02495.2000.

[181] T. K. Chen, G. O. Luo, and A. G. Ewing, "Amperometric Monitoring of Stimulated Catecholamine Release from Rat Pheochromocytoma (Pc12) Cells at the Zeptomole Level," *Anal Chem*, vol. 66, no. 19, pp. 3031–3035, 1994, doi: 10.1021/ac00091a007.

[182] L. A. Greene and G. Rein, "Release, storage and uptake of catecholamines by a clonal cell line of nerve growth factor (NGF) responsive pheochromocytoma cells," *Brain Res*, vol. 129, no. 2, pp. 247–263, 1977, doi: 10.1016/0006-8993(77)90005-1.

[183] S. E. Zerby and A. G. Ewing, "The latency of exocytosis varies with the mechanism of stimulated release in PC12 cells," *J Neurochem*, vol. 66, no. 2, pp. 651–657, 1996, doi: 10.1046/j.1471-4159.1996.66020651.x.

[184] D. Schubert, S. Heinemann, and Y. Kidokoro, "Cholinergic metabolism and synapse formation by a rat nerve cell line," *Proc Natl Acad Sci USA*, vol. 74, no. 6, pp. 2579–2583, 1977, doi: 10.1073/pnas.74.6.2579.

[185] R. Bauerfeind, A. Régnier-Vigouroux, T. Flatmark, and W. B. Huttner, "Selective storage of acetylcholine, but not catecholamines, in neuroendocrine synaptic-like microvesicles of early endosomal origin," *Neuron*, vol. 11, no. 1, pp. 105–121, 1993, doi: 10.1016/0896-6273(93)90275-V.

[186] R. H. S. Westerink, A. De Groot, and H. P. M. Vijverberg, "Heterogeneity of catecholamine-containing vesicles in PC12 cells," *Biochem Biophys Res Commun*, vol. 270, no. 2, pp. 625–630, 2000, doi: 10.1006/bbrc.2000.2470.

[187] R. D. Adams and A. B. Harkins, "PC12 cells that lack synaptotagmin i exhibit loss of a subpool of small dense core vesicles," *Biophys J*, vol. 107, no. 12, pp. 2838–2849, 2014, doi: 10.1016/j.bpj.2014.10.060.

[188] T. L. Colliver, S. J. Pyott, M. Achalabun, and A. G. Ewing, "VMAT-mediated changes in quantal size and vesicular volume," *J Neurosci*, vol. 20, no. 14, pp. 5276–5282, 2000, doi: 10.1523/jneurosci.20-14-05276.2000.

[189] E. N. Pothos, S. Przedborski, V. Davila, Y. Schmitz, and D. Sulzer, "D2-like dopamine autoreceptor activation reduces quantal size in PC 12 cells," *J Neurosci*, vol. 18, no. 15, pp. 5575–5585, 1998, doi: 10.1523/jneurosci.18-15-05575.1998.

[190] R. H. S. Westerink and A. G. Ewing, "The PC12 cell as model for neurosecretion," *Acta Physiol.*, vol. 192, p. 273, 2008.

[191] C. Gu, A. Larsson, and A. G. Ewing, "Plasticity in exocytosis revealed through the effects of repetitive stimuli affect the content of nanometer vesicles and the fraction of transmitter released," *Pro Nat Acad Sci*, vol. 116, no. 43, pp. 21409–21415, Oct. 2019, doi: 10.1073/PNAS.1910859116.

[192] X. Li, J. Dunevall, and A. G. Ewing, "Using Single-Cell Amperometry To Reveal How Cisplatin Treatment Modulates the Release of Catecholamine

Transmitters during Exocytosis," *Angew Chem - Inter Ed*, vol. 55, no. 31, 2016, doi: 10.1002/anie.201602977.

[193] Z. Wang, X. He, K. Long Le Vo, and A. G. Ewing, "Electrochemical and Mass Spectrometric Measurement of Enhanced Intravesicular Catecholamine Content and Exocytotic Frequency at Subanaesthetic Ketamine Doses," *Analysis & Sensing*, vol. 1, no. 4, pp. 166–170, 2021, doi: 10.1002/anse.202100026.

[194] X. Li, A. S. Mohammadi, and A. G. Ewing, "Single cell amperometry reveals curcuminoids modulate the release of neurotransmitters during exocytosis from PC12 cells," *J Electroanal Chem*, vol. 781, pp. 30–35, 2016, doi: 10.1016/j.jelechem.2016.10.025.

[195] L. A. Sombers, M. M. Maxson, and A. G. Ewing, "Loaded dopamine is preferentially stored in the halo portion of PC12 cell dense core vesicles," *J Neurochem*, vol. 93, no. 5, pp. 1122–1131, 2005, doi: 10.1111/j.1471-4159.2005.03087.x.

[196] L. A. Sombers *et al.*, "The Effects of Vesicular Volume on Secretion through the Fusion Pore in Exocytotic Release from PC12 Cells," *J Neurosc*, vol. 24, no. 2, pp. 303–309, 2004, doi: 10.1523/JNEUROSCI.1119-03.2004.

[197] L. Ren, M. Dowlatshahi Pour, P. Malmberg, and A. G. Ewing, "Altered Lipid Composition of Secretory Cells Following Exposure to Zinc Can Be Correlated to Changes in Exocytosis," *Chemistry*, vol. 25, no. 21, pp. 5406–5411, 2019, doi: 10.1002/chem.201900010.

[198] J. Lovrić *et al.*, "Nano Secondary Ion Mass Spectrometry Imaging of Dopamine Distribution Across Nanometer Vesicles," *ACS Nano*, vol. 11, no. 4, pp. 3446–3455, 2017, doi: 10.1021/acsnano.6b07233.

[199] A. Thomen *et al.*, "Subcellular Mass Spectrometry Imaging and Absolute Quantitative Analysis across Organelles," *ACS Nano*, vol. 14, no. 4, pp. 4316–4325, 2020, doi: 10.1021/acsnano.9b09804.

[200] K. Takahashi *et al.*, "Induction of pluripotent stem cells from adult human fibroblasts by defined factors.," *Cell*, vol. 131, no. 5, pp. 861–72, Nov. 2007, doi: 10.1016/j.cell.2007.11.019.

[201] K. Takahashi and S. Yamanaka, "Induction of Pluripotent Stem Cells from Mouse Embryonic and Adult Fibroblast Cultures by Defined Factors," *Cell*, vol. 126, no. 4, pp. 663–676, 2006, doi: 10.1016/j.cell.2006.07.024.

[202] M. Nakagawa *et al.*, "Generation of induced pluripotent stem cells without Myc from mouse and human fibroblasts," *Nat Biotechnol*, vol. 26, no. 1, pp. 101–106, 2008, doi: 10.1038/nbt1374.

[203] M. C. Marchetto, K. J. Brennand, L. F. Boyer, and F. H. Gage, "Induced pluripotent stem cells (iPSCs) and neurological disease modeling: Progress and promises," *Hum Mol Genet*, vol. 20, no. R2, pp. 109–115, 2011, doi: 10.1093/hmg/ddr336.

[204] J. Yu *et al.*, “Induced pluripotent stem cell lines derived from human somatic cells,” *Science*, vol. 318, pp. 1917–1920, 2007, doi: https://doi.org/10.1126/science.1151526.

[205] F. Soldner *et al.*, “Parkinson’s Disease Patient-Derived Induced Pluripotent Stem Cells Free of Viral Reprogramming Factors,” *Cell*, vol. 136, no. 5, pp. 964–977, 2009, doi: 10.1016/j.cell.2009.02.013.

[206] K. Kaji, K. Norrby, A. Paca, M. Mileikovsky, P. Mohseni, and K. Woltjen, “Virus-free induction of pluripotency and subsequent excision of reprogramming factors,” *Nature*, vol. 458, no. 7239, pp. 771–775, 2009, doi: 10.1038/nature07864.

[207] A. Revilla *et al.*, “Current advances in the generation of human iPS cells: implications in cell-based regenerative medicine,” *J Tissue Eng Regen Med*, vol. 10, pp. 893–907, 2016, doi: 10.1002/term.

[208] M. Stadtfeld, M. Nagaya, J. Utikal, G. Weir, and K. Hochedlinger, “Induced Pluripotent Stem Cells Generated Without Viral Integration,” *Science*, vol. 322, pp. 945–949, 2008, doi: https://doi.org/10.1126/science.1162494.

[209] N. Fusaki, H. Ban, A. Nishiyama, K. Saeki, and M. Hasegawa, “Efficient induction of transgene-free human pluripotent stem cells using a vector based on Sendai virus, an RNA virus that does not integrate into the host genome,” *Proc Jpn Acad Ser B Phys Biol Sci*, vol. 85, no. 8, pp. 348–362, 2009, doi: 10.2183/pjab.85.348.

[210] K. Okita, M. Nakagawa, H. Hyenjong, T. Ichisaka, and S. Yamanaka, “Generation of Mouse Induced Pluripotent Stem Cells Without Viral Vectors,” *Science*, vol. 322, pp. 949–954, 2008, doi: https://doi.org/10.1126/science.1164270.

[211] J. Yu *et al.*, “Human Induced Pluripotent Stem Cells Free of Vector and Transgene Sequences,” *Science*, vol. 324, pp. 797–802, 2009, doi: https://doi.org/10.1126/science.1172482.

[212] F. Jia *et al.*, “A nonviral minicircle vector for deriving human iPS cells,” *Nat Methods*, vol. 7, no. 3, pp. 197–199, 2010, doi: 10.1038/nmeth.1426.

[213] L. Warren *et al.*, “Highly efficient reprogramming to pluripotency and directed differentiation of human cells with synthetic modified mRNA,” *Cell Stem Cell*, vol. 7, no. 5, pp. 618–630, 2010, doi: 10.1016/j.stem.2010.08.012.

[214] S. L. Lin, D. C. Chang, C. H. Lin, S. Y. Ying, D. Leu, and D. T. S. Wu, “Regulation of somatic cell reprogramming through inducible mir-302 expression,” *Nucleic Acids Res*, vol. 39, no. 3, pp. 1054–1065, 2011, doi: 10.1093/nar/gkq850.

[215] N. Miyoshi *et al.*, “Reprogramming of mouse and human cells to pluripotency using mature microRNAs,” *Cell Stem Cell*, vol. 8, no. 6, pp. 633–638, 2011, doi: 10.1016/j.stem.2011.05.001.

[216] D. Kim *et al.*, "Generation of Human Induced Pluripotent Stem Cells by Direct Delivery of Reprogramming Proteins," *Cell Stem Cell*, vol. 4, no. 6, pp. 472–476, 2009, doi: 10.1016/j.stem.2009.05.005.

[217] H. Zhou *et al.*, "Generation of Induced Pluripotent Stem Cells Using Recombinant Proteins," *Cell Stem Cell*, vol. 4, no. 5, pp. 381–384, 2009, doi: 10.1016/j.stem.2009.04.005.

[218] D. Huangfu *et al.*, "Induction of pluripotent stem cells by defined factors is greatly improved by small-molecule compounds," *Nat Biotechnol*, vol. 26, no. 7, pp. 795–797, 2008, doi: 10.1038/nbt1418.

[219] S. Zhu *et al.*, "Reprogramming of human primary somatic cells by OCT4 and chemical compounds," *Cell Stem Cell*, vol. 7, no. 6, pp. 651–655, 2010, doi: 10.1016/j.stem.2010.11.015.

[220] J. Silva, O. Barrandon, J. Nichols, J. Kawaguchi, T. W. Theunissen, and A. Smith, "Promotion of reprogramming to ground state pluripotency by signal inhibition," *PLoS Biol*, vol. 6, no. 10, pp. 2237–2247, 2008, doi: 10.1371/journal.pbio.0060253.

[221] W. Li *et al.*, "Generation of human-induced pluripotent stem cells in the absence of exogenous Sox2," *Stem Cells*, vol. 27, no. 12, pp. 2992–3000, 2009, doi: 10.1002/stem.240.

[222] Y. Shi, J. T. Do, C. Desponts, H. S. Hahm, H. R. Schöler, and S. Ding, "A Combined Chemical and Genetic Approach for the Generation of Induced Pluripotent Stem Cells," *Cell Stem Cell*, vol. 2, no. 6, pp. 525–528, 2008, doi: 10.1016/j.stem.2008.05.011.

[223] C. A. Lyssiotis *et al.*, "Reprogramming of murine fibroblasts to induced pluripotent stem cells with chemical complementation of Klf4," *Proc Natl Acad Sci USA*, vol. 106, no. 22, pp. 8912–8917, 2009, doi: 10.1073/pnas.0903860106.

[224] J. K. Ichida *et al.*, "A Small-Molecule Inhibitor of Tgf-β Signaling Replaces Sox2 in Reprogramming by Inducing Nanog," *Cell Stem Cell*, vol. 5, no. 5, pp. 491–503, 2009, doi: 10.1016/j.stem.2009.09.012.

[225] W. Li *et al.*, "Generation of Rat and Human Induced Pluripotent Stem Cells by Combining Genetic Reprogramming and Chemical Inhibitors," *Cell Stem Cell*, vol. 4, no. 1, pp. 16–19, 2009, doi: 10.1016/j.stem.2008.11.014.

[226] Y. Shi, C. Desponts, J. T. Do, H. S. Hahm, H. R. Schöler, and S. Ding, "Induction of Pluripotent Stem Cells from Mouse Embryonic Fibroblasts by Oct4 and Klf4 with Small-Molecule Compounds," *Cell Stem Cell*, vol. 3, no. 5, pp. 568–574, 2008, doi: 10.1016/j.stem.2008.10.004.

[227] T. S. Mikkelsen *et al.*, "Dissecting direct reprogramming through integrative genomic analysis," *Nature*, vol. 454, no. 7200, pp. 49–55, 2008, doi: 10.1038/nature07056.

[228] T. Lin *et al.*, "A chemical platform for improved induction of human iPSCs," *Nat Methods*, vol. 6, no. 11, pp. 805–808, 2009, doi: 10.1038/nmeth.1393.

[229] R. M. Marton and J. P. A. Ioannidis, “A Comprehensive Analysis of Protocols for Deriving Dopaminergic Neurons from Human Pluripotent Stem Cells,” *Stem Cells Transl Med*, vol. 8, no. 4, pp. 366–374, 2019, doi: 10.1002/sctm.18-0088.

[230] S. M. Chambers, C. A. Fasano, E. P. Papapetrou, M. Tomishima, M. Sadelain, and L. Studer, “Highly efficient neural conversion of human ES and iPS cells by dual inhibition of SMAD signaling,” *Nat Biotechnol*, vol. 27, no. 3, pp. 275–280, 2009, doi: 10.1038/nbt.1529.

[231] N. J. Laping *et al.*, “Inhibition of transforming growth factor (TGF)-β1-induced extracellular matrix with a novel inhibitor of the TGF-β type I receptor kinase activity: SB-431542,” *Mol Pharmacol*, vol. 62, no. 1, pp. 58–64, 2002, doi: 10.1124/mol.62.1.58.

[232] W. C. Smith and R. M. Harland, “Expression cloning of noggin, a new dorsalizing factor localized to the Spemann organizer in Xenopus embryos,” *Cell*, vol. 70, no. 5, pp. 829–840, 1992, doi: 10.1016/0092-8674(92)90316-5.

[233] S. Ye *et al.*, “Pleiotropy of glycogen synthase kinase-3 inhibition by CHIR99021 promotes self-renewal of embryonic stem cells from refractory mouse strains,” *PLoS One*, vol. 7, no. 4, 2012, doi: 10.1371/journal.pone.0035892.

[234] C. Chiang *et al.*, “Cyclopia and defective axial patterning in mice lacking Sonic hedgehog gene function,” *Nature*, vol. 383, pp. 407–413, 1996. doi: 10.1038/383407a0.

[235] M. Jefri *et al.*, “Stimulation of L-type calcium channels increases tyrosine hydroxylase and dopamine in ventral midbrain cells induced from somatic cells,” *Stem Cells Transl Med*, vol. 9, no. 6, pp. 697–712, 2020, doi: 10.1002/sctm.18-0180.

[236] L. F. H. Lin, D. H. Doherty, J. D. Lile, S. Bektesh, and F. Collins, “GDNF: A glial cell line - Derived neurotrophic factor for midbrain dopaminergic neurons,” *Science*, vol. 260, no. 5111, pp. 1130–1132, 1993, doi: 10.1126/science.8493557.

[237] Y. A. Barde, D. Edgar, and H. Thoenen, “Purification of a new neurotrophic factor from mammalian brain.,” *EMBO J*, vol. 1, no. 5, pp. 549–553, 1982, doi: 10.1002/j.1460-2075.1982.tb01207.x.

[238] Patapoutian A and Reichardt LF, “Trk receptors: mediators of neurotrophin action Patapoutian and Reichardt 273 Trk-mediated signaling,” *Curr Opin Neurobiol*, vol. 11, no. 3, pp. 272–280, 2001. doi: 10.1016/s0959-4388(00)00208-7.

[239] B. Bilican *et al.*, “Mutant induced pluripotent stem cell lines recapitulate aspects of TDP-43 proteinopathies and reveal cell-specific vulnerability,” *Proc Natl Acad Sci USA*, vol. 109, no. 15, pp. 5803–5808, 2012, doi: 10.1073/pnas.1202922109.

[240] H. W. Horch and L. C. Katz, “BDNF release from single cells elicits local dendritic growth in nearby neurons,” *Nat Neurosci*, vol. 5, no. 11, pp. 1177–1184, 2002, doi: 10.1038/nn927.

[241] M. J. Sanderson, I. Smith, I. Parker, and M. D. Bootman, “Fluorescence microscopy,” *Cold Spring Harb Protoc*, vol. 2014, no. 10, 2014, doi: 10.1101/pdb.top071795.

[242] E. Abbe, “Beiträge zur Theorie des Mikroskops und der mikroskopischen Wahrnehmung,” *Archiv f mikrosk Anatomie*, vol. 9, 1873, pp. 413–468 doi: 10.1007/BF02956173

[243] E. Betzig *et al.*, “Imaging intracellular fluorescent proteins at nanometer resolution,” *Science*, vol. 313, no. 5793, pp. 1642–1645, 2006, doi: 10.1126/science.1127344.

[244] M. J. Rust, M. Bates, and X. Zhuang, “Sub-diffraction-limit imaging by stochastic optical reconstruction microscopy (STORM),” *Nat Methods*, vol. 3, no. 10, pp. 793–795, 2006, doi: 10.1038/nmeth929.

[245] M. Bates, B. Huang, GT. Dempsey, and X. Zhuang, “Multicolor Super-resolution Imaging with Photo-switchable Fluorescent Probes,” *Science*, vol. 317, no. 5845, pp. 1749–1753, 2007, doi: doi:10.1126/science.1146598.

[246] S. J. Sahl, S. W. Hell, and S. Jakobs, “Fluorescence nanoscopy in cell biology,” *Nat Rev Mol Cell Biol*, vol. 18, no. 11, pp. 685–701, 2017 doi: 10.1038/nrm.2017.71.

[247] C. Bond, A. N. Santiago-Ruiz, Q. Tang, and M. Lakadamyali, “Technological advances in super-resolution microscopy to study cellular processes,” *Mol Cell*, vol. 82, no. 2, pp. 315–332, 2022, doi: 10.1016/j.molcel.2021.12.022.

[248] S. W. Hell and J. Wichmann, “Breaking the diffraction resolution limit by stimulated emission : stimulated-emission-depletion fluorescence microscopy,” *Opt Lett*, vol. 19, no. 11, pp. 780–782, 1994.

[249] T. A. Klar and S. W. Hell, “Subdiffraction resolution in far-field fluorescence microscopy,” 1999. *Opt Lett*, vol. 24, no. 14, pp. 954–956

[250] F. Göttfert *et al.*, “Coaligned dual-channel STED nanoscopy and molecular diffusion analysis at 20 nm resolution,” *Biophys J*, vol. 105, no. 1, pp. 6–8, 2013, doi: 10.1016/j.bpj.2013.05.029.

[251] T. A. Klar, S. Jakobs, M. Dyba, A. Egner, and S. W. Hell, “Fluorescence microscopy with diffraction resolution barrier broken by stimulated emission,” *Proc Nat Acad Sci*, vol. 97, no. 15, pp. 8206–8210, 2000, doi: 10.1073/PNAS.97.15.8206.

[252] F. Bottanelli *et al.*, “Two-colour live-cell nanoscale imaging of intracellular targets,” *Nat Commun*, vol. 7, no. 10778, 2015, pp. 1–5, 2016, doi: 10.1038/ncomms10778.

[253] X. Duan, M. Zhang, and Y. H. Zhang, “Organic fluorescent probes for live-cell super-resolution imaging,” *Front Optoelectron*, vol. 16, no. 34, pp. 1–12, 2023, doi: 10.1007/s12200-023-00090-3.

[254] H. Schneckenburger *et al.*, “Light exposure and cell viability in fluorescence microscopy,” *J Microsc*, vol. 245, no. 3, pp. 311–318, 2012, doi: 10.1111/j.1365-2818.2011.03576.x.

[255] S. Waldchen, J. Lehmann, T. Klein, S. Van De Linde, and M. Sauer, “Light-induced cell damage in live-cell super-resolution microscopy,” *Sci Rep*, vol. 5, no. 15348, 2015, doi: 10.1038/srep15348.

[256] Y. Han, M. Li, F. Qiu, M. Zhang, and Y. H. Zhang, “Cell-permeable organic fluorescent probes for live-cell long-term super-resolution imaging reveal lysosome-mitochondrion interactions,” *Nat Commun*, vol. 8, no. 1307, 2017, doi: 10.1038/s41467-017-01503-6.

[257] D. Si, Q. Li, Y. Bao, J. Zhang, and L. Wang, “Fluorogenic and Cell-Permeable Rhodamine Dyes for High-Contrast Live-Cell Protein Labeling in Bioimaging and Biosensing,” *Angew Chem - Int Ed*, vol. 62, no. 45, 2023, doi: 10.1002/anie.202307641.

[258] A. Ettinger and T. Wittmann, “Fluorescence Live Cell Imaging,” in *Methods in Cell Biol*, pp. 77–94. 2014, doi: 10.1016/B978-0-12-420138-5.00005-7.

[259] M. Moradi *et al.*, “Differential roles of α-, β-, and γ-actin in axon growth and collateral branch formation in motoneurons,” *J Cell Biol*, vol. 216, no. 3, pp. 793–814, 2017, doi: 10.1083/jcb.201604117.

[260] U. Vielkind and S. H. Swierenga, “A simple fixation procedure for immunofluorescent detection of different cytoskeletal components within the same cell,” *Histochemistry*, vol. 91, no. 1, pp. 81–88, 1989, doi: 10.1007/BF00501916.

[261] K. N. Richter *et al.*, “Glyoxal as an alternative fixative to formaldehyde in immunostaining and super-resolution microscopy,” *EMBO J*, vol. 37, no. 1, pp. 139–159, 2018, doi: 10.15252/embj.201695709.

[262] G. Farr and K. Nakane, “Immunohistochemistry with Enzyme Labeled Antibodies: A Brief Review,” *J Immunol Methods*, vol. 47, no. 2, pp. 129–144, 1981. doi: 10.1016/0022-1759(81)90114-9.

[263] M. Hayat, “Factors Affecting Antigen Retrieval,” in *Microscopy, Immunohistochemistry, and Antigen Retrieval Methods*, Springer, Boston, 2002, doi: https://doi.org/10.1007/0-306-47599-5_4.

[264] Y. H. Tan, M. Liu, B. Nolting, J. G. Go, J. Gervay-hague, and G. Liu, “A Nanoengineering Approach for Investigation and Regulation of Protein Immobilization,” *ACS Nano*, vol. 2, no. 11, pp. 2374–2384, 2008. doi: 10.1021/nn800508f.

[265] A. Pedreáñez, J. Mosquera-Sulbarán, N. Muñóz, D. Tene, and J. Robalino, “Nanoantibodies: Small molecules, big possibilities,” *Biotechnologia*, vol. 102, no. 3, pp. 321–336, 2021, doi: 10.5114/bta.2021.108724.

[266] E. Ruska, “The Development of the Electron Microscope and of Electron Microscopy (Nobel Lecture),” *Angew Chem Int Ed Eng*, vol. 26, no. 7, pp. 595–605, 1987, doi: 10.1002/anie.198705953.

[267] M. Knoll and E. Ruska, “Das Elektronenmikroskop,” *Z Physik*, vol. 78, pp. 318–339, 1932, doi: 10.1007/BF01342199

[268] C. Kisielowski et al. “Detection of Single Atoms and Buried Defects in Three Dimensions by Aberration-Corrected Electron Microscope with 0.5-Å Information Limit” *Microsc Microanal*, vol. 14, pp. 469-477, 2008, doi:10.1017/S1431927608080902

[269] D. Rathkey, “Evolution and Comparison of Electron Sources,” *Micros Today*, vol. 1, no. 4, pp. 16–17, 1993, doi: 10.1017/s1551929500067432.

[270] R. F. Egerton, *Physical Principles of Electron Microscopy*. Springer, 2016.

[271] A. Konkol, G. R. Booker, and P. R. Wilshaw, “Backscattered electron contrast on cross sections of interfaces and multilayers in the scanning electron microscope,” *Ultramicroscopy*, vol. 58, pp. 233–237, 1995. doi: 10.1016/0304-3991(95)00039-4

[272] P. A. Penczek, “Resolution Measures in Molecular Electron Microscopy,” *Methods Enzymol*, vol. 482, no. 10, pp. 73–100, 2010, doi: 10.1016/S0076-6879(10)82003-8.

[273] M. C. Jamur and C. Oliver, “Cell fixatives for immunostaining.,” *Methods Mol Biol*, vol. 588, pp. 55–61, 2010, doi: 10.1007/978-1-59745-324-0_8.

[274] K. Okuda, I. Urabe, Y. Yamada, and H. Okada, “Reaction of glutaraldehyde with amino and thiol compounds,” *J Ferment Bioeng*, vol. 71, no. 2, pp. 100–105, 1991, doi: 10.1016/0922-338X(91)90231-5.

[275] H. Singh, K. A. Bishen, D. Garg, H. Sukhija, D. Sharma, and U. Tomar, “Fixation and Fixatives: Roles and Functions—A Short Review,” *Dent J of Adv Stud*, vol. 07, no. 02, pp. 051–055, 2019, doi: 10.1055/s-0039-1693098.

[276] I. Migneault, C. Dartiguenave, M. J. Bertrand, and K. C. Waldron, “Glutaraldehyde: Behavior in aqueous solution, reaction with proteins, and application to enzyme crosslinking,” *Biotechniques*, vol. 37, no. 5, pp. 790–802, 2004, doi: 10.2144/04375rv01.

[277] T. J. A. Johnson, “Glutaraldehyde Fixation Chemistry A Scheme for Rapid Crosslinking and Evidence for Rapid Oxygen Consumption,” vol. 4, no. 1, 1985. Scan Electron Microsc Available at: https://digitalcommons.usu.edu/electron/vol4/iss1/5

[278] M. J. Karnovsky, “A Formaldehyde-Glutaraldehyde Fixative of High Osmolality for Use in Electron Microscopy,” *J Cell Biol*, vol. 27, no. 2, pp. 1A-149A, 1965.

[279] Y. Li *et al.*, “The effects of chemical fixation on the cellular nanostructure,” *Exp Cell Res*, vol. 358, no. 2, pp. 253–259, 2017, doi: 10.1016/j.yexcr.2017.06.022.

[280] S. Liu, I. D. Pokrovskaya, and B. Storrie, “High-Pressure Freezing Followed by Freeze Substitution: An Optimal Electron Microscope Technique to Study Golgi Apparatus Organization and Membrane Trafficking,” *Methods Mol Biol*, pp. 211–223, 2023, doi: 10.1007/978-1-0716-2639-9_13.

[281] K. L. McDonald and M. Auer, “High-pressure freezing, cellular tomography, and structural cell biology,” *Biotechniques*, vol. 41, no. 2, pp. 137–143, 2006, doi: 10.2144/000112226.

[282] A. Frankl, M. Mari, and F. Reggiori, “Electron microscopy for ultrastructural analysis and protein localization in saccharomyces cerevisiae,” *Microbial Cell*, vol. 2, no. 11, pp. 412–428, 2015, doi: 10.15698/mic2015.11.237.

[283] M. Komorowska, M. Koter, G. Bartosz, and J. Gomulkiewicz, “The Effects of Glutaraldehyde and Osmium Tetroxide on the Erythrocyte Membrane,” *Biochim Acta*, vol. 686, pp. 94–98, 1982.

[284] M. Winey, J. B. Meehl, E. T. O’Toole, and T. H. Giddings, “Conventional transmission electron microscopy,” *Mol Biol Cell*, vol. 25, no. 3, pp. 319–323, 2014, doi: 10.1091/mbc.E12-12-0863.

[285] F. Lange, P. Agüi-Gonzalez, D. Riedel, N. T. N. Phan, S. Jakobs, and S. O. Rizzoli, “Correlative fluorescence microscopy, transmission electron microscopy and secondary ion mass spectrometry (CLEM-SIMS) for cellular imaging,” *PLoS One*, vol. 16, no. 5 May 2021, pp. 1–17, 2021, doi: 10.1371/journal.pone.0240768.

[286] J. J. Thomson, “Rays of Positive Electricity,” *Phil. Mag.*, vol. 21, no. 122, pp. 225–249, 1911.

[287] R. M. Caprioli, T. B. Farmer, and J. Gile, “Molecular Imaging of Biological Samples: Localization of Peptides and Proteins Using MALDI-TOF MS,” *Anal Chem*, vol. 69, no. 23, pp. 4751–4760, 1997, doi: 10.1021/ac970888i.

[288] K. Skupakova, B. Balluff, C. Tressler, T. Adelaja, R.M.A. Heeren, K. Glunde, G. Ertaylan, ”Cellular resolution in clinical MALDI mass spectrometry imaging: the latest advancements and current challenges” *Clin Chel Lab Med* vol. 58, no. 6, pp. 914-929, 2020, doi:10.1515/cclm-2019-0858.

[289] X. Ma and F. M. Fernández, “Advances in mass spectrometry imaging for spatial cancer metabolomics,” *Mass Spectrom Rev*, no. May, pp. 1–34, 2022, doi: 10.1002/mas.21804.

[290] M. Niehaus, J. Soltwisch, M. E. Belov, and K. Dreisewerd, “Transmission-mode MALDI-2 mass spectrometry imaging of cells and tissues at subcellular resolution,” *Nat Methods*, vol. 16, no. 9, pp. 925–931, 2019, doi: 10.1038/s41592-019-0536-2.

[291] J. M. Wiseman, D. R. Ifa, Q. Song, and R. G. Cooks, “Tissue imaging at atmospheric pressure using Desorption Electrospray Ionization (DESI) mass spectrometry,” *Angew Chem - Int Ed*, vol. 45, no. 43, pp. 7188–7192, 2006, doi: 10.1002/anie.200602449.

[292] M. Yang, D. Unsihuay, H. Hu, F. N. Meke, Z. Qu, Z. Zhang, J. Laskin, ”Nano-DESI Mass Spectrometry Imaging of Proteoforms in Biological Tissues with High Spatial Resolution” *Anal Chem*, vol. 95, pp. 5214-5222, 2023, doi.org/10.1021/acs.analchem.2c04795

[293] R. F. K. Herzog and F. P. Viehböck, “Ion Source for Mass Spectrometry,” *Phys Rev*, vol. 76, pp. 855–856, 1949, doi: 10.1103/PhysRev.76.855.

[294] N. Ogrinc Potočnik, G. L. Fisher, A. Prop, and R. M. A. Heeren, “Sequencing and Identification of Endogenous Neuropeptides with Matrix-Enhanced Secondary Ion Mass Spectrometry Tandem Mass Spectrometry,” *Anal Chem*, vol. 89, no. 16, pp. 8223–8227, 2017, doi: 10.1021/acs.analchem.7b02573.

[295] V. Kertesz and G. J. Van Berkel, “Fully automated liquid extraction-based surface sampling and ionization using a chip-based robotic nanoelectrospray platform,” *J Mass Spectrom*, vol. 45, no. 3, pp. 252–260, 2010, doi: 10.1002/jms.1709.

[296] P. Nemes and A. Vertes, “Laser ablation electrospray ionization for atmospheric pressure molecular imaging mass spectrometry,” *Methods Mol Biol*, vol. 656, no. 21, pp. 159–171, 2010, doi: 10.1007/978-1-60761-746-4_9.

[297] A. L. Gray, “Solid Sample Introduction by Laser Ablation for Inductively Coupled Plasma Source Mass Spectrometry,” *Analyst*, vol. 110, pp. 551–556, 1985.

[298] P. van der Heide, “Secondary ion mass spectrometry: An introduction to principles and practices”. 2014. doi: 10.1016/0042-207x(84)90085-x.

[299] D. A. Brenes, B. J. Garrison, N. Winograd, Z. Postawa, A. Wucher, and P. Blenkinsopp, “Fluid flow and effusive desorption: Dominant mechanisms of energy dissipation after energetic cluster bombardment of molecular solids,” *J Phys Chem Lett*, vol. 2, no. 16, pp. 2009–2014, 2011, doi: 10.1021/jz200708j.

[300] N. Winograd, “Gas Cluster Ion Beams for Secondary Ion Mass Spectrometry,” *Annu Rev Anal Chem*, vol. 11, pp. 29–48, 2018, doi: 10.1146/annurev-anchem-061516-045249.

[301] A. V. Steele, A. Schwarzkopf, J. J. McClelland, and B. Knuffman, “High-brightness cs focused ion beam from a cold-atomic-beam ion source,” *Nano Futures*, vol. 1, no. 1, pp. 0–9, 2017, doi: 10.1088/2399-1984/aa6a48.

[302] N. Davies, D. E. Weibel, P. Blenkinsopp, N. Lockyer, R. Hill, and J. C. Vickerman, “Development and experimental application of a gold liquid metal ion source,” *Appl Surf Sci*, vol. 203–204, pp. 223–227, 2003, doi: 10.1016/S0169-4332(02)00631-1.

[303] S. Rabbani, A. M. Barber, J. S. Fletcher, N. P. Lockyer, and J. C. Vickerman, “TOF-SIMS with argon gas cluster ion beams: A comparison with C 60+,” *Anal Chem*, vol. 83, no. 10, pp. 3793–3800, 2011, doi: 10.1021/ac200288v.

[304] T. B. Angerer, P. Blenkinsopp, and J. S. Fletcher, “High energy gas cluster ions for organic and biological analysis by time-of-flight secondary ion mass spectrometry,” *Int J Mass Spectrom*, vol. 377, no. 1, pp. 591–598, 2015, doi: 10.1016/j.ijms.2014.05.015.

[305] H. Tian, D. Maciazek, Z. Postawa, B. J. Garrison, and N. Winograd, "C-O bond dissociation and induced chemical ionization using high energy (CO2)n+ gas cluster ion beam," *J Am Soc Mass Spectrom*, vol. 30, no. 3, pp. 476–481, 2019, doi: 10.1007/s13361-018-2102-z.

[306] Ionoptika, "GCIB70," Ionoptika webpage. [Online]. Available: https://ionoptika.com/products/ion-beams/gas-cluster-ion-beams/gcib-sm/

[307] K. Dimovska Nilsson, A. Karagianni, I. Kaya, M. Henricsson, and J. S. Fletcher, "(CO2)n+, (H2O)n+, and (H2O)n+ (CO2) gas cluster ion beam secondary ion mass spectrometry: analysis of lipid extracts, cells, and Alzheimer's model mouse brain tissue," *Anal Bioanal Chem*, vol. 413, no. 16, pp. 4181–4194, 2021, doi: 10.1007/s00216-021-03372-x.

[308] A. Wucher, J. Cheng, L. Zheng, and N. Winograd, "Three-dimensional depth profiling of molecular structures," *Anal Bioanal Chem*, vol. 393, no. 8, pp. 1835–1842, 2009, doi: 10.1007/s00216-008-2596-5.

[309] J. Bailey *et al.*, "3D ToF-SIMS imaging of polymer multilayer films using argon cluster sputter depth profiling," *ACS Appl Mater Interfaces*, vol. 7, no. 4, pp. 2654–2659, 2015, doi: 10.1021/am507663v.

[310] H. Tian *et al.*, "Secondary-Ion Mass Spectrometry Images Cardiolipins and Phosphatidylethanolamines at the Subcellular Level," *Angew Chem Int Ed*, vol. 58, no. 10, pp. 3156–3161, 2019, doi: 10.1002/anie.201814256.

[311] M. F. Russo, I. A. Wojciechowski, and B. J. Garrison, "Sputtering of amorphous ice induced by C 60 and Au 3 clusters," *Appl Surf Sci*, vol. 252, no. 19, pp. 6423–6425, 2006, doi: 10.1016/j.apsusc.2006.02.243.

[312] P. Williams, "Secondary Ion Mass Spectrometry," *Ann Rev Mater Sci*, vol. 15, pp. 517–548, 1985, doi: 10.1021/ac00292a600.

[313] K. K. Murray, "Resolution and Resolving Power in Mass Spectrometry," *J Am Soc Mass Spectrom*, vol. 33, no. 12, pp. 2342–2347, 2022, doi: 10.1021/jasms.2c00216.

[314] Q. P. Vanbellingen, N. Elie, M. J. Eller, S. Della-Negra, D. Touboul, and A. Brunelle, "Time-of-flight secondary ion mass spectrometry imaging of biological samples with delayed extraction for high mass and high spatial resolutions," *Rapid Commun Mass Spectrom*, vol. 29, no. 13, pp. 1187–1195, 2015, doi: 10.1002/rcm.7210.

[315] Ionoptika, "How the J105 SIMS works." [Online]. Available: https://ionoptika.com/how-the-j105-sims-works/

[316] M. K. Passarelli *et al.*, "The 3D OrbiSIMS - Label-free metabolic imaging with subcellular lateral resolution and high mass-resolving power," *Nat Methods*, vol. 14, no. 12, pp. 1175–1183, 2017, doi: 10.1038/nmeth.4504.

[317] L. J. Gamble and C. R. Anderton, "Secondary Ion Mass Spectrometry Imaging of Tissues, Cells, and Microbial Systems," *Micros Today*, vol. 24, no. 2, pp. 24–31, 2016, doi: 10.1017/s1551929516000018.

[318] F. Li, E. F. Fornasiero, T. M. Dankovich, V. Kluever, and S. O. Rizzoli, "A Reliable Approach for Revealing Molecular Targets in Secondary Ion Mass

Spectrometry," *Int J Mol Sci*, vol. 23, no. 9, 2022, doi: 10.3390/ijms23094615.

[319] S. Kabatas *et al.*, "Boron-Containing Probes for Non-optical High-Resolution Imaging of Biological Samples" *Angew Chem Int Ed*, pp. 3438–3443, 2019, doi: 10.1002/anie.201812032.

[320] I. C. Vreja *et al.*, "Secondary-ion mass spectrometry of genetically encoded targets," *Angew Chem Int Ed*, vol. 54, no. 19, pp. 5784–5788, 2015, doi: 10.1002/anie.201411692.

[321] M. Angelo *et al.*, "Multiplexed ion beam imaging of human breast tumors," *Nat Med*, vol. 20, no. 4, pp. 436–442, 2014, doi: 10.1038/nm.3488.

[322] C. He *et al.*, "High-resolution visualization and quantification of nucleic acid-based therapeutics in cells and tissues using Nanoscale secondary ion mass spectrometry (NanoSIMS)," *Nucleic Acids Res*, vol. 49, no. 1, pp. 1–14, 2021, doi: 10.1093/nar/gkaa1112.

[323] G. Slodzian, B. Daigne, F. Girard, F. Boust, and F. Hillion, "Scanning secondary ion analytical microscopy with parallel detection," *Biol Cell*, vol. 74, no. 1, pp. 43–50, 1992, doi: 10.1016/0248-4900(92)90007-N.

[324] C. Lechene *et al.*, "High-resolution quantitative imaging of mammalian and bacterial cells using stable isotope mass spectrometry," *J Biol*, vol. 5, no. 6, p. 20, 2006, doi: 10.1186/jbiol42.

[325] R. Herzog and J. Mattauch, "Ueber einen neuen Massenspektrographen," *Ann. Phys.*, vol. 19, pp. 786–795, 1934. doi: 10.1007/BF01341392

[326] G. Slodzian, F. Hillion, F. J. Stadermann, and E. Zinner, "QSA influences on isotopic ratio measurements," *Appl Surf Sci*, vol. 231–232, pp. 874–877, 2004, doi: 10.1016/j.apsusc.2004.03.155.

[327] J. F. Frisz *et al.*, "Sphingolipid domains in the plasma membranes of fibroblasts are not enriched with cholesterol.," *J Biol Chem*, vol. 288, no. 23, pp. 16855–61, 2013, doi: 10.1074/jbc.M113.473207.

[328] J. F. Frisz *et al.*, "Direct chemical evidence for sphingolipid domains in the plasma membranes of fibroblasts," *Proceedings of the National Academy of Sciences*, vol. 110, no. 8, pp. E613–E622, 2013, doi: 10.1073/PNAS.1216585110.

[329] J. Lovrić *et al.*, "Correlative High-Resolution Imaging of Iron Uptake in Lung Macrophages," *Anal Chem*, vol. 94, no. 37, pp. 12798–12806, 2022, doi: 10.1021/acs.analchem.2c02675.

[330] S. E. Senyo *et al.*, "Mammalian heart renewal by pre-existing cardiomyocytes," *Nature*, vol. 493, no. 7432, pp. 433–436, 2013, doi: 10.1038/nature11682.

[331] A. A. Legin *et al.*, "Nano-scale imaging of dual stable isotope labeled oxaliplatin in human colon cancer cells reveals the nucleolus as a putative node for therapeutic effect," *Nanoscale Adv*, vol. 3, no. 1, pp. 249–262, 2021, doi: 10.1039/d0na00685h.

[332] C. Becquart *et al.*, “Intracellular Absolute Quantification of Oligonucleotide Therapeutics by NanoSIMS,” *Anal Chem*, vol. 94, no. 29, pp. 10549–10556, 2022, doi: 10.1021/acs.analchem.2c02111.

[333] A. Meibom *et al.*, “Correlated cryo-SEM and CryoNanoSIMS imaging of biological tissue,” *BMC Biol*, vol. 21, no. 1, pp. 1–13, 2023, doi: 10.1186/s12915-023-01623-0.

[334] J. Malm, D. Giannaras, M. O. Riehle, N. Gadegaard, and P. Sjövall, “Fixation and drying protocols for the preparation of cell samples for time-of-flight secondary ion mass spectrometry analysis,” *Anal Chem*, vol. 81, no. 17, pp. 7197–7205, 2009, doi: 10.1021/ac900636v.

[335] S. Chandra, “Challenges of biological sample preparation for SIMS imaging of elements and molecules at subcellular resolution,” *Appl Surf Sci*, vol. 255, no. 4, pp. 1273–1284, 2008, doi: 10.1016/j.apsusc.2008.05.073.

[336] E. B. Monroe, J. C. Jurchen, J. Lee, S. S. Rubakhin, and J. V. Sweedler, “Vitamin E imaging and localization in the neuronal membrane,” *J Am Chem Soc*, vol. 127, no. 35, pp. 12152–12153, 2005, doi: 10.1021/ja051223y.

[337] I. Lanekoff, N. T. Phan, C. T. Van Bell, N. Winograd, P. Sjövall, and A. G. Ewing, “Mass spectrometry imaging of freeze-dried membrane phospholipids of dividing Tetrahymena pyriformis,” *Surface and Interface Analysis*, vol. 45, no. 1, pp. 211–214, 2012, doi: 10.1002/sia.5017.

[338] P. Agüi-Gonzalez, S. Jähne, and N. T. N. Phan, “SIMS imaging in neurobiology and cell biology,” *J Anal At Spectrom*, vol. 34, no. 7, pp. 1355–1368, 2019, doi: 10.1039/c9ja00118b.

[339] T. P. Roddy, D. M. Cannon, S. G. Ostrowski, N. Winograd, and A. G. Ewing, “Identification of cellular sections with imaging mass spectrometry following freeze fracture,” *Anal Chem*, vol. 74, no. 16, pp. 4020–4026, 2002, doi: 10.1021/ac025574w.

[340] W. A. Ausserer, S. Chandra, and G. H. Morrison, “Morphological and elemental integrity of freeze-fractured, freeze-dried cultured cells during ion microscopic analysis,” *J Microsc*, vol. 154, no. 1, pp. 39–57, 1989, doi: 10.1111/j.1365-2818.1989.tb00566.x.

[341] J. Lovrić, P. Malmberg, B. R. Johansson, J. S. Fletcher, and A. G. Ewing, “Multimodal Imaging of Chemically Fixed Cells in Preparation for NanoSIMS,” *Anal Chem*, vol. 88, no. 17, pp. 8841–8848, 2016, doi: 10.1021/acs.analchem.6b02408.

[342] M. V. King, “Dimensional changes in cells and tissues during specimen preparation for the electron microscope,” *Cell Biophys*, vol. 18, no. 1, pp. 31–55, 1991, doi: 10.1007/BF02990514.

[343] N. R. Meyer, J. L. Fortney, and A. E. Dekas, “NanoSIMS sample preparation decreases isotope enrichment: magnitude, variability and implications for single-cell rates of microbial activity,” *Environ Microbiol*, vol. 23, no. 1, pp. 81–98, 2021, doi: 10.1111/1462-2920.15264.

[344] H. Jiang *et al.*, “Stable isotope imaging of biological samples with high resolution secondary ion mass spectrometry and complementary techniques,” *Methods*, vol. 68, no. 2, pp. 317–324, 2014, doi: 10.1016/j.ymeth.2014.02.012.

[345] H. Jiang, M. R. Kilburn, J. Decelle, and N. Musat, “NanoSIMS chemical imaging combined with correlative microscopy for biological sample analysis,” *Curr Opin Biotechnol*, vol. 41, pp. 130–135, 2016, doi: 10.1016/j.copbio.2016.06.006.

[346] S. Huang *et al.*, “Subcellular Partitioning of Arsenic Trioxide Revealed by Label-Free Imaging,” *Anal Chem*, vol. 94, no. 40, pp. 13889–13896, 2022, doi: 10.1021/acs.analchem.2c02770.

[347] W. Song *et al.*, “The lipoprotein lipase that is shuttled into capillaries by GPIHBP1 enters the glycocalyx where it mediates lipoprotein processing,” *Proc Nat Acad Sci*, vol. 120, no. 44, 2023, doi: 10.1073/pnas.

[348] A. Ferrari *et al.*, “Aster-dependent nonvesicular transport facilitates dietary cholesterol uptake,” *Science*, vol. 382, no. 6671, 2023, doi: 10.1126/science.adf0966.

[349] C. He *et al.*, “High-resolution visualization and quantification of nucleic acid-based therapeutics in cells and tissues using Nanoscale secondary ion mass spectrometry (NanoSIMS),” *Nucleic Acids Res*, vol. 49, no. 1, pp. 1–14, 2021, doi: 10.1093/nar/gkaa1112.

[350] X. Heiligenstein and M. S. Lucas, “One for All, All for One: A Close Look at In-Resin Fluorescence Protocols for CLEM,” *Front Cell Dev Biol*, vol. 10, pp. 1–14, 2022, doi: 10.3389/fcell.2022.866472.

[351] H. Xiong *et al.*, “Chemical reactivation of quenched fluorescent protein molecules enables resin-embedded fluorescence microimaging,” *Nat Commun*, vol. 5, 2014, doi: 10.1038/ncomms4992.

[352] D. Jeong and D. Kim, “Recent Developments in Correlative Super-Resolution Fluorescence Microscopy and Electron Microscopy,” *Mol Cells*, vol. 45, no. 1, pp. 41–50, 2022, doi: 10.14348/molcells.2021.5011.

[353] M. W. Tuijtel *et al.*, “Inducing fluorescence of uranyl acetate as a dual-purpose contrast agent for correlative light-electron microscopy with nanometre precision,” *Sci Rep*, vol. 7, no. 1, pp. 1–12, 2017, doi: 10.1038/s41598-017-10905-x.

[354] S. K. Saka, A. Vogts, K. Kröhnert, F. Hillion, S. O. Rizzoli, and J. T. Wessels, “Correlated optical and isotopic nanoscopy,” *Nat Commun*, vol. 5, p. 3664, 2014, doi: 10.1038/ncomms4664.

[355] D. Woebken *et al.*, “Identification of a novel cyanobacterial group as active diazotrophs in a coastal microbial mat using NanoSIMS analysis,” *ISME J*, vol. 6, no. 7, pp. 1427–1439, 2012, doi: 10.1038/ismej.2011.200.

[356] D. Woebken *et al.*, “Revisiting N2 fixation in Guerrero Negro intertidal microbial mats with a functional single-cell approach,” *ISME J*, vol. 9, no. 2, pp. 485–496, 2015, doi: 10.1038/ismej.2014.144.

[357] S. E. Senyo *et al.*, “Mammalian heart renewal by pre-existing cardiomyocytes,” *Nature*, vol. 493, no. 7432, pp. 433–436, 2013, doi: 10.1038/nature11682.

[358] T. Wirtz, O. De Castro, J. N. Audinot, A. Biesemeier, and Q. H. Huang, “Advanced multimodal analytical capabilities on FIB instruments using SIMS: New developments, applications and prospects,” *Wiley Analytical Science.* [Online] Available: https://analyticalscience.wiley.com/content/article-do/advanced-multimodal-analytical-capabilities-fib-instruments-using-sims-new-developments

[359] R. Van De Plas, J. Yang, J. Spraggins, and R. M. Caprioli, “Image fusion of mass spectrometry and microscopy: A multimodality paradigm for molecular tissue mapping,” *Nat Methods*, vol. 12, no. 4, pp. 366–372, 2015, doi: 10.1038/nmeth.3296.